University of Zurich[UZH]

INSELSPITAL
UNIVERSITÄTSSPITAL BERN
HOPITAL UNIVERSITAIRE DE BERNE
BERN UNIVERSITY HOSPITAL

MASTER THESIS

Optimized gantry-table path for non-isocentric dynamic trajectory radiotherapy by means of a dosimetrically motivated path finding

Kyriakos X. Rossis

DEPARTMENT OF PHYSICS
UZH ZURICH

DIVISION OF MEDICAL RADIATION PHYSICS
INSELSPITAL – UNIVERSITY HOSPITAL OF BERN

Supervisor:
Prof. Dr. Jan Unkelbach

Advisors:
Dr. Silvan Mueller
Prof. Dr. Peter Manser
Prof. Dr. Michael K. Fix

May 19, 2023

Acknowledgements

Firstly, I would like to express my sincere gratitude to Prof. Dr. Peter Manser and Prof. Dr. Michael Fix, from the Division of Medical Radaition Physics, Inselspital Bern, for offering to me the opportunity to work as a part of their group on this advanced master thesis project. I would also like to thank them for their great supervision and support during this one-year collaboration. In addition, I would like to thank Prof. Dr. Jan Unkelbach, from the Department of Radiation Oncology, University Hospital Zurich and UZH, for his support and encouragement towards the collaboration of the UZH and the Inselspital. Moreover, I would like to sincerely thank him for managing this research project of high importance. Furthermore, I would like to extend my heartfelt thanks to Dr. Silvan Mueller and Mr. Gian Guyer for the invaluable guidance, support and encouragement, as well as the motivation which were vital for the completion of the project. I am also thankful to Dr. Werner Volken for helping me to understand basic tools needed for this project. I find myself blessed for being a part of this group with Dr. Daniel Frei, Dr. Jenny Bertholet, Dr. med. Paul-Henry Mackerprang, Mr. Hannes Anton Loebner, Ms Chengchen Zhu and all people contributing to this study, for gladly sharing their knowledge and for always being friendly and cheerful. Finally, I want to express immeasurable gratitude towards my family and close friends for always being supportive during my master thesis.

Abstract

By utilizing non-coplanar beam trajectories, DTRT delivers radiation along a path connecting multiple beam directions, and the addition of table translations to gantry and table rotations can potentially improve dosimetric results. This study aims to develop a treatment planning process (TPP) capable of generating DTRT plans utilizing both gantry and table rotations, as well as table translations, to provide a more effective means of delivering radiation to a wider range of tumors. The project investigates a dosimetrically motivated path-finding approach for DTRT and evaluates dosimetric results for different tumor cases, contributing to the development of more effective treatment options for cancer patients. The TPP developed consists of two main parts, the first one being the generation of a DTRT path and the second one focusing on the intensity modulation along that path. For the generation of the path, Fluence Map Optimization (FMO) is used in iterations with an additional step of eliminating part of the available beam directions. Outcome of this process is the generation of a suitable set of beam directions, called anchor points, based on a scoring quantity. The anchor points are then connected by a path-finding algorithm. Then, the second part of the TPP takes place where the intensity modulation is achieved by the use of Hybrid- Direct Aperture Optimization (H-DAO) and a final dose calculation with a monitor unit (MU) weighted re-optimization performed by the Swiss Monte Carlo Plan (SMCP) [3], [4] dose calculation. Treatment plans were created for four unique tumor cases utilizing a static isocenter position. These cases include a brain, a nasopharyngeal, a breast and a prostate tumor. Through these cases, proper functionality of the developed DTRT TPP was validated by comparing to plans of well-known treatment techniques such as VMAT. To investigate the advantages and disadvantages of the dosimetrically motivated DTRT TPP for non-isocentric cases, two craniospinal tumor cases and a bilateral breast tumor case were studied. Parameters which influence the DTRT path generation were investigated, and a suitable set of parameters was chosen to create the dosimetrically motivated DTRT plans. Following an isocentric approach, relatively similar or even better dosimetric results can be achieved using the developed DTRT TPP compared to treatment plans based on other treatment modalities. Regarding the non-isocentric approach, similar dosimetric

results were obtained by the developed DTRT TPP compared to treatment plans utilizing other treatment techniques. In conclusion, a dosimetrically motivated DTRT TPP is successfully implemented to generate DTRT plans with a continuously changing isocenter position. The well-functioning TPP and the promising first results motivate further research in the field of non-isocentric DTRT.

Contents

1. Introduction

Radiotherapy is a non-invasive and very effective cancer treatment approach. It is frequently regarded as preferred due to its ability to precisely target tumors while causing minimal damage to adjacent healthy tissue. Advanced radiotherapy techniques such as intensity modulated radiotherapy (IMRT) and volumetric modulated arc therapy (VMAT) have considerably increased radiotherapy efficacy. IMRT is a technology that employs several beams of various intensities of radiation to give a more targeted dose of radiation to the tumor. This approach is especially beneficial for tumors that are close to vital organs or tissues that must be avoided [5]. VMAT, on the other hand, is a method of delivering radiation in a continuous arc while altering the intensity of the beam. When compared to previous approaches, this technology enables beam delivery from more beam directions and shorter treatment times [6]. While these strategies have been shown to improve treatment outcomes, researchers have continued to look for new ways to further improve the discipline of radiation.

Dynamic trajectory radiotherapy (DTRT) is one of the most recent treatments being researched. The idea behind DTRT is to transmit continuous radiation along a path connecting various beam directions using non-coplanar beam trajectories. This is accomplished by utilizing multiple degrees of freedom (DoFs), such as gantry and table rotations, while the beam is turned on constantly. This allows the radiation dose distribution to be delivered more effectively, as tumor control can be achieved while sparing healthy tissue. This is especially crucial for tumors that are close to vital organs or tissues that must be avoided. In preliminary investigations, DTRT showed encouraging dosimetric results, with the potential to improve treatment outcomes and reduce side effects [3], [7].

The primary research question that needs to be answered is whether adding table translations to the traditional gantry and table rotations utilized in DTRT treatment plans can result in enhanced dosimetric results. The importance of this study stems from the requirement to create a treatment planning process (TPP) capable of generating DTRT plans using both gantry and table rotations, as well as table translations. A TPP of this type might be useful for treating a broader range of tumors, regardless of size, shape, or location. Table translations, in particular, could potentially provide a more effective technique of administering radiation to large or concave-shaped tumors by allowing the beam to be focused to multiple isocenter positions in DTRT schemes. This study is motivated by the desire to advance the current state of DTRT treatment planning and improve the quality of care for cancer patients [8].

The goal of this research is to create and investigate a dosimetrically motivated path-finding approach for DTRT that uses gantry and table rotations, as well as table translations, to improve the dosimetric plan quality for various tumor situations. We created a TPP that uses the new DTRT path-finding algorithm and utilized it to assess the dosimetric findings of various tumor instances. A brain case, a nasopharyngeal

case, a breast case, a prostate case, two craniospinal cases, and a bilateral breast case were investigated. By attaining this goal, this study aims to contribute to the creation of more effective cancer treatment alternatives.

2. Materials and Methods

2.1. Treatment Planning Process

The Treatment Planning Process (TPP) developed to create a dosimetrically motivated dynamic trajectory radiotherapy (DTRT) treatment plan, considering both gantry and table rotations, as well as table translations, is an 8-step process, as it is presented in **Figure 1**.

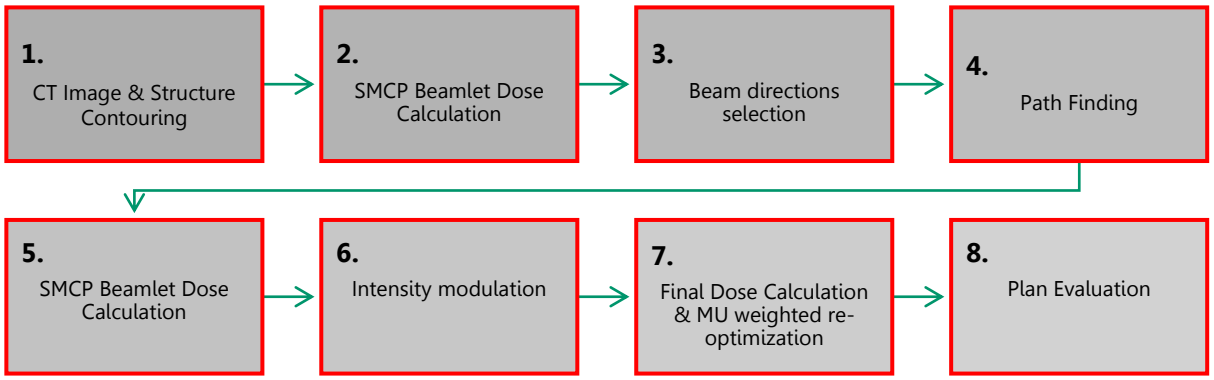

Figure 1: The workflow of the TPP for the dosimetrically motivated DTRT treatment plan.

Parameters used in each step of a TPP might differ depending on the location, size and shape of the tumor. Treatment plans for small and non-concave tumors were performed using a static isocenter position along the generated DTRT path (isocentric cases), while large or concave tumor cases were studied by introducing a DTRT path of a continuously changing isocenter position (non-isocentric cases). A gantry and table rotation were used for isocentric cases, whilst table translations were allowed additionally for non-isocentric cases. Each step of the TPP is explained in detail in this section.

2.1.1. CT image & Structure Contouring

The initial stage in the TPP involves the importation of the planning computed tomography (CT) image set into a research version of the commercial Eclipse treatment planning system (TPS) version 13.6, developed by Varian Medical Systems Palo Alto, CA. The TPS enables the incorporation of clinically contoured structures or the user-defined delineation of such structures. These contoured structures encompass the

target volumes, organs at risk (OARs), and avoidance structures. For the purpose of this study, clinically contoured structures were used. **Figure 2** shows an example of a nasopharyngeal tumor (Head & Neck case).

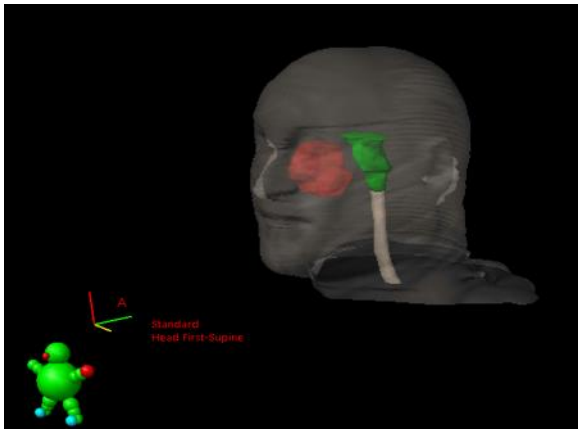

Figure 2: A CT image imported in Eclipse TPS and examples of contoured structures. Planning target volume is indicated as red, brainstem as green and spinal cord as white.

2.1.2.SMCP Beamlet Dose Calculation

With the CT image imported and all the structures of interest contoured, a "dummy" field is manually introduced in Eclipse TPS defining the beam particle type, energy and the isocenter position. A photon beam of 6MV was used for this study. The determination of a grid with the desired beam directions is required, which involves the selection of axes from a set of available degrees of freedom (DoF), including gantry rotation, table rotation, as well as lateral, vertical, and longitudinal table translations. The formed grid resembles a map, and each map point corresponds to a different beam direction. Map points that intersect with the defined avoidance regions are disregarded. Specifically, this pertains to the directions entering through the CT's end, where patient data is absent, as well as the directions that pose a risk of collisions between the treatment machine and either itself or the patient during treatment delivery. Harnessing the defined "dummy" field, a Monte Carlo (MC) beamlet dose calculation is carried out using the Eclipse interfaced Swiss Monte Carlo Plan (SMCP) in order to calculate the Dose-Influence matrix (D_{ij}) for each available beam direction [4]. The Dose-Influence matrix provides the dose in Gray per monitor units $\left[\frac{Gy}{MU}\right]$ delivered to each CT voxel i by each beamlet j. As beamlet, a narrow photon beam is defined which can either have a 5x5 mm^2 or a 5x10 mm^2 size [1].

The photon Monte Carlo (MC) treatment planning framework involves the use of Eclipse within Aria (Version 7.5.42) and a specialized plug-in, Research API, for the initiation of the external component of the framework. Prior to initiating the MC beamlet dose calculation, various parameters are specified, including field settings, source settings, beam modifier settings, dose engine settings, and research settings..

The beamlet dose calculation was performed using pre-patient phase-space (at the exit plane of the treatment head) as the source. Multiple photon beam phase-space sources were pre-computed up until the monitor unit (MU) chamber and right before the jaws in the treatment head, using the BEAMnrc package [9],[10]. The volume element (voxel) resolution and the CT image resolution were both set at 0.5x0.5x0.5 cm^3, and the Voxel-based Monte Carlo (VMC++) dose calculation algorithm was utilized [4].

Additionally, the selection of treatment approach, whether it is an isocentric or non-isocentric approach, led to the utilization of varying parameters pertaining to collimator rotation and jaw positioning. In treatment plans created using an isocentric approach, a multi-leaf collimator (MLC) was incorporated into the "dummy" field. As said, using SMCP beamlet dose calculation, the dose delivered to each voxel is calculated considering all feasible beam direcitons. According to the beam's eye view (BEV) for each available beam direction, the MLC was configured to conform to the Planning Target Volume (PTV), with an additional 0.5 cm margin. For the available beam directions, the jaws opening was defined based on the shape of the MLC so that it encompasses every MLC aperture, while maintaining the jaws opening to a minimum. Regarding the MLC, a dynamic collimator rotation was implemented to align the patient's superior-inferior axis with each beam direction. In contrast, when treatment plans involved a continuously moving isocenter position, the size of the treatment field and, therefore, the position of the jaws were determined by the "dummy" field created in Eclipse. Concerning the MLC rotation, it was fixed at a non-zero-degree angle (such as 2^o or 5^o) due to the absence of an algorithm to determine the appropriate dynamic MLC rotation for non-isocentric cases. A static angle was selected as a substitute. Additionally, the MLC rotation angle was not set to zero to avoid the overlap of radiation leakage through the MLC.

2.1.3.Beam directions selection

After performing the beamlet dose calculation for the available beam directions, the subsequent step involves the identification and selection of favorable beam directions for administering radiation therapy to the patient. To determine the ideal beam directions, each of the available beam directions needs to be evaluated and assigned a specific score that reflects its level of importance. This process is done over iterations using Fluence Map Optimization (FMO) with an additional elimination step over the available map points.

Fluence Map Optimization is a mathematical problem that seeks to determine the best distribution of radiation fluence for a given set of beam directions. The FMO algorithm employs a mathematical model that incorporates both the physical

characteristics of the radiation beam and the patient's anatomy. The beam is represented as a collection of discrete, narrow beamlets, and using the beamlets fluence (weights) calculated by FMO, the radiation dose delivered by each beamlet to each small voxel within the patient's body can also be estimated. The goal is to minimize an objective function by calculating the optimal weight, measured in monitor units (MU), for each beamlet of each field [1], [11]. **Equation 1** shows the mathematical model that FMO is based on. The Dose-Influence matrix D_{ij} already calculated by the SMCP beamlet dose calculation is used for the FMO.

$$d_i = \sum_{j=1}^{N} D_{ij} \cdot x_j \quad (1)$$

Equation 1: The mathematical model that FMO is based on. di is the dose at voxel i, Dij is the Dose-Influence matrix storing the dose in Gray per monitor units delivered to each voxel i from each beamlet j. xj is the weight of beamlet j measured in MU and N is the number of beamlets delivered from every field.

The total objective function is described as a sum over weighted objective functions for the different structures in the body.

$$f(d) = \sum_{k} w_k f_k(d) \quad (2)$$

Equation 2: The total objective function $f(d)$ is described as a sum over the different structures k in the body multiplying each objective function for each structure with a certain weight w_k.

The optimization process may employ various objective functions, including a quadratic penalty function that imposes quadratic penalties on the deviations from the upper and lower dose-volume objectives, a normal tissue objective that defines the desired dose fall-off as a function of the distance from the PTV to achieve dose conformity, or a tissue-specific generalized equivalent uniform dose objective[1]. The resulting value of the objective function serves as an indicator of the quality of the treatment plan. Ideally, an objective function value of 0 would indicate that all the mathematical functions, defined to achieve treatment objectives, have been fully satisfied. These objectives typically involve minimizing the delivery of radiation doses to certain anatomical structures, such as the spinal cord. As the degree of deviation from the objectives increases, the objective function value also increases. Thus, a higher objective function value indicates a less optimal treatment plan.

Harnessing the calculated information (d_i), two different quantities are introduced so that each map point can be characterized by a certain value. These values which describe the map points will be later used to eliminate a certain part of the map points. The first quantity relates to the objective function value, while the second is based on the mean PTV dose and the irradiated part of the PTV. **Figure 3** is a representation of the first optimization, for both scoring quantities introduced, considering all the available map points using FMO.

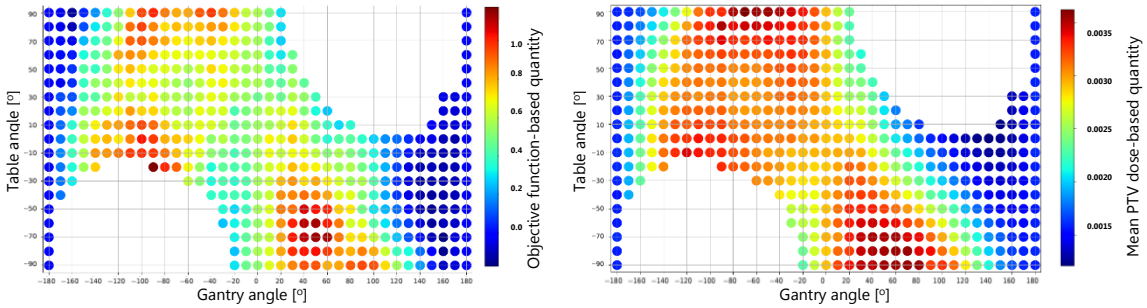

Figure 3: A map including all the available map points for a brain case is presented. White areas indicate the areas where collision betwwen the treatment machine components or between the tratment machine and the patient occur. a) The available map points are characterized by a quantity introduced related to the objective function-based quantity as shown by the colour bar. b) The map points are characterized by a quantity based on the mean PTV dose-based quantity.

The introduction of the two quantities was necessitated by the requirement to identify the most suitable beam directions, referred to as anchor points, for radiation delivery and subsequently connect them using a developed path-finding algorithm. Upon scoring each available map point with either of the two quantities, an elimination process ensues. To facilitate this process, a predetermined number of anchor points and a specific threshold percentage are established. The map points with the lowest quantity values are then eliminated based on the chosen threshold percentage. **Figure 4** is an illustrative diagram explaining how FMO & Elimination process is conducted while **Figure 5** shows an FMO & Elimination process performed when an objective function-based quantity was used with a threshold percentage of 50% and a requested number of 15 anchor points.

The FMO & Elimination method is an iterative procedure that concludes upon the production of the predetermined number of selected anchor points. These anchor points serve as the fundamental building blocks for generating the dosimetrically motivated DTRT path via the path-finding algorithm which follows.

2.1.3.1. Objective Function Value-based quantity

As previously stated, the optimal fluence for each beamlet is calculated, which generates the fluence map or weight map. Using this weight map, the delivered radiation dose to each voxel from each beam direction can be calculated. The objective function value is then computed by considering all the available beam directions. Subsequently, for each map point, the objective function value is recalculated by considering all the available map points except itself. The difference between the recalculated objective function value and the total objective function value (computed by considering all the available map points) is quantified. This difference is then expressed as a relative quantity by being multiplied by 100% and divided by the total objective function value as shown in **Equation 3**.

$$Q_{mp}^{Obj.func} = [f(d)^{erased\ mp} - f(d)^{tot}] \cdot \frac{100}{f(d)^{tot}} \quad (3)$$

Equation 3: $Q_{mp}^{Obj.func}$ is a measure of the relative difference in the objective function value between two scenarios: one in which a specific map point is included in the pool of available map points and the other in which it is excluded. $f(d)^{erased\ mp}$ refers to the objective function value calculated after the specific map point has been removed, while $f(d)^{tot}$ represents the objective function value calculated using all the available map points.

The higher this value is, the more important the observed map point is to radiate from. This is because, when a map point is excluded from the objective function value calculation, the higher the objective function value gets, this means that this specific map point is needed to minimize the objective function value. In contrast, if the quantity calculated is not high enough, then this means that other existing map points achieve similar goals and so the investigated map point does not lead to a significant decrease of the objective function value.

2.1.3.2. Mean PTV dose-based quantity

The second quantity is the mean dose delivered to the PTV over the irradiated region of the PTV from the map point under investigation. As previously described, the dose delivered to each voxel from each beam direction is calculated (d_i). Using the structural information from the contoured regions, specifically the PTV, the relative mean dose delivered to the PTV is computed for each map point. The sum of the number of PTV voxels irradiated by each of the beamlets of that map point is then estimated. The value that characterizes each map point is the relative mean dose to the PTV over the total number of PTV voxels irradiated by all the beamlets of that map point.

$$D_{PTV\ mean} = \frac{\sum_{i=1}^{N} d_i}{N} \quad (4)$$

Equation 4: The mean dose delivered to the PTV by every available map point. d_i is the dose delivered to voxel i of the PTV by the set of map points and N is the number of PTV voxels

$$D_{PTV\ mean}^{m} = \frac{\sum_{i=1}^{N^m} d_i^m}{N^m} \quad (5)$$

Equation 5: The mean dose delivered to the PTV only by a specific map point m. d_i^m is the dose delivered to voxel i of the PTV from the map point m, N^m is the number of PTV voxels radiated by the map point m.

To calculate the relative mean dose delivered to the PTV by each map point, **Equation 6** is used.

$$(d_{mean})_{mp}^{rel} = \frac{D_{PTV\ mean}^{m}}{D_{PTV\ mean}} \quad (6)$$

Equation 6: Relative mean dose delivered to the PTV by map point m.

The quantity describing each map point is presented in **Equation 7**.

$$Q_m^{meanPTVdose/irr.PTV} = \frac{(d_{mean})_m^{rel}}{\sum_{j=1}^{n} k_j^m} \quad (7)$$

Equation 7: The relative mean dose delivered to the PTV by map point m over the number of PTV voxels k_j^m irradiated by each beamlet j of the map point m. n is the number of beamlets included in map point m.

To ensure that both isocentric and non-isocentric cases are appropriately evaluated, the scoring quantity for map points must be generalized. In non-isocentric cases, various map points can irradiate different parts of the tumor, leading to unequal radiation of the tumor volume by each map point. Therefore, to account for this variability and to evaluate each map point equally, the mean PTV dose delivered by each map point is divided by the number of PTV voxels being irradiated by each beamlet of the particular map point. Neglecting the irradiated tumor volume may result in map points that radiate a larger part of the PTV being favored as the best beam directions, leading to an underdose of the PTV if only these map points are used for radiation delivery. It has been demonstrated that excluding the irradiated tumor volume into the scoring quantity leads to a suboptimal selection of map points to radiate the entire PTV.

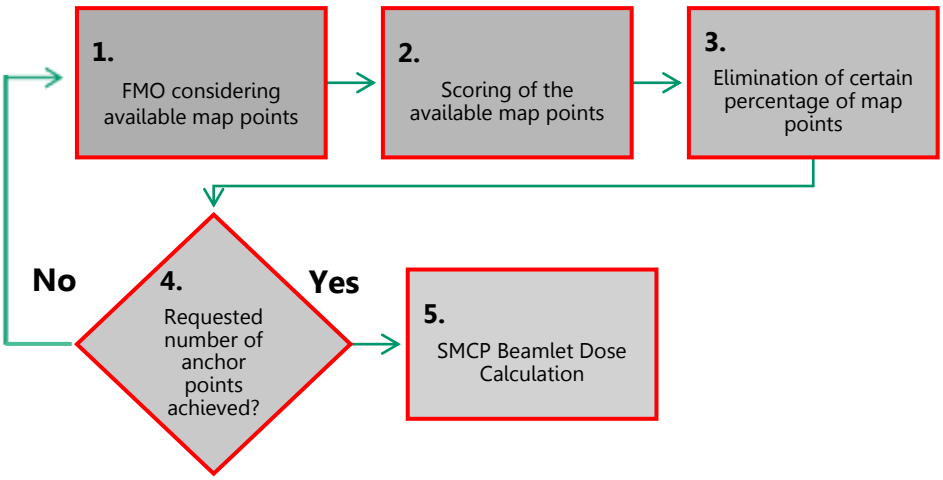

Figure 4: A diagram explaining the function of FMO & Elimination process.

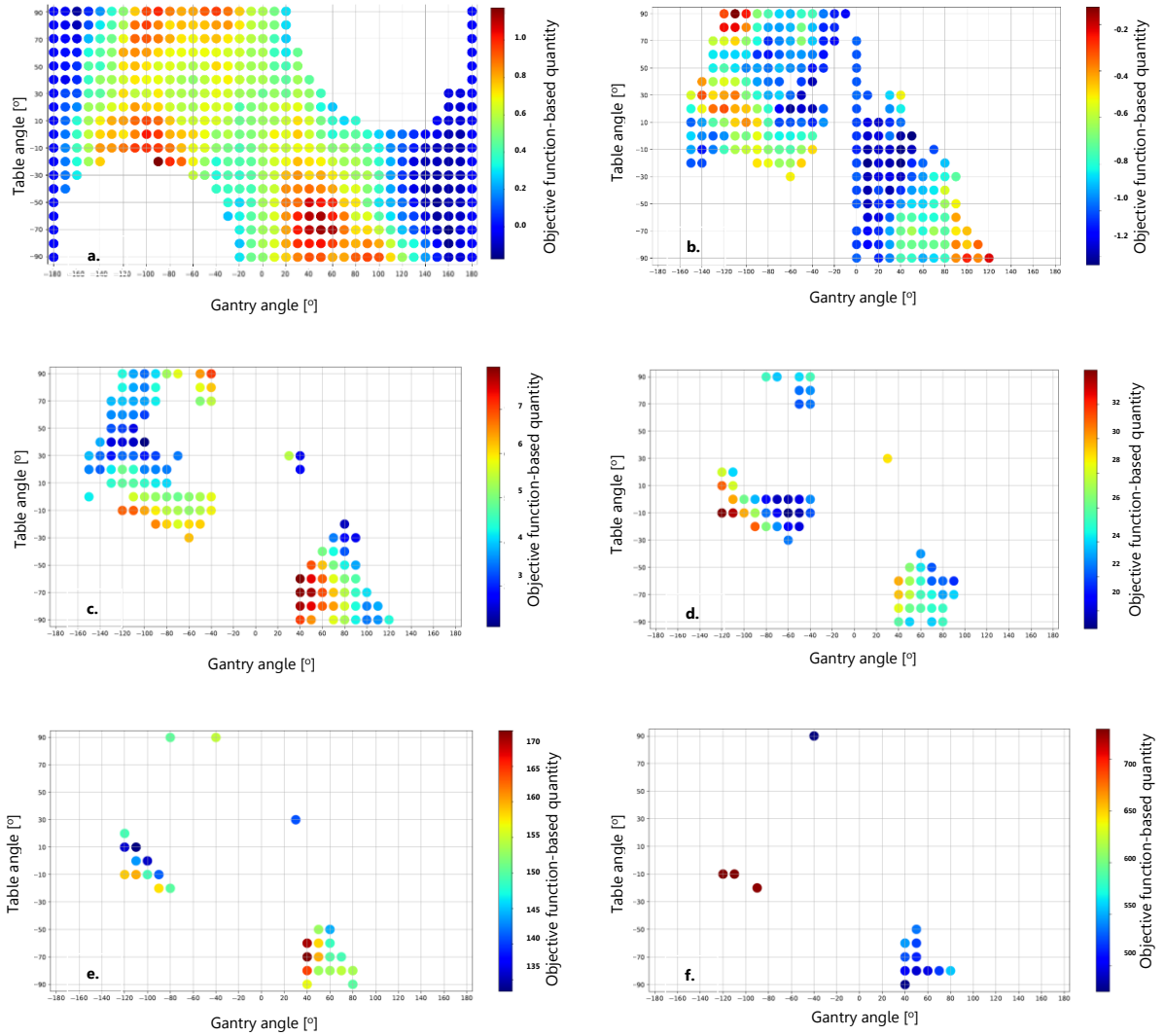

Figure 5: The application of the FMO & Elimination process to map points that have been scored using the objective function-based quantity for a brain case. A 50% of the available map points is eliminated in each iteration until 15 anchor points are generated (f). Figures (a)-(f) represent the optimization and elimination iterations. In each iteration, the remaining points are scored with a different value. That is because less map points are considered for the optimization between each iteration.

2.1.4.Path-finding algorithm

With the anchor points generated, the upcoming task is to find the optimal path to connect them which will represent a DTRT path. The idea to produce such a path was first to use the A* algorithm to calculate paths with the lowest cost connecting each pair of anchor points, and then utilize a Traveling Salesman problem (TSP) solver algorithm to identify the ordering of the anchor points along a path.

The A* algorithm is a highly prevalent path-finding technique employed in the fields of computer science and artificial intelligence [12]. Its fundamental purpose is to compute the best path between two designated nodes on a grid, taking into account both the expenses of traversing each node and the projected cost of reaching the final

node. The algorithm proceeds by exploring the grid in a systematic fashion, prioritizing the nodes that appear most promising in terms of reaching the optimal outcome. To accomplish this, the algorithm navigates through the grid and utilizing the cost between each pair of grid points, finds the optimal paths (lowest-cost paths) connecting each different pair of anchor points and saves them. Grid points in the collision areas are marked as inaccessible points and so A* algorithm recognizes that paths developed cannot pass through these regions. An example of an A* algorithm path between a starting point and a stopping point is shown in **Figure 6**. Consequently, the A* algorithm is a suitable tool for addressing path-finding challenges, such as finding the shortest route between two nodes on a grid [13].

The Traveling Salesman Problem (TSP) is a classic optimization problem that has been studied extensively in computer science and operations research. The problem involves finding the shortest possible route that visits each of a given set of points exactly once. In mathematical terms, the TSP is defined as a complete graph, in which each point is connected to every other point with a certain cost assigned to it. The objective is to determine a Hamiltonian cycle, which is a cycle that visits every point exactly once, with the minimum possible total cost. The TSP is considered a highly challenging problem in terms of computational time, especially for large problem sizes [14].

For the purpose of this project, to create the DTRT path that links the anchor points, the A* algorithm is firstly utilized to calculate the most efficient paths connecting each pair of anchor points (sub-paths) and their corresponding cost. Next, the TSP solver is employed to determine the optimal sequence in which to visit the anchor points. A grid of all the available map points and the anchor points produced, are taken as input in the A* algorithm. When the first iteration of the FMO & Elimination process was performed, each map point was scored with a value according to the scoring quantity used. These values are then used to characterize the grid points. Harnessing these values, a cost between each pair of neighbouring grid points is calculated.

When the objective function value-based quantity is used, the grid points are initially described by this value. Then this value is reversed, so that important grid points will be described by a high negative value, while less important grid points will have a low negative or even a positive value. Due to the reversion, negative values are produced which can mislead the navigation of A* algorithm through the grid. In order to prevent having negative values, every value is shifted by the absolute value of the highest negative value generated. This way, the lowest value characterizing a grid point will be 0. **Equation 8** shows how the cost between 2 neighbouring grid points is calculated. On the other hand, when using the mean PTV dose-based quantity, the grid points are characterized by this value and the cost between two neighbouring grid points is calculated as shown in **Equation 9**.

The total costs of the paths connecting 2 different anchor points are used to produce a cost matrix which will later on be used by the TSP solver developed.

$$Cost^{Obj.Func} = \frac{1}{2}\left[\left(-Q_{m_a}^{Obj.func} + \left|Q_{highest}^{Obj.func}\right|\right) + \left(-Q_{m_b}^{Obj.func} + \left|Q_{highest}^{Obj.func}\right|\right)\right] \quad (8),$$

Equation 8: The cost between two neighbouring points a and b. $Q_{m_a}^{Obj.func}$ and $Q_{m_b}^{Obj.func}$ are the values for points a and b calculated by $Q_m^{Obj.func}$, which was previously explained in Equation 3. $Q_{highest}^{Obj.func}$ is the highest value calculated by the objective function-based quantity for a map point.

$$Cost^{meanPTVdose/irr.PTV} = \frac{1}{2}\left[\frac{1}{Q_{m_a}^{meanPTVdose/irr.PTV}} + \frac{1}{Q_{m_b}^{meanPTVdose/irr.PTV}}\right] \quad (9)$$

Equation 9: The cost between grid points a and b when they are described by the value $Q_m^{meanPTVdose/irr.PTV}$ as shown in Equation 7. The inverse of the $Q_m^{meanPTVdose/irr.PTV}$ values is used so important points with a high value will lead to a low cost.

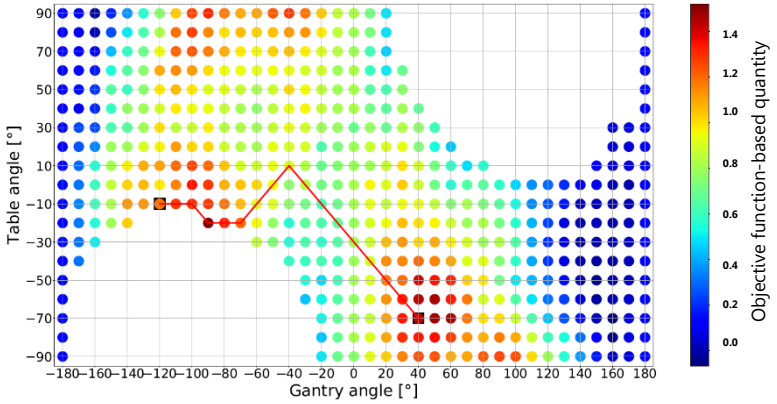

Figure 6: A path generated by A algorithm to connect two points (marked in black squares). Areas marked in white are inaccessible areas and so the path cannot pass through them. The path is indicated with a red line.*

To determine the optimal sequence of anchor points along a path, a TSP solver was implemented. The TSP solver utilizes the cost matrix generated by the A* algorithm, which indicates the cost between each anchor point. Two algorithms were developed to determine the order of the anchor points: a greedy algorithm and a combination of a greedy algorithm with a backtracking algorithm (Hybrid TSP solver algorithm). These algorithms were used to find the best possible ordering of the anchor points, ultimately producing the final path connecting the anchor points.

The greedy algorithm is a pathfinding technique that begins with a given starting point and selects the subsequent point with the lowest cost from the current point to establish a path. A repetitive process is performed over various starting points to determine the path with the least cost discovered by the greedy algorithm. Although the greedy algorithm is quick to execute, it does not ensure that the optimal low-cost path will be found.

The second algorithm developed to tackle the TSP is the Hybrid TSP solver algorithm, which involves a combination of the greedy algorithm and a backtracking algorithm. The backtracking algorithm usually examines every conceivable sequence

of anchor points, which can be extremely computationally demanding. To minimize the computational time while still finding the lowest-cost path, the conjugation of the greedy and backtracking algorithms was devised. Initially, the greedy algorithm is used as described above to identify a low-cost path, which is then used as input for the backtracking algorithm. The backtracking algorithm begins to calculate all feasible orderings of the anchor points. When a possible path exceeds the cost of the path identified by the greedy algorithm, that path is discarded, and its calculation stops. The paths that are less expensive than the path determined by the greedy algorithm are thoroughly calculated, and the path with the lowest cost is chosen from them. **Figure 7** depicts the usage of the greedy and backtracking algorithms in the TSP solver.

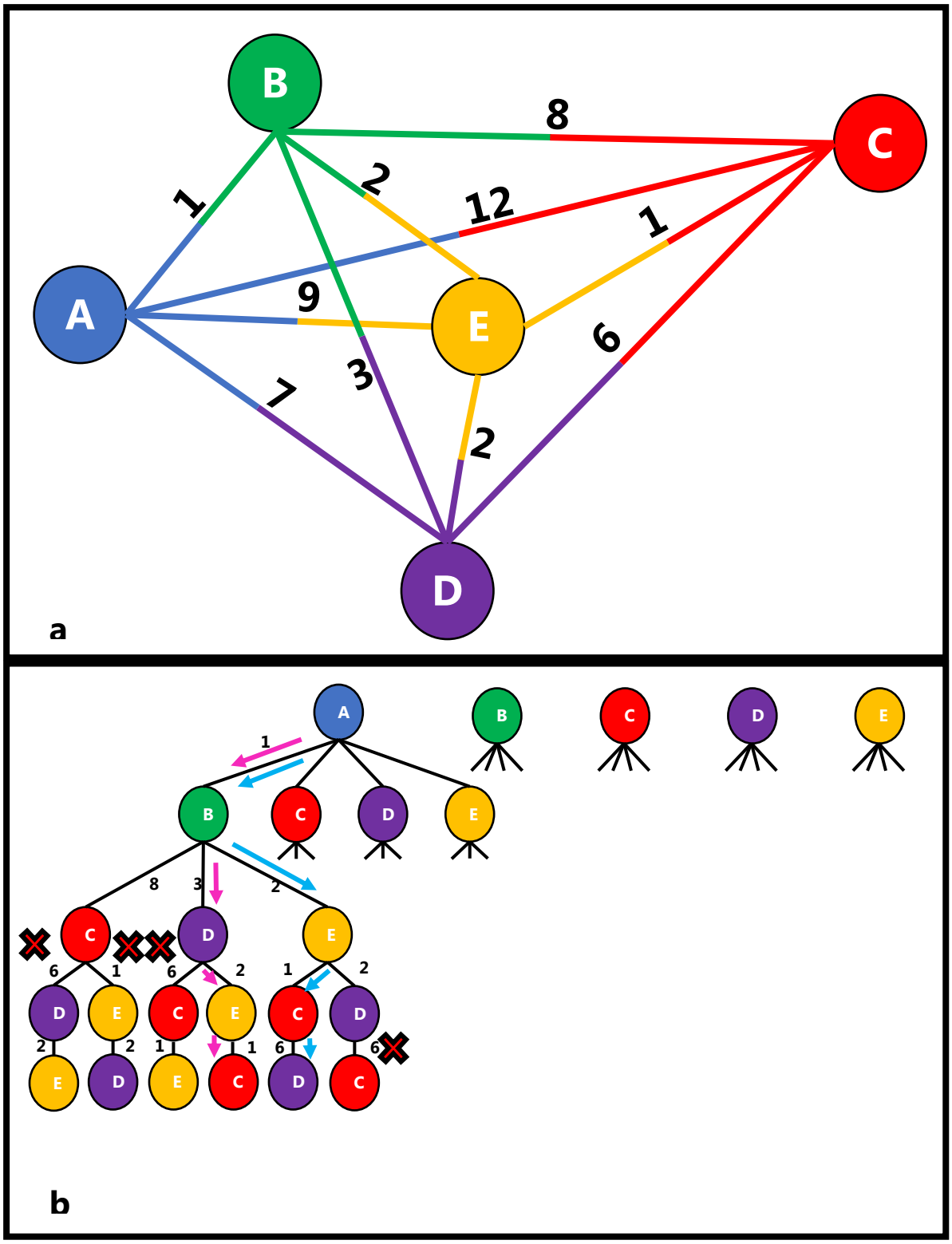

Figure 7: A schematical illustration interpreting the function of the Hybrid TSP solver algorithm. The top diagram (a) represents an example of 5 anchor points (A-B-C-D-E) and the cost between each pair of them. The diagram at the bottom (b) illustrates different orderings of the anchor points. The arrows in light blue colour show the path found by the greedy algorithm (A-B-E-C-D) with a total cost of 10. To arrows in pink colour, indicate the path found by the backtracking algorithm (A-B-D-E-C) with a total cost of 7. Red crosses indicate how greedy algorithm is used to prevent backtracking algorithm perform unnecessary calculations. Path calculations stop, when a cost equal or higher than the cost coming from the path, found by greedy algorithm, is obtained.

Subsequently, by combining the sequence provided by the TSP solver with the optimal sub-paths produced by the A* algorithm, the DTRT path is constructed, which navigates through the least expensive areas as shown in **Figure 8**. When the path is defined, interpolation takes place so that points along the path will be generated every 5° for table and gantry rotations and every 2 cm for table translations. These points are called optimization points because they will be considered by H-DAO to perform the intensity modulation along the path. Creating the optimization points leads to more apertures along the path, as the H-DAO will generate an aperture for each optimization point.

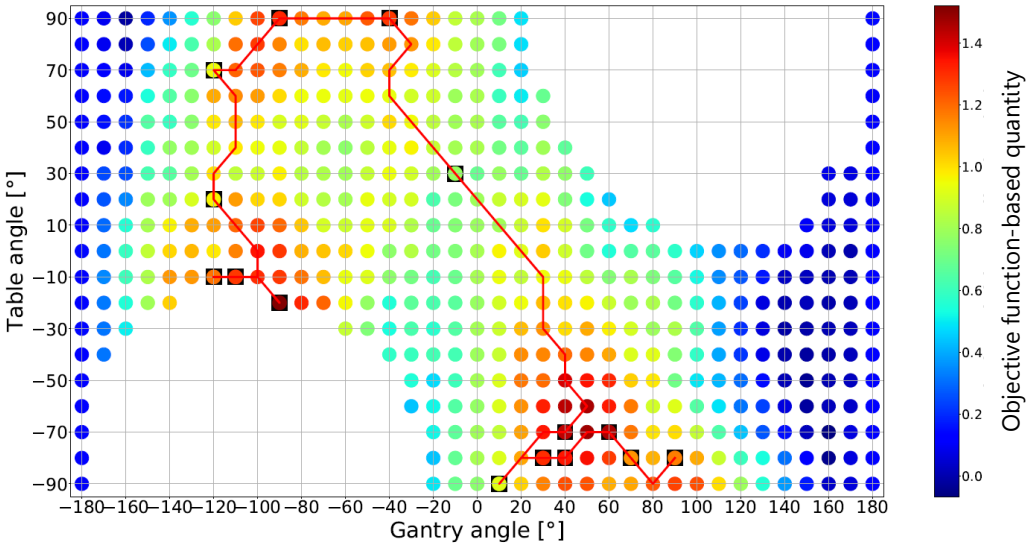

Figure 8: An example of a DTRT path generated by the path-finding algorithm referring to a brain case. The red line indicates the DTRT path and points enclosed in black squares indicate the anchor points.

2.1.5.SMCP-path-Beamlet Dose Calculation

The dosimetrically motivated DTRT path is generated and another SMCP beamlet dose calculation is performed along the path using a CT image resolution of $0.25x0.25\text{x}0.25\ cm^3$ to improve the dosimetric accuracy. As previously mentioned, in isocentric cases, the jaws opening is determined by the MLC apertures along the path, which are conformal to the PTV with an additional 0.5 cm margin, and the minimum opening that can include all MLC apertures is used. The MLC is also rotated to align with the patient's superior-inferior axis. For non-isocentric cases, the field size and jaws opening are the same as those for the "dummy" field, and the MLC is set to a static 2° or 5° angle as described earlier.

2.1.6.H-DAO

The FMO technique is used to determine the best fluence map for each beam direction. However, the fluence maps obtained through FMO cannot be practically delivered due to machine limitations imposed by the MLC, such as constraints on leaf movement. Consequently, an optimization algorithm to convert the optimized intensity maps into a set of feasible aperture shapes, which can be delivered, is needed, resulting in a reduction in plan quality [16].

To account also for the limitations imposed by the MLC and generate realistic aperture shapes, for each optimization point along the path, a Direct Aperture Optimization (DAO) algorithm is used [17]. For the purpose of this project, the Hybrid-DAO (H-DAO) [18] was used, which is an optimization algorithm combining the column generation-based DAO (CG-DAO) [19] and the simulated annealing-based DAO (SA-DAO) [2].

The CG-DAO algorithm initializes an empty pool of apertures and then iteratively selects and adds promising apertures until there is one aperture available for each optimization point. The process involves the generation of new and promising apertures, and the selection of the aperture with the lowest cost. The MUs weight is optimized using the gradient descent approach which is obtained by the L-BFGS quasi-Newton method [20], [21]. The optimization process is terminated once every optimization point has an aperture, or else it is continued by generating a new set of promising apertures.

The SA-DAO method employs a fixed number of apertures and optimizes the modulation of the MUs weights and aperture shapes using a random number generator. The method selects a random aperture and modifies either the MU weight or the position of one MLC leaf during each iteration. The change is accepted or rejected based on the objective function value. If the objective function value decreases, the change is accepted. Conversely, if the objective function value increases or remains the same, the change is accepted with a probability to potentially avoid getting stuck in a local minimum [20].

The H-DAO algorithm begins with an empty aperture pool and generates new promising apertures. The most promising aperture, identified as the one with the lowest cost based on the objective function gradient, is selected and added to the pool. The MU weights of the apertures are then optimized using the gradient descent method. Any apertures whose MU weights fall below the minimum threshold are eliminated. In the next step, the MU weights or shapes of randomly chosen apertures are modified, followed by a re-optimization of MU weights. Apertures with MU weights below the minimum allowable value are discarded. The procedure stops when all optimization points, along the DTRT path, have an aperture, otherwise, the algorithm proceeds to the next iteration by generating new apertures. The workflow of the H-DAO is illustrated in **Figure 9**.

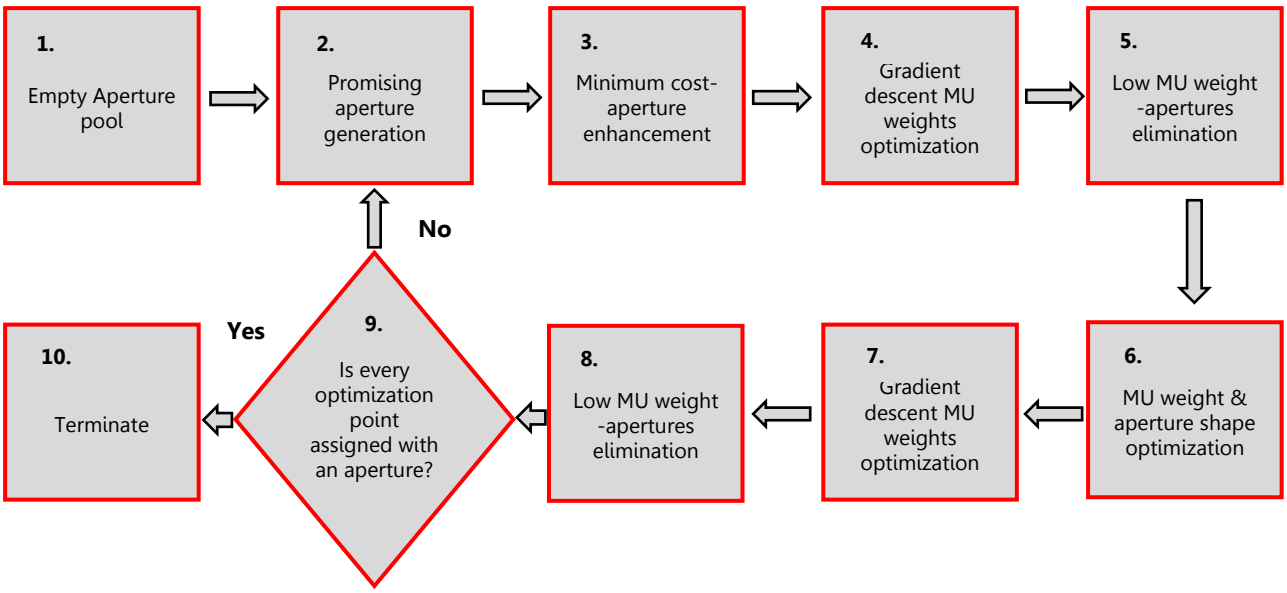

Figure 9: The workflow of H-DAO.

2.1.7.Final dose calculation

After optimizing the weights and shapes of the apertures, a final dose calculation is performed using the SMCP dose calculation, which calculates the dose delivered to each voxel by considering the position of the jaws, the MLC apertures along the path, the impact of the MLC leaf transmission and the interleaf leakage based on the particle simulation. The simulation utilizes pre-simulated phase-space data at a plane above the secondary collimators as the source for the dose calculation. VMC++ software is used to simulate the patient-specific components of the treatment head, including the jaws and MLC, and to perform the dose calculation within the patient [22].

Following the SMCP final dose calculation, the MU weights of the ranges between adjacent optimization points are re-optimized, with consideration given to the delivery-efficiency constraints that were applied during the initial optimization. Subsequently, the final dose calculation is multiplied by the re-optimized MU weights, and the resultant re-optimized dose for the trajectories is calculated [2].

2.1.8.Evaluation

Visualizing the calculated dose distribution of the treatment plan, evaluation of the treatment plan can be achieved. The final dose calculated, after the MU weighted re-optimization, is loaded back to Eclipse TPS and visualized. Evaluation of the plan can be done also by looking the dose volume histograms (DVHs).

2.2. Other treatment plan approaches

A variety of treatment methods are available for creating treatment plans, each with their own advantages and disadvantages that may vary depending on the specific tumor case. These methods include IMRT, VMAT, geometrically motivated DTRT and manually defined DTRT. In order to assess the dosimetric performance of the dosimetrically motivated DTRT plan, a comparative analysis was performed with treatment plans generated using other modalities. For each treatment modality, the beamlet dose calculation was carried out using the SMCP dose calculation, and intensity modulation was achieved using H-DAO. In addition, the final dose calculation was performed using SMCP with weighted MU re-optimization for all treatment plans.

2.2.1.IMRT

Intensity-Modulated Radiation Therapy (IMRT) is an advanced form of radiation therapy that enables highly precise targeting of tumor tissue while minimizing radiation exposure to surrounding healthy tissue. This is achieved by using the MLC which allow the modulation of the intensity of the radiation beam, which can be delivered from multiple beam directions. IMRT also employs advanced optimization algorithms to optimize the shape and intensity of the beam and minimize the dose to healthy tissue while maximizing the dose to the tumor. This process involves the segmentation of the tumor into different regions with unique dose requirements, allowing for customization of the dose delivered to each specific region. The accuracy and precision of IMRT has been shown to lead to improved tumor control rates, while minimizing the risk of side effects such as damage to surrounding organs or tissues. IMRT is used to treat a wide range of cancers, including prostate, breast, head and neck, and brain tumors [11].

2.2.2.VMAT

Volumetric Modulated Arc Therapy (VMAT) is a type of intensity-modulated radiation therapy (IMRT) that offers the ability to deliver a highly precise radiation dose to the tumor volume while minimizing the dose to the surrounding healthy tissues. In VMAT, the radiation beam is continuously delivered around the patient in a dynamic manner, using a 360-degree arc, and the shape and intensity of the beam are continuously adjusted during the rotation. This allows for more flexibility in radiation dose delivery compared to traditional IMRT, which uses fixed beam directions. The optimization of VMAT treatment plans involves the application of advanced algorithms to optimize both the shape and intensity of the radiation beam to achieve the desired

dose distribution. VMAT is a proven effective treatment modality for various types of cancer, such as prostate, lung, head and neck, and brain tumors, with high local tumor control rates and low risk of side effects [23].

2.2.3.Geometrically motivated DTRT

To generate a path for geometrically motivated DTRT plans, a map of the overlap between the target structure and organs at risk (OARs) is created based on the beam's eye view (BEV) of the treatment head. However, since the CT scan has a limited length, beam directions that enter the end slice of the CT data set are excluded from the optimizer because the tissues and OARs beyond that slice cannot be considered [24].

To ensure safe and efficient delivery of dynamic trajectory radiotherapy, collision avoidance is addressed by constructing a collision map and incorporating it into the optimization of the gantry-table path. A path finding algorithm based on A* search is applied to the restricted gantry-table map to determine the path with minimal overlap between the organs at risk and the target volume. In addition, a gantry-collimator map is generated by minimizing the area between the target contour and the MLC leaves, without any constraint on the path selection. The same A* algorithm is utilized to search for the optimal gantry-collimator path [25].

The geometrically motivated DTRT path is generated by defining optimization points at 5-degree intervals in both the table and gantry rotations. This approach reduces the computational time required to perform intensity modulation along the path.

2.2.4.DTRT manually defined

An alternative approach to generate a treatment plan is by manually delineating a DTRT path. This method involves the identification of optimization points, which may also focus on different isocenter positions, to form a path that utilizes various degrees of freedom to investigate the impact of beam directions on different planes on dosimetric outcomes. Such treatment plans, referred to as non-coplanar plans, aim to improve the accuracy and precision of dose delivery by enabling radiation to be delivered from multiple angles in non-coplanar planes. This approach seeks to achieve optimal dose distributions that minimize exposure to healthy tissues while maximizing the dose to the tumor [8].

2.3. Cases studied

To evaluate the effectiveness of the dosimetrically motivated DTRT TPP, seven cases of tumors were analyzed. For each case, treatment plans were devised, including a brain case, a head and neck case concerning a nasopharyngeal tumor, a breast case, a prostate case, two craniospinal cases, and a bilateral breast case. Notably, the brain tumor, nasopharynx tumor, breast tumor, and prostate tumor were investigated with a fixed isocenter approach, wherein only gantry and table rotations were enabled. On the other hand, the remaining tumor cases were investigated using a non-isocentric approach, where table translations were allowed. For the two cranispinal irradiation cases, a gantry rotation and a longitudinal table translation were allowed, while for the bilateral breast case, a gantry rotation and a lateral table translation were enabled.

2.3.1. Cases investigated with a fixed isocenter position

For the treatment plan creation following an isocentric approach, both SMCP beamlet dose calculations - one before the generation of the path and one after - were calculated with the MLC aligned with the superior-inferior axis of the patient, while the jaws were adjusted to the minimum aperture size that could accommodate all feasible MLC openings from all conceivable beam directions. As for the parameters used for the DTRT path generation, a 10% threshold to eliminate map points in each FMO & Elimination process iteration, a number of 15 anchor points, the objective function-based quantity to score the map points and the Hybrid TSP solver to generate the path, were utilized.

2.3.1.1. Brain case

The patient diagnosed with a brain tumor was subjected to a clinical treatment involving a two-partial-arc VMAT plan and so another plan of the same nature was devised to evaluate the resulting dosimetric outcomes concerning the dosimetrically motivated DTRT plan developed. The first partial arc had the gantry initially set right below the patient (-180^{o}) and a clockwise rotation of the gantry was performed until the gantry was rotated at the left side of the patient (90^{o}). The collimator rotation was set to 5^{o} for the first arc. The second partial arc was exactly the same as the first, only reversed and the collimator rotation was set to 355^{o}. Both arcs employed a field size of 13cm x 10cm defined by the jaws, while the MLC was set conformal to the PTV with

a 0.5cm margin. The center of the PTV was selected to be placed at the isocenter position. The VMAT setup is illustrated in **Figure 10**.

Furthermore, a geometrically motivated DTRT treatment plan was created for the brain tumor. The collision areas were duly considered, and as previously stated, a path was defined to enable avoidance of organ overlap. During the generation of the gantry-table path, the patient's physical dimensions, the placement of the arms in the body's vicinity, and the delineated anatomical structures were taken into account. The isocenter position remained fixed at the center of the PTV throughout the path, and a two-paths treatment plan was created.

In the context of the dosimetrically motivated DTRT plan, a two-path approach was utilized during the generation of the treatment plan. An isocentric approach was used in the creation of the plan, with the isocenter located at the center of the PTV.

Every one of the above-described plans was created considering an objective function described by the objectives presented in **Table 1**, while a dose normalization at the 50% of the PTV was considered with a prescribed dose of 60 Gy.

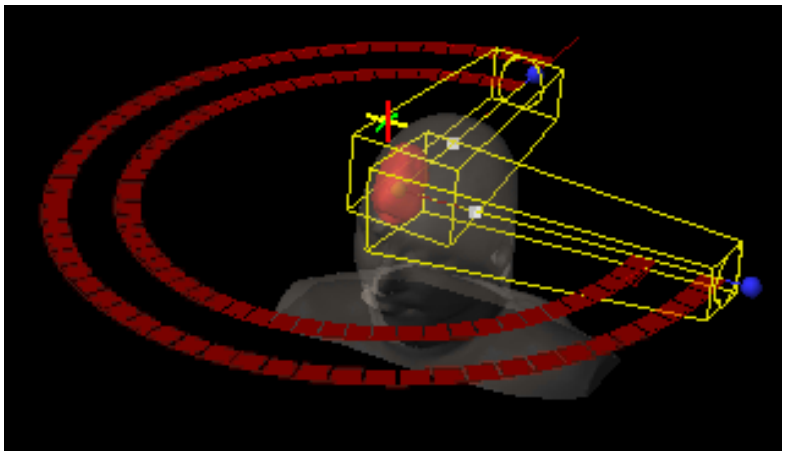

Figure 10: The beam set up for a VMAT plan is shown regarding a brain tumor.

Table 1: Objectives used for the contoured structures for the patient with a brain tumor.

Structure	Objective Type	Priority	Relative Dose	Relative Volume
PTV	Upper Dose	200	102	0
PTV	Lower Dose	200	98	100
Left Eye	Upper Dose	15	10	0
Right Eye	Upper Dose	15	10	0
Chiasm	Upper Dose	15	55	0

Chiasm – 2mm marg.	Upper Dose	15	80	0
Brain	Upper Dose	30	35	30
Brain	Upper Dose	30	60	20
Brain	Upper Dose	30	90	15
Brainstem	Upper Dose	15	70	0
Brainstem	Upper Dose	15	40	5
Brainstem	Upper Dose	15	10	45
Right Lens	Upper Dose	15	4	0
Left Lens	Upper Dose	15	4	0
Left Optical nerve	Upper Dose	15	12	0
Right Optical nerve	Upper Dose	30	60	0
Right Optical nerve – 2mm marg.	Upper Dose	30	80	0
Left Lacrimal gland	Mean Dose	15	8	0
Right Lacrimal gland	Mean Dose	15	10	0

Structure	Priority	Relative Dose	Relative Volume	Start Distance	End Dose	Fall Off	Optimization parameter
Normal tissue	15	90	0	0.5	40	0.1	End Dose

2.3.1.2. Head & Neck case

A two-partial-arc VMAT plan was employed to clinically treat a nasopharyngeal tumor. The plan consisted of two partial arcs, with the first starting with the gantry at a certain angle below the patient and on his right side (222°), while a clockwise rotation would follow until the gantry would achieve a symmetric position below the patient and on his left side (136°). The collimator rotation would be fixed at 5° for the first arc. The second partial arc would follow the same path as the first arc, but only with opposite direction and having a collimator angle of 355°. The field size defined by the jaws was selected to be 13.5cm x 8cm for both arcs, while the MLC was defined to be conformal to the PTV with a 0.5cm margin. The nasopharyngeal tumor was treated with a static-isocenter approach, with the isocenter placed at the PTV's geometric center. The VMAT setup is illustrated in **Figure 11**.

Similar to the approach used for the brain case, a geometrically driven DTRT treatment plan was devised for the nasopharyngeal case. The DTRT path aimed to target a stationary isocenter located at the center of the PTV and a two-path treatment plan was developed.

A dosimetrically motivated DTRT plan was generated with the same procedure as described for the brain case, only this time, the static isocenter used was placed at the center of the PTV delineated for this case.

The above-described plans were produced considering an objective function which describes the objectives presented in **Table 2**, while a dose normalization at the 95% of the PTV was considered with a prescribed dose of 50 Gy.

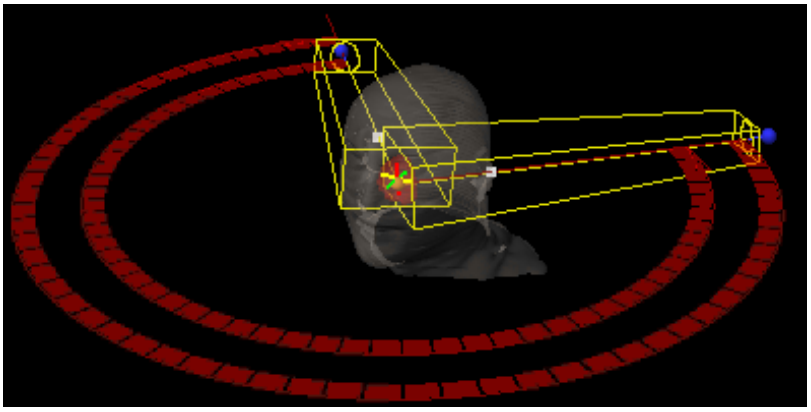

Figure 11: The beam set up for a VMAT plan is shown regarding a nasopharyngeal tumor.

Table 2: Objectives used for the contoured structures for the patient with a nasopharyngeal tumor.

Structure	Objective Type	Priority	Relative Dose	Relative Volume
PTV	Upper Dose	5000	105	0
PTV	Lower Dose	5000	100	100
PTV	Lower Dose	5000	100	95
PTV	Lower Dose	5000	95	100
Spinal Cord	Upper Dose	20	35	0
Spinal Cord – 2mm marg.	Upper Dose	20	9	0
Right Carotid - 2mm marg.	Upper Dose	20	6	47
Right Carotid - 2mm marg.	Upper Dose	20	14	27
Right Carotid - 2mm marg.	Upper Dose	20	26	7
Right Carotid - 2mm marg.	Upper Dose	20	60	0

Brainstem	Upper Dose	20	20	0
Brainstem - 2mm marg.	Upper Dose	20	33	0
Left Parotid gland	Mean Dose	20	6	0
Right Parotid gland	Mean Dose	20	2	0
Oral Cavity	Mean Dose	20	55	0
Left Optical nerve	Upper Dose	20	82	0
Right Optical nerve	Upper Dose	20	46	0
Optic Chiasm	Upper Dose	20	65	0
Lips	Upper Dose	20	45	0
Lips	Mean Dose	20	8	0
Left Lacrimal gland	Mean Dose	20	7	0
Right Lacrimal gland	Mean Dose	20	7	0
Left Eye	Upper Dose	20	52	0
Left Eye	Mean Dose	20	23	0
Right Eye	Upper Dose	20	33	0
Right Eye	Mean Dose	20	18	0
Right Cochlea	Upper Dose	20	7	0
Left Cochlea	Upper Dose	20	18	0
Normal tissue	Upper Dose	50000	98	0

Structure	Priority	Relative Dose	Relative Volume	Start Distance	End Dose	Fall Off	Optimization parameter
Normal tissue	30	90	0	0.5	10	0.15	End Dose

2.3.1.3. Breast case

The clinical treatment of a breast case was based on two partial VMAT arcs. To demonstrate the clinical treatment, a VMAT plan with 2 partial arcs was created. The first arc was set to start with the gantry right below the patient (-180°), while a clockwise rotation would follow until the gantry would stop at the left side of the patient (90°). The collimator rotation would be fixed at 5° for the first arc. The second

partial arc would follow the same path as the first arc, but only with opposite direction and having a collimator angle of 355°, while a field spit technique was used. The first arc was focusing the beam irradiation to one half of the breast tumor, while the other arc was focusing on the other half of the tumor. The isocenter position was static at the center of the PTV for both arcs. The VMAT setup is illustrated in **Figure 12**.

In addition, a plan for DTRT was developed for the breast case, using the same geometric approach as the plans created for the brain and nasopharyngeal cases. The differences in this plan were that the isocenter was positioned at the center of the PTV located in the right breast, the patient had her arms raised above her head and the 2-paths produced also used the field-split technique.

Furthermore, a dosimetrically motivated DTRT plan made of 2 paths, was produced for the breast case using the same approach previously described. The plan created was dealt as an isocentric approach.

The objectives used for the three plans produced for the breast case are shown in **Table 3**. A dose normalization at the 50% of the PTV was used with a prescribed dose of 42.7 Gy.

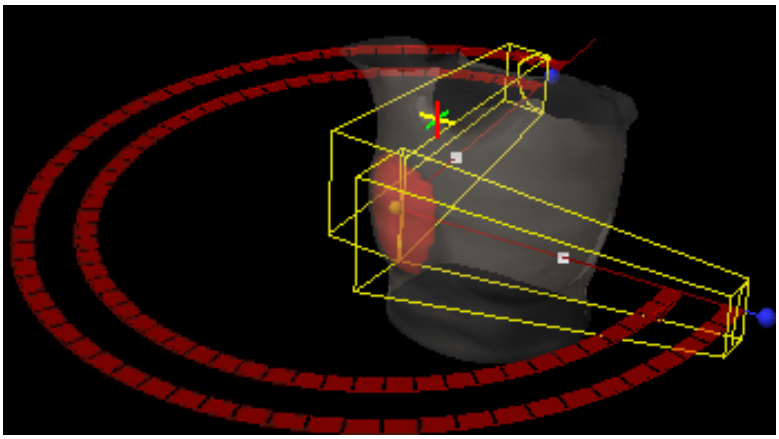

Figure 12: The beam set up for a VMAT plan is shown regarding a right breast tumor.

Table 3: Objectives used for the contoured structures for the patient with a breast tumor.

Structure	Objective Type	Priority	Relative Dose	Relative Volume
PTV	Upper Dose	188956800	102	0
PTV	Lower Dose	188956800	98	100
Spinal Canal	Upper Dose	3276800	10	0
Lung total	Upper Dose	3276800	10	20
Right Lung	Upper Dose	3276800	35	10
Left Lung	Upper Dose	3276800	25	0

Heart	Mean Dose	3276800	2	0
Normal tissue	Upper Dose	3276800	90	0

Structure	Priority	Relative Dose	Relative Volume	Start Distance	End Dose	Fall Off	Optimization parameter
Normal tissue	15	95	0	0.5	40	0.1	End Dose

2.3.1.4. Prostate case

The prostate case was clinically treated using two full VMAT arcs. To represent the clinical treatment, a VMAT plan with two full arcs was created, where the MLC was set to 5° for the first arc and 355° for the second arc, and the field size was set at 10cm x 8cm. The isocenter position remained static at the center of the PTV for both arcs. The VMAT setup is illustrated in **Figure 13.**

Additionally, a geometrically motivated DTRT treatment plan with 2 DTRT paths was developed for the prostate case, using the same parameters used for the brain case. The dosimetrically motivated DTRT plan involved using 2 DTRT paths and investigating the prostate tumor with an isocentric approach.

Table 4 shows the objectives for the contoured structures delineated for the prostate case. A dose normalization at the 50% of the Planning Target Volume (PTV) was used with a prescribed dose of 80 Gy.

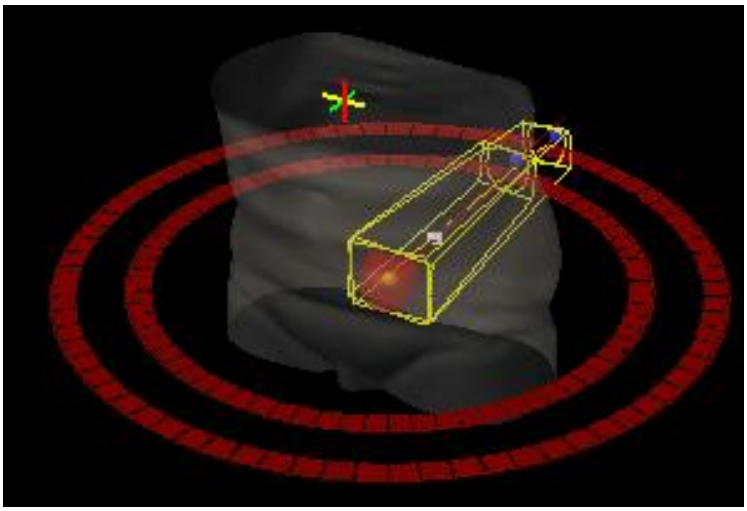

Figure 13: The beam set up for a VMAT plan is shown regarding a right breast tumor.

Table 4: Objectives used for the contoured structures for the patient with a prostate tumor.

Structure	Objective Type	Priority	Relative Dose	Relative Volume
PTV	Lower Dose	320000000	98	100
PTV	Upper Dose	320000000	102	0
Bowel	Upper Dose	3276800	5	0
Rectum Wall	Upper Dose	3276800	15	43
Rectum Wall	Upper Dose	3276800	67	20
Rectum Wall	Upper Dose	3276800	76	12
Rectum Wall	Upper Dose	3276800	90	0
Rectum	Upper Dose	3276800	14	42
Rectum	Upper Dose	3276800	63	18
Rectum	Upper Dose	3276800	73	10
Rectum	Upper Dose	3276800	85	3
Right Femoral Head	Upper Dose	3276800	5	0
Right Femoral Head	Mean Dose	3276800	13	0
Left Femoral Head	Upper Dose	3276800	5	0
Left Femoral Head	Mean Dose	3276800	13	0
Bladder	Upper Dose	3276800	18	36
Bladder	Upper Dose	3276800	54	14
Bladder	Upper Dose	3276800	90	5
Bladder Wall	Upper Dose	3276800	24	36
Bladder Wall	Upper Dose	3276800	61	16
Normal Tissue	Upper Dose	320000000	100	0

Structure	Priority	Relative Dose	Relative Volume	Start Distance	End Dose	Fall Off	Optimization parameter
Normal tissue	10000000	90	0	0.5	40	0.1	End Dose

2.3.2. Cases investigated with a continuously changing isocenter position

For the treatment plan creation following a non-isocentric approach, both SMCP beamlet dose calculations - one before the generation of the path and one after - were calculated with the jaws positioned as defined in the "dummy" field. As for the parameters used for the DTRT path generation, a 10% threshold to eliminate map points in each FMO & Elimination process iteration, a number of 18 anchor points, the objective function-based quantity to score the map points and the Hybrid TSP solver to generate the path, were utilized.

2.3.2.1. Craniospinal Irradiation case I

A case of craniospinal tumor was investigated to evaluate the efficacy of the dosimetrically motivated DTRT plan for a large tumor covering a wide area of the patient's body. The clinical treatment of this case employed the IMRT technique, for which a treatment plan was generated using 6 fields to target the tumor. Of these, 2 fields were focused on the brain region while the remaining 4 fields were directed at the spinal cord. The plan utilized a total of 60 apertures, allowing for 10 apertures per beam direction for beam delivery.

A different treatment plan using 3 full VMAT arcs was created to investigate this tumor case. The three arcs were delivering dose to three different parts of the target so that each voxel of the target would be radiated. The MLC was rotated at a static angle of 2^{o}.

Another treatment plan was produced, generated by a manually defined DTRT path. The beam delivery follows a path along the spinal cord from the bottom to the top to reach the patient's head. As for the brain region, a partial arc was used with the gantry initially placed below the patient at a certain angle on his right side (-150^{o}). The gantry rotates clockwise around the patient until it stops at the symmetrical position on the left side of the patient (150^{o}). Then the path follows again to the lower part of the spinal cord. The MLC was rotated at a 2^{o} angle during the whole DTRT path. A 2-paths plan was generated. **Figure 14** illustrates the beam set up for the IMRT, VMAT and manually defined DTRT plans.

Finally, the dosimetrically motivated DTRT plan was generated for the craniospinal case, which was approached as a non-isocentric case. The plan was designed with two degrees of freedom to produce the DTRT path, namely the gantry rotation and table longitudinal translation. This approach allowed for changing the isocenter position during beam delivery, ensuring full radiation coverage of the target volume. In contrast to isocentric cases, where the MLC is aligned with the superior-

inferior axis of the patient, the MLC rotation was set static to a 2-degree angle during beam delivery for non-isocentric cases. Additionally, given that the isocenter position was continuously changing, the jaws were not adjusted to conform to any MLC apertures, as was done in the isocentric cases. Again a 2-paths plan was generated. The objectives considered for the objective function value calculation for each of the aforementioned plans, are presented in **Table 5**. A dose normalization at the 50% of the PTV was used with a prescribed dose of 12 Gy.

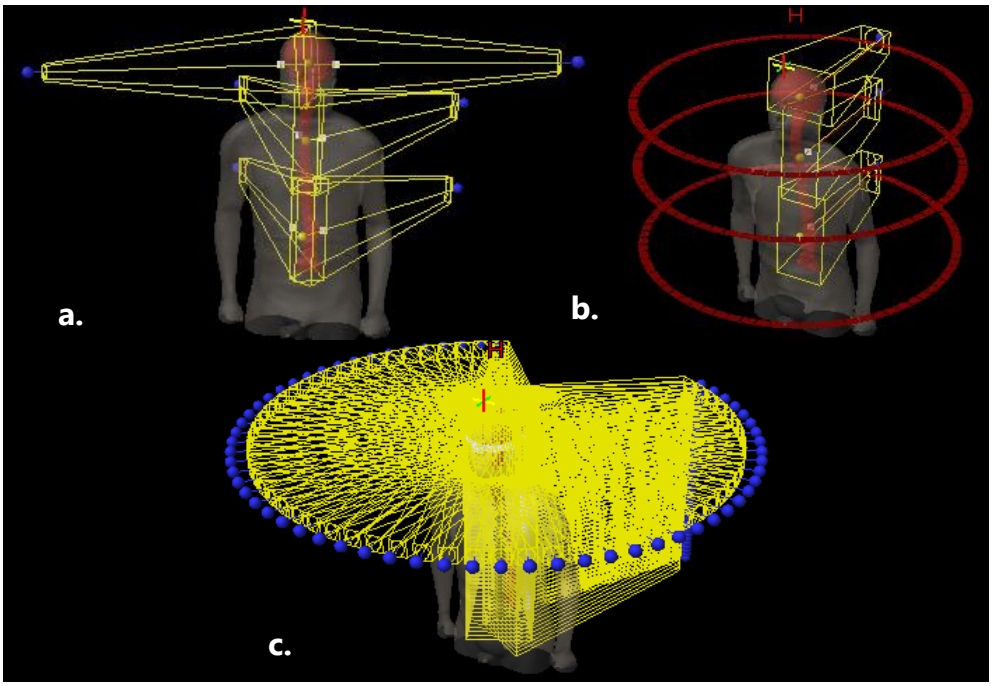

Figure 14: The beam set up for an a) IMRT plan and a b) VMAT plan are shown regarding a craniospinal tumor.

Table 5: Objectives used for the contoured structures for the patient with a craniospinal tumor.

Structure	Objective Type	Priority	Relative Dose	Relative Volume
PTV	Lower Dose	759375	98	100
PTV	Upper Dose	75937	105	0
Heart	Upper Dose	3125	10	50
Heart	Upper Dose	3125	40	0
Heart	Mean Dose	3125	15	0
Left Lens	Mean Dose	7776	20	0
Right Lens	Mean Dose	7776	20	0
Left Eye	Upper Dose	7776	95	0

Left Eye	Mean Dose	3125	30	0
Right Eye	Mean Dose	3125	30	0
Right Eye	Upper Dose	7776	95	0
Left Lung	Upper Dose	7776	10	30
Right Lung	Upper Dose	7776	10	30
Right Lung	Mean Dose	7776	8	0
Left Lung	Mean Dose	7776	8	0
Right Kidney	Mean Dose	3125	4	0
Left Kidney	Mean Dose	3125	4	0
Liver	Mean Dose	3125	5	0
Thyroid	Mean Dose	3125	30	0
Large Bowel	Mean Dose	2430	15	0
Larynx	Upper Dose	2430	40	0
Bladder Wall	Upper Dose	3125	61	16
Normal Tissue	Upper Dose	759375	100	0

Structure	Priority	Relative Dose	Relative Volume	Start Distance	End Dose	Fall Off	Optimization parameter
Normal tissue	75937	95	0	0.25	30	0.1	End Dose

2.3.2.2. Craniospinal Irradiation case II

A second craniospinal tumor was investigated. This case was also treated clinically with the IMRT treatment modality. As described in the previous craniospinal case, similar treatment plans were developed. A similar 6 field-IMRT plan, a VMAT plan using 3 full arcs and the dosimetrically motivated DTRT plan using 2 paths, were created. **Figure 15** illustrates the beam set up for the IMRT and VMAT plans. The plans were performed considering a dose normalization at the 50% of the PTV with a prescribed dose of 7.2 Gy and the objectives used during the whole TPP are shown in **Table 6**.

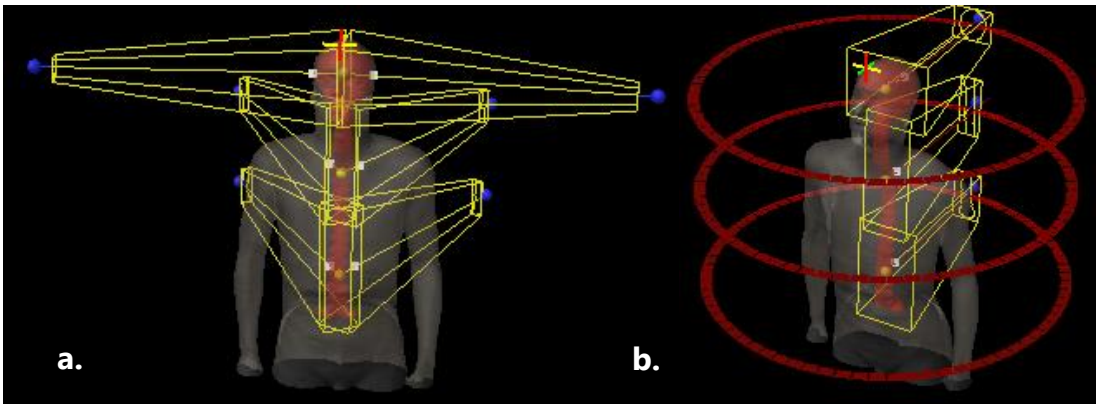

Figure 15: The beam set up for an a) IMRT plan and a b) VMAT plan are shown regarding a craniospinal tumor.

Table 6: Objectives used for the contoured structures for the patient with a craniospinal tumor.

Structure	Objective Type	Priority	Relative Dose	Relative Volume
PTV	Min Dose	759375	98	100
PTV	Max Dose	759375	105	0
Avoid	Mean Dose	7776	20	0
Heart	Max Dose	7776	40	0
Heart	Mean Dose	7776	15	0
Left Lens	Mean Dose	7776	15	0
Right Lens	Mean Dose	7776	15	0
Left Eye	Max Dose	7776	95	0
Left Eye	Mean Dose	3125	30	0
Right Eye	Mean Dose	3125	30	0
Right Eye	Max Dose	7776	95	0
Left Lung	Max Dose	7776	20	0
Right Lung	Max Dose	7776	20	0
Right Lung	Mean Dose	7776	8	0
Left Lung	Mean Dose	7776	8	0
Right Kidney	Mean Dose	3125	4	0
Left Kidney	Mean Dose	3125	4	0
Liver	Mean Dose	3125	5	0
Thyroid	Mean Dose	3125	30	0

Bowel	Mean Dose	2430	15	0
Larynx	Max Dose	2430	40	0
Esophagus	Mean Dose	3125	40	0
Spleen	Mean Dose	2430	15	0
Stomach	Mean Dose	2430	15	0
Left Retina	Mean Dose	7776	20	0
Right Retina	Mean Dose	7776	20	0
Normal Tissue	Max Dose	759375	100	0

Structure	Priority	Relative Dose	Relative Volume	Start Distance	End Dose	Fall Off	Optimization parameter
Normal tissue	75937	95	0	0.25	30	0.1	End Dose

2.3.2.3. Bilateral breast case

A bilateral breast case was clinically treated using a VMAT treatment plan. To demonstrate this plan, a VMAT plan with two different isocenter positions was created. The first isocenter position was located at the center of the tumor in the left breast, while the second isocenter position was at the center of the tumor in the right breast. Two partial arcs were created to deliver dose at the first isocenter. The first arc had the gantry initially below the patient at her right side and a clockwise arc was performed until the gantry stopped above the patient at a certain angle on her left side (45°). The collimator angle was fixed at 5° for the first arc. The second arc focusing on the same isocenter followed the same path, only with the opposite direction and with a fixed collimator angle at 355°. Regarding the second isocenter position, focusing on the left breast, two partial arcs were defined samewise as for the first isocenter position, only now rotating from the left side of the patient. The 2 partial arcs for each breast used the field split technique.

A manually defined DTRT plan was created. Optimization points were placed so that the beam delivery would follow tangential beam directions around the patient's chest. This way, the tumor located at the two breasts would be radiated, while critical organs such as lungs, heart and spinal cord are not radiated at all. The manually defined path was doubled and using the doubled path, the treatment plan was performed. **Figure 16** illustrates the beam set up for the VMAT and the manually defined DTRT plans.

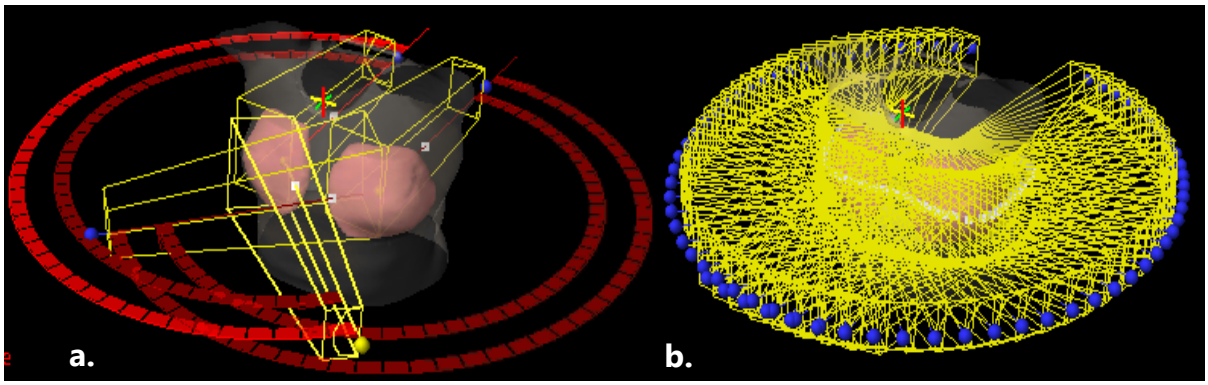

Figure 16: The beam set up for a VMAT plan are shown regarding a bilateral breast tumor.

In addition, the dosimetrically motivated DTRT plan was created using 2 DTRT paths. The DOFs allowed for the generation of the DTRT path were the gantry rotation and the lateral table translation. The MLC rotation was also set to static at a 2° angle along the path.

The plan was performed considering a dose normalization at the 50% of the Planning Target Volume (PTV) with a prescribed dose of 50 Gy and the objectives used during the whole TPP are shown in **Table 7**.

Table 7: Objectives used for the contoured structures for the patient with a bilateral breast tumor.

Structure	Objective Type	Priority	Relative Dose	Relative Volume
PTV	Upper Dose	18452	101.5	0
PTV	Lower Dose	18452	98.5	100
PTV	Lower Dose	131030	100	50
Spinal Canal	Upper Dose	1845	20	0
Lung total	Upper Dose	5521	0	50
Lung total	Upper Dose	4094	40	5
Lung total	Upper Dose	5521	20	20
Heart	Mean Dose	5390	5	0
Heart	Upper Dose	4094	10	0

Structure	Priority	Relative Dose	Relative Volume	Start Distance	End Dose	Fall Off	Optimization parameter
Normal tissue	15	100	0	0.5	30	0.12	End Dose

2.4. Parameter investigation

The dosimetrically motivated DTRT treatment plan can be divided into two major components. The first component involves generating a DTRT path as described in section **Treatment Planning Process** using the methods described from section **CT image & Structure Contouring** up to section **Path-finding algorithm**. The second component involves modulating the intensity of the generated path to achieve a final dose distribution in the patient. The shape of the generated dosimetrically motivated DTRT path is significantly influenced by various parameters. Once the path is generated, the focus shifts to the intensity modulation along that path. If the generated path does not ensure complete coverage of the target, for example, then part of the PTV may be underdosed. Therefore, the parameters that affect the path generation process were investigated to identify a favorable set of parameters for generating the path. The parameters were firstly examined for cases utilizing an isocentric approach in order to validate the performance of the developed DTRT TPP. Subsequently, according to the results received by using an isocentric approach, the parameters were investigated also for a non-isocentric approach.

2.4.1.Threshold for map points elimination

A parameter used during the construction of the DTRT path is the threshold percentage of map points to be eliminated, from the pool of the available map points, after each FMO iteration. Considering that after each elimination process another FMO is performed for the remaining map points, regarding how many and which map points remain, different fluence maps can be calculated for the map points that are still available. By this meaning, the fluence maps generated can be influenced by the thresholding percentage. The fluence maps have a direct influence on the scoring of each map point which indicates the map points that are more likely to be eliminated at the current elimination iteration. This indicates that the selected threshold to eliminate map points may have an impact on the DTRT plan generated. DTRT plans were created using a different threshold in order to investigate the impact that this parameter may have on the treatment plan. For cases investigated by an isocentric approach, DTRT plans using thresholds of 10%, 25%, 50% and 90% where created, while for cases examined by a non-isocentric approach, DTRT plans utilizing thresholds of 10%, 25% and 50% where generated.

2.4.2.Anchor points number selection

Another parameter that potentially has a substantial impact on the DTRT path creation, is the selected number of anchor points. By selecting a higher or lower number of anchor points to be produced, at the end of the FMO & Elimination process, can have an influence on the length of the DTRT path. It can also affect the plan objective function value of the plan regarding the shape, the size and the location of the target. For example, we assume that large tumors, such as a craniospinal tumor, need no less than a certain amount of anchor points, in order for a path, which will fully cover the target, to be generated. For cases investigated by an isocentric approach, DTRT plans using a number of 3, 9, 12 and 15 anchor points where created, while for cases examined by a non-isocentric approach, DTRT plans utilizing 15 and 18 anchor points where generated.

2.4.3.Ordering of the anchor points along the path

As explained earlier, in order to specify the ordering of the anchor points along the path, the TSP is solved using two different methods, one by using a greedy algorithm and one by using a Hybrid TSP solver algorithm. The TSP solver method can have an impact on the formed DTRT path. It is expected that paths generated by the two methods will differ, resulting a beam delivery from a set of different beam directions. For this purpose, the two TSP solver methods are investigated to understand their influence on the dosimetrically motivated DTRT plan.

2.4.4.Map points and grid points scoring

The scoring of the map points and therefore the grid points, which the A* algorithm will navigate to find the optimal sub-paths between two anchor points, can influence the creation of the DTRT path. This parameter has a double impact on the DTRT path generation.

Firstly, by scoring the available map points with either the objective function-based quantity $Q_{mp}^{Obj.func}$ (**Equation 3**) , or the mean PTV dose-based quantity $Q_{mp}^{meanPTVdose/irr.PTV}$ (**Equation 7**), leads to a different set of map points to be eliminated in each elimination iteration until the final set of anchor points is gathered. Eliminating different set of map points will therefore lead to a different set of anchor points at the end of FMO & Elimination process. So, it is expected that a different set of anchor points will lead to a different DTRT path.

In addition, the same scoring method used for the elimination of the map points, is also used for the scoring of the grid points on the grid that is used as an input for the A* algorithm to find optimal sub-paths between different pairs of anchor points. According to the scoring method used, a different cost between 2 neighbouring grid points was given, as it was defined in Equation 8 and Equation 9. It is assumed that different cost between neighbouring grid points can have an impact on the selection of the sub-paths between 2 anchor points.

Taking into consideration the above said, the two scoring methods were investigated to find out how they affect a DTRT plan.

3. Results

In this chapter, the dosimetrically motivated DTRT TPP, which was developed for this project, was used and the dosimetric results are presented in the current section. A thorough investigation was carried out to determine the optimal set of parameters for the DTRT path generation process, which was then used to create treatment plans for all tumor cases studied. The dosimetric results for the isocentric cases are presented in this chapter, and the developed DTRT TPP is validated by comparing its results with the ones obtained using other treatment modalities. For non-isocentric DTRT plans, the dosimetric results are compared with results drawn out plans created using other treatment techniques in order to further explore the benefits and drawbacks of the developed TPP.

3.1. Parameter investigation

The DTRT treatment plans presented for the parameter investigation were created by using the SMCP beamlet dose calculation, the FMO & Elimination process, the path-finding algorithm, a second beamlet dose calculation along the generated path and the H-DAO for the intensity modulation of the path. Results for the parameter investigation are only shown for an isocentric DTRT approach for a brain case, where gantry and table rotations were allowed, and a non-isocentric DTRT approach for a craniospinal irradiation case, where gantry rotation and longitudinal table translation were enabled.

3.1.1. Threshold for map points elimination

In this section the threshold selected during FMO & Elimination process is investigated. The plans presented were created by selecting a number of 15 anchor points, eliminating beam directions arising from the objective function-based quantity and using the Hybrid TSP solver for the ordering of the anchor points.

3.1.1.1. Brain Case

The outcoming paths when different thresholds were used to eliminate map points for the brain case, are shown in **Figure 17**. The DTRT path generated by a 90% threshold is substantially shorter than the others. It seems that a higher threshold led to the selection of anchor points which are located closer to each other. The x-axis

represents the gantry angle which as -180° and +180° indicates the position of the gantry right below the patient, while 0° indicates a gantry right above the patient. From -180° towards +180° the gantry rotates clockwise. The y-axis represents the table angle which from -90° to +90° rotates in a counter clockwise direction.

Treatment plans were created based on the paths shown in **Figure 17**. The resulting DVHs for specific structures, which were produced after a H-DAO, are shown in **Figure 18**, while the objective function values, different dose values referring to the selected structures and calculation times, are presented in **Table 8**.

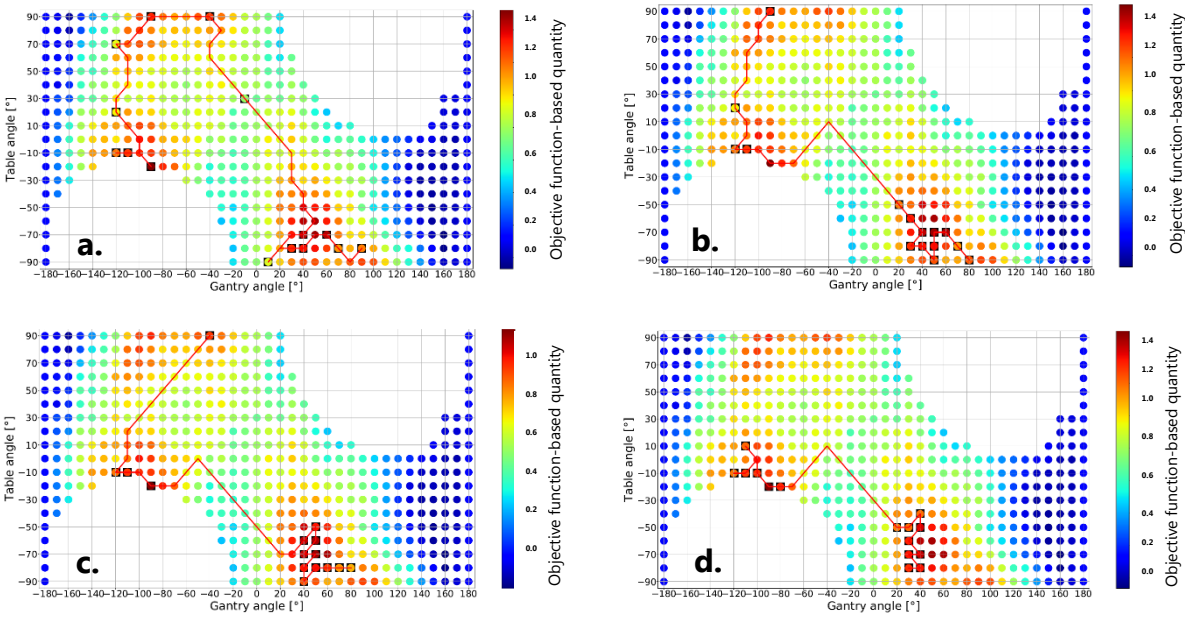

Figure 17: The DTRT paths generated by path-finding algorithm, using different thresholds during FMO & Elimination process, are presented in a red line. Paths generated by using a threshold of a) 10%, b) 25%, c) 50% and d) 90% are shown. Each point on the graphs represents an available beam direction of a gantry and table angle. White areas demonstrate inaccessible beam directions due to collisions of the treatment machine units. Points marked in black squares express the anchor points, while the colour bar presents the scoring of each map point by the objective function-based quantity.

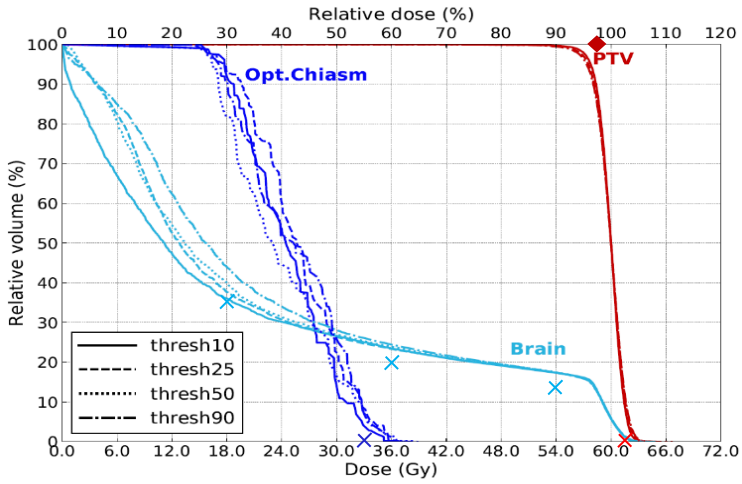

Figure 18: A comparison of DVHs for the PTV (red), the optic chiasm (blue) and the brain (light blue) between a threshold of 10%, 25%, 50% and 90%. Upper dose objectives are marked with crosses, while lower dose objectives are marked with rhombus.

Table 8: The objective function value of the plans and dose values for the selected structures for plans created using a threshold of 10%, 25%, 50% and 90%.

	10%	25%	50%	90%
Objective function value	0.024322	0.031234	0.032756	0.043587
Anchor points generation calc time [s]	1928.566	927.515	2323.343	277.241
DTRT Path calc time [s]	14.701	753.424	326.041	53.232
H-DAO calc time [s]	752.122	423.999	467.972	261.181
PTV $D_{98\%}$	94.9%	94.2%	94.1%	93.7%
PTV $D_{2\%}$	103.6%	104.0%	103.9%	104.2%
Brain Mean Dose	34.0%	36.7%	37.1%	39.2%
Brain Max Dose	108.0%	107.1%	107.0%	108.1%
Optic Chiasm Max Dose	61.9%	64.0%	64.9%	62.0%

The plan using a threshold of 10% produces a lower objective function value and a more homogeneous dose to the PTV compared to the plans utilizing higher thresholds. The mean dose at the brain and the maximum dose at the optic chiasm are kept to lower values for a plan of a 10% threshold. The maximum dose delivered at the brain is high for every plan as expected, because the PTV is in the brain area. The algorithms, used to create the DTRT plan, perform the calculations in short calculation times for every threshold case investigated.

This path starts with the table slightly rotated clockwise (-10°) and the gantry at an angle below the patient and on his right side (-120°). The table then begins a counter clockwise until the patient is fully rotated to a horizontal position, while the gantry makes small shifts around the initial angle. After that, both the table and gantry rotate clockwise. At the very end of the path slight shifts at both gantry and table rotations occur, leading to the gantry radiating from the left side of the patient (90°) and the table rotated to an almost horizontal position (-80°). The gantry stays close to the patient's head during the path.

3.1.1.2. Craniospinal case II

The outcoming paths that were generated by the pathfinding algorithm are shown in **Figure 19**. The x-axis represents the gantry angle which as -180° and +180° indicates the position of the gantry right below the patient, while 0° indicates a gantry right above the patient. From -180° towards +180° the gantry rotates clockwise. The

y-axis represents the longitudinal table translation which at -2cm indicates that the very top of the patient's head is placed at the isocenter position, while a -78cm longitudinal table position indicates that the lower part of the spinal cord is placed at the isocenter.

Treatment plans were created based on the above DTRT paths. The resulting DVHs for specific structures, which were produced after a H-DAO, are shown in **Figure 20**, while the objective function values, different dose values referring to the selected structures and calculation times, are presented in **Table 9**.

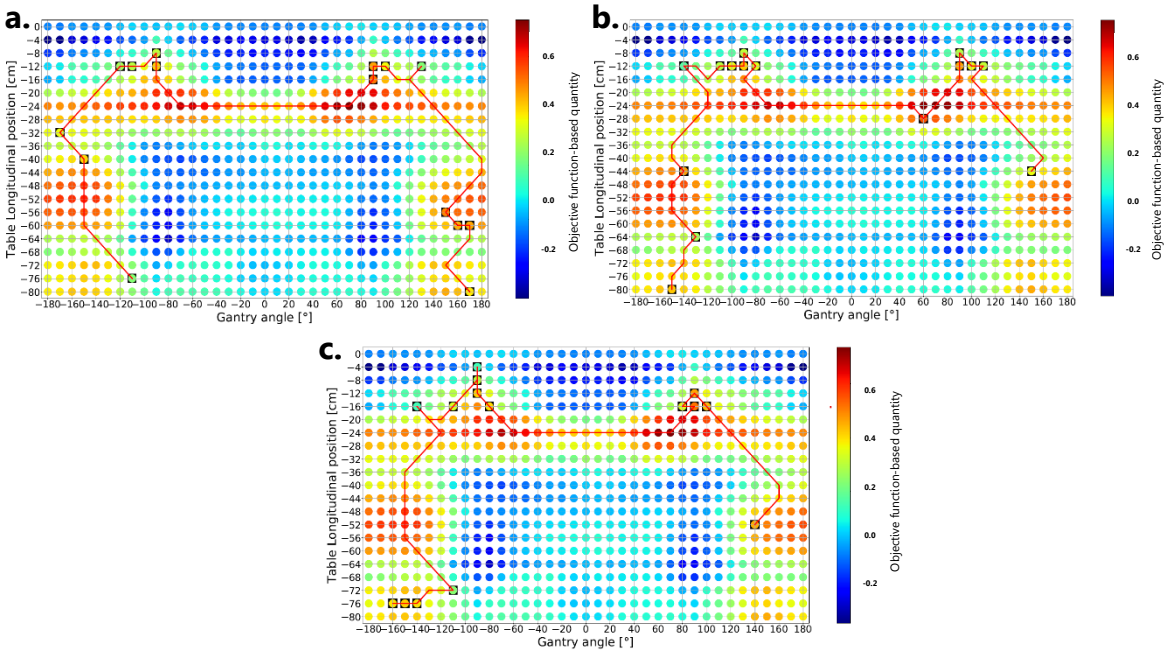

Figure 19: The DTRT paths generated by path-finding algorithm, using different thresholds through FMO & Elimination process, are presented in a red line. Paths using a threshold of a) 10%, b) 25%, and c) 50% were created. Each point on the graphs represents an available beam direction of a gantry angle and a longitudinal table position. Points marked in black squares express the anchor points, while the colour bar presents the scoring of each map point by the objective function-based quantity.

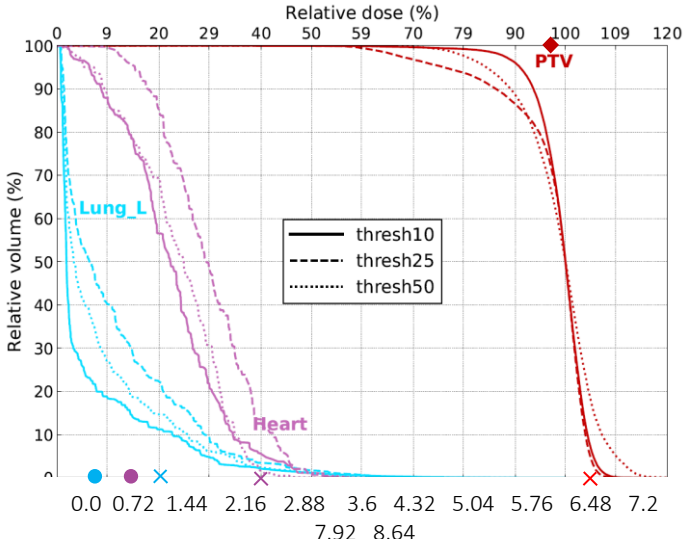

Figure 20: A comparison of DVHs for the PTV (red), the left lung (light blue) and the heart (pink) between a threshold of 10, 25 and 50. Upper dose objectives are marked with a cross, lower dose objectives are marked with a rhombus and mean dose objectives are marked with a circle.

Table 9: The objective function value of the plans and dose values for the selected structures for plans created using a threshold of 10%, 25% and 50%.

	10%	25%	50%
Objective Function value	2.027044	11.052111	9.875811
Anchor points generation calc time [s]	7924.760	3460.318	1617.730
DTRT Path calc time [s]	65.317	229.533	110.067
H-DAO calc time [s]	1276.608	1189.558	1344.021
PTV $D_{98\%}$	87.0%	66.0%	79.2%
PTV $D_{2\%}$	106.8%	105.9%	112.5%
Left Lung Mean Dose	6.5%	11.5%	8.7%
Left Lung Max Dose	99.8%	92.8%	97.7%
Heart Mean Dose	22.6%	29.8%	23.6%
Heart Max Dose	65.0%	58.9%	53.6%

The DTRT path created by a threshold of 10% differs from the paths generated by a threshold of 25% and 50% as the first path starts by radiating the lowest part of the spinal cord, it then moves up to the brain region, it makes a partial arc around the brain area and then it moves back to the lowest part of the spinal cord. The two other paths follow a similar scheme, only they stop at the abdomen area and not the end of the spinal cord.

The plan using a threshold of 10% produces a lower objective function value and a more homogeneous dose to the PTV compared to the plans utilizing higher thresholds. The mean dose at the left lung and the heart are kept to lower values for a plan of a 10% threshold, while the maximum doses for the 2 structures were higher than the plans produced by higher thresholds. The FMO & Elimination process to generate the anchor points, takes approximately 2.20 hours when using a threshold of 10%. The rest of the algorithms, used to create the DTRT plan, perform the calculations in short calculation times for every threshold case investigated.

3.1.2. Anchor points number selection

In this section the number of anchor points demanded at the end of FMO & Elimination process is investigated. The plans presented were created by selecting a threshold of 10%, eliminating beam directions arising from the objective function-based quantity and using the Hybrid TSP solver for the ordering of the anchor points.

3.1.2.1. Brain case

The outcoming paths that were generated by pathfinding algorithm are shown in **Figure 21**. The two axes are illustrating gantry and table rotation as explained in section **3.1.1.1**.

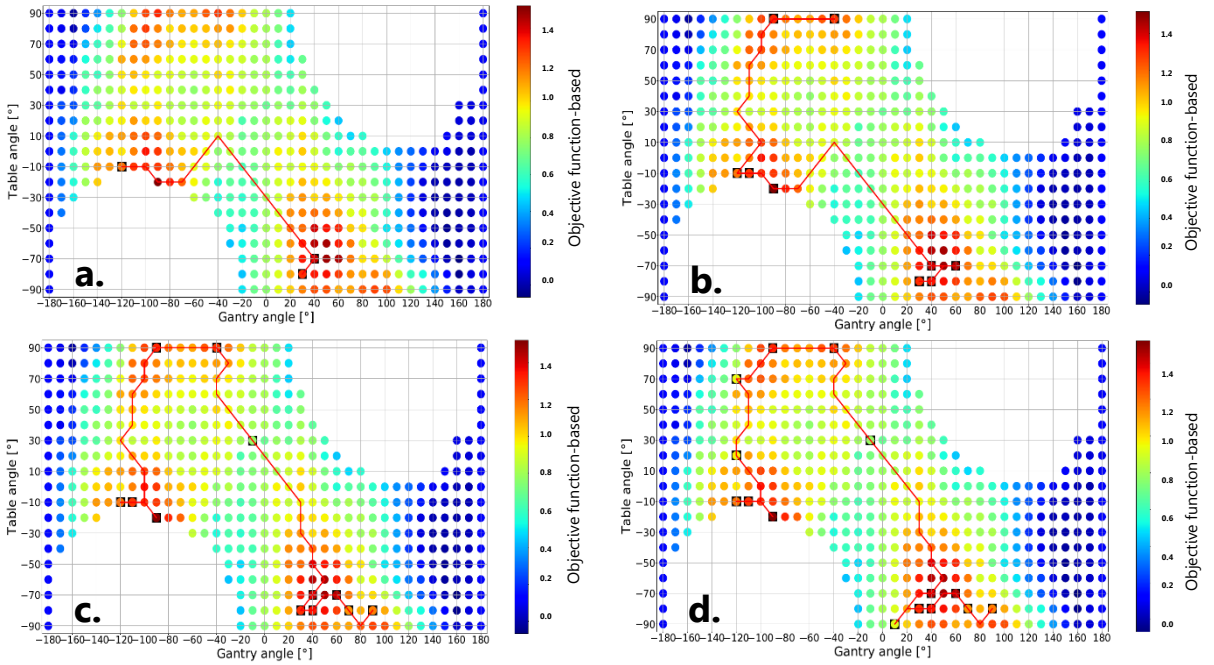

Figure 21: The DTRT paths generated by path-finding algorithm, asking for a different number of anchor points at the end of FMO & Elimination process, are presented in a red line. Paths generated by demanding a) 3, b) 9, c) 12 and d) 15 anchor points are shown. Each point on the graphs represents an available beam direction of a gantry and table angle. White areas demonstrate inaccessible beam directions due to collisions of the treatment machine units. Points marked in black squares express the anchor points, while the colour bar presents the scoring of each map point by the objective function-based quantity.

The DTRT path produced by a demanding 3 anchor points, is shorter than the rest. Even the path with 9 anchor points is shorter than the paths having 12 and 15 anchor points. The last 2 paths are fairly similar. It seems that the amount of beam directions that the path will go through, saturates after a certain amount of anchor points.

Treatment plans were created based on the paths shown in the aforementioned figure. The resulting DVHs for specific structures, which were produced after a H-DAO, are shown in **Figure 21**, while the objective function values, different dose values referring to the selected structures and calculation times, are presented in **Table 10**.

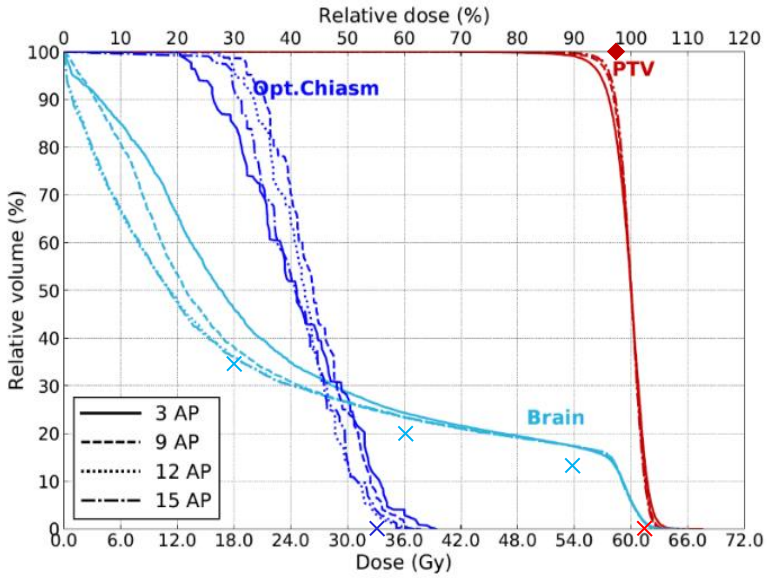

Figure 22: A comparison of DVHs for the PTV (red), the optic chiasm (blue) and the brain (light blue) between a threshold of 10, 25, 50 and 90. Upper dose objectives are marked with crosses, while lower dose objectives are marked with a rhombus.

Table 10: The objective function value of the plans and dose values for the selected structures for plans created using a number of 3, 9, 12 and 15 anchor points.

	3 A.P.	9 A.P.	12 A.P.	15 A.P.
Objective function value	0.063259	0.031440	0.023891	0.024322
Anchor points generation calc time [s]	2031.649	2159.563	2133.618	1928.566
DTRT Path calc time [s]	0.000	0.002	0.177	14.701
H-DAO calc time [s]	172.035	499.087	626.169	752.122
PTV $D_{98\%}$	92.3%	94.2%	95.0%	94.9%
PTV $D_{2\%}$	104.5%	103.9%	103.7%	103.6%
Brain Mean Dose	39.8%	36.6%	34.0%	34.0%
Brain Max Dose	110.0%	106.8%	108.4%	108.0%
Optic Chiasm Max Dose	65.6%	62.8%	62.7%	61.9%

.

The plans using a 12 and 15 anchor points produce lower objective function values and a better tumor control compared to the other plans. The maximum dose at the brain and the optic chiasm are kept to lower values for a plan of 15 anchor points. The path follows the same scheme described in the section of the threshold investigation for the **Brain Case**. The algorithms, used to create the DTRT plan, perform the calculations in short calculation times for every case investigated having a different number of anchor points.

3.1.2.2. Craniospinal Irradiation case II

The outcoming paths that were generated by pathfinding algorithm are shown in **Figure 23**. The two axes are illustrating gantry rotation and longitudinal table translation as explained in section **3.1.1.2**.

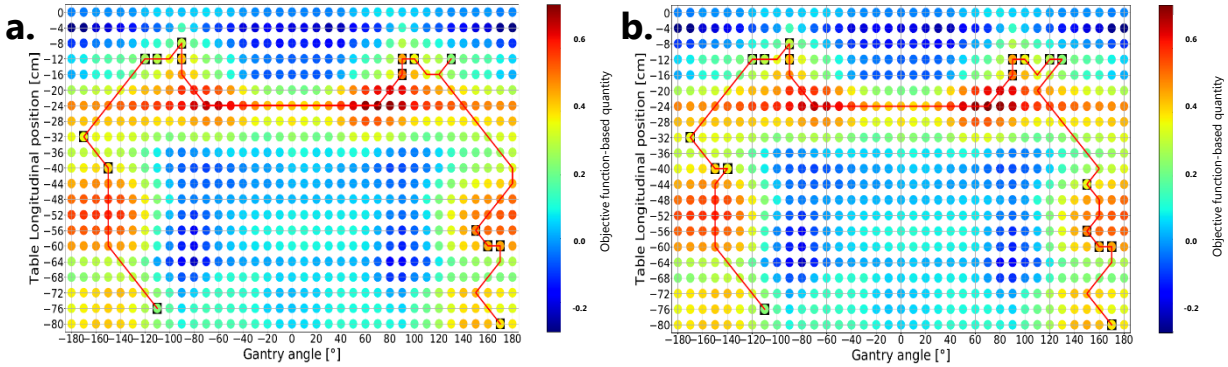

Figure 23: The DTRT paths generated by path-finding algorithm, demanding a different number of anchor points at the end of FMO & Elimination process, are presented in a red line. Paths with a number of a) 15 and b) 18 anchor points were created. Each point on the graphs represents an available beam direction of a gantry angle and a longitudinal table position. Points marked in black squares express the anchor points, while the colour bar presents the scoring of each map point by the objective function-based quantity.

The two DTRT paths have a similar form as the beam delivery starts at the lowest part of the spinal cord, it then moves up to the brain region, it makes a partial arc around the brain area and then it moves back to the lowest part of the spinal cord.

Treatment plans were created based on the paths shown in the aforementioned figure. The resulting DVHs for specific structures, which were produced after a H-DAO, are shown in **Figure 24**, while the objective function values, different dose values referring to the selected structures and calculation times, are presented in **Table 11**.

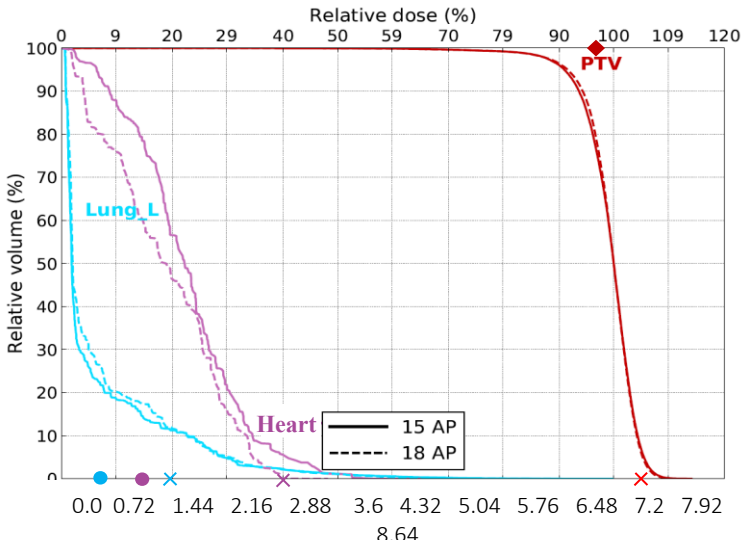

Figure 24: A comparison of DVHs for the PTV (red), the left lung (light blue) and the heart (pink) between a set of 15 and 18 anchor points. Upper dose objectives are marked with a cross, lower dose objectives are marked with a rhombus and mean dose objectives are marked with a circle.

Table 11: The objective function value of the plans and dose values for the selected structures for plans created using a number of 15 and 18 anchor points.

	15 A.P.	18 A.P.
Objective function value	0.274655	0.259579
Anchor points generation calc time [s]	7924.760	9074.336
DTRT Path calc time [s]	65.317	7297.400
H-DAO calc time [s]	1276.608	1304.414
PTV $D_{98\%}$	87.0%	87.1%
PTV $D_{2\%}$	106.8%	106.5%
Left Lung Mean Dose	6.5%	7.1%
Left Lung Max Dose	99.8%	98.5%
Heart Mean Dose	22.6%	18.7%
Heart Max Dose	65.0%	48.2%

The plan created by having a set of 18 anchor points produces a lower objective function value and a better sparing of the heart is achieved. A craniospinal case is a tumor that starts from the bottom of the spinal cord and continues up to the brain as it conforms to the spinal cord and the brain. Because of that, it was expected that a high number of anchor points would be needed to achieve a high plan quality. The FMO & Elimination process to generate the anchor points, takes approximately 2.20 hours when using a 15 anchor points, while for 18 anchor points it takes almost 2.52 hours. In addition, increasing the number of anchor points to 18 leads to an increase of the path-finding calculation time towards approximately 2.03 hours.

3.1.3.Ordering of the anchor points along the path

In this section the two different path-finding algorithms are investigated. The plans presented were created by selecting a threshold of 10%, eliminating beam directions arising from the objective function-based quantity while for the brain case 15 anchor points were used and 18 for the craniospinal irradiation case.

3.1.3.1. 1 Brain case

The outcoming paths that were generated by the two pathfinding algorithms are shown in **Figure 25**. The two axes are illustrating gantry and table rotation as explained in section **3.1.1.1**.

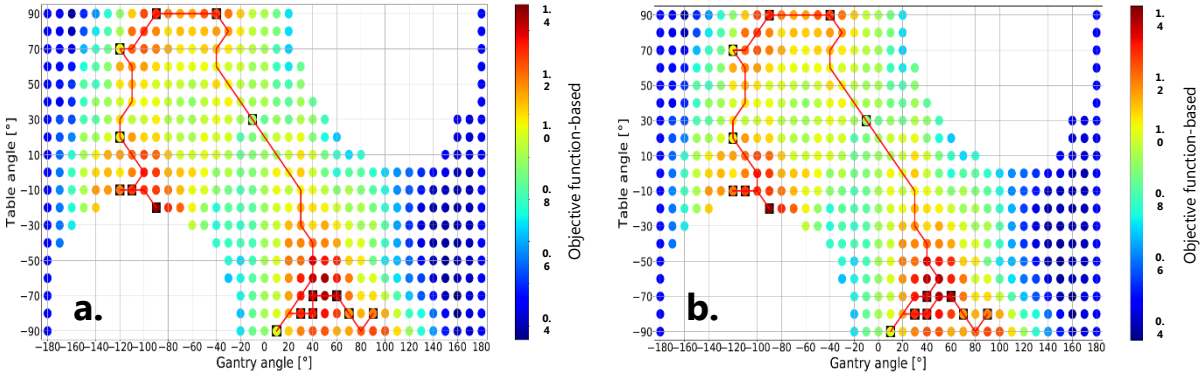

Figure 25: The DTRT paths generated when using the two TSP solver algorithms implemented, are presented in a red line. Paths generated by the use of a) greedy and b) hybrid TSP solver algorithms are shown. Each point on the graphs represents an available beam direction of a gantry and table angle. White areas demonstrate inaccessible beam directions due to collisions of the treatment machine units. Points marked in black squares express the anchor points, while the colour bar presents the scoring of each map point by the objective function-based quantity.

The two DTRT paths generated are almost the same and follow the scheme described in section **3.1.1.1**. Only minor changes between the paths exist and for that, the dosimetric results are expected to be similar.

Treatment plans were created based on the paths shown in the aforementioned figure. The resulting DVHs for specific structures, which were produced after a H-DAO, are shown in **Figure 26**, while the objective function values, different dose values referring to the selected structures and calculation times, are presented in **Table 12**.

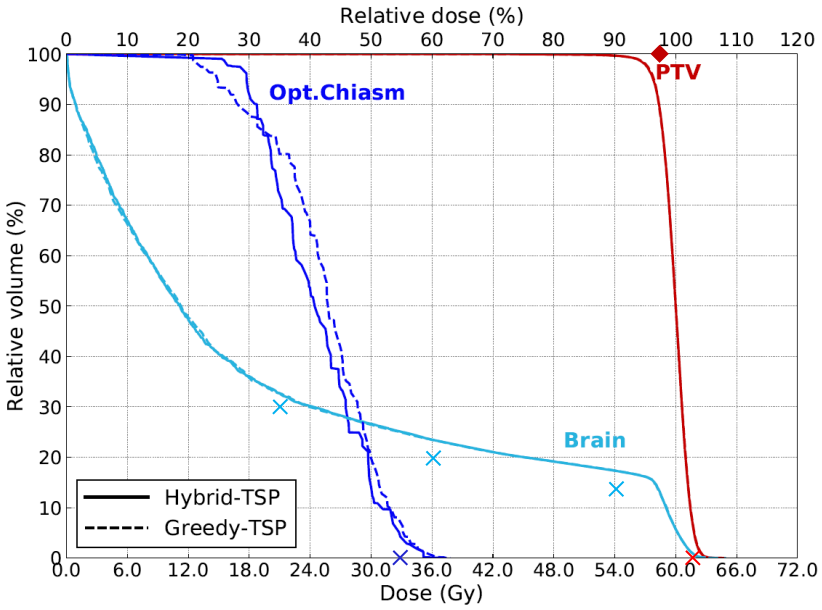

Figure 26: A comparison of DVHs for the PTV (red), the optic chiasm (blue) and the brain (light blue) between the use of the greedy algorithm and the hybrid TSP solver algorithm for the ordering of map points. Upper dose objectives are marked with crosses, while lower dose objectives are marked with a rhombus.

Table 12: The objective function value of the plans and dose values for the selected structures for plans created using the greedy and the hybrid TSP solver algorithm.

	Greedy algorithm	Hybrid TSP solver algorithm
Objective function value	0.024424	0.024322
Anchor points generation calc time [s]	1928.566	1928.566
DTRT Path calc time [s]	0.000	14.701
H-DAO calc time [s]	800.772	752.122
PTV $D_{98\%}$	95.0%	94.9%
PTV $D_{2\%}$	103.7%	103.6%
Brain Mean Dose	33.9%	34.0%
Brain Max Dose	106.7%	108.0%
Optic Chiasm Max Dose	63.0%	61.9%

The 2 plans share similar results as expected because the two DTRT paths have only minor differences.

3.1.3.2. Craniospinal Irradiation case II

The outcoming paths that were generated by the two pathfinding algorithms are shown in **Figure 27** using a number of 18 anchor points. The two axes are illustrating gantry rotation and longitudinal table translation as explained in section **3.1.1.2**.

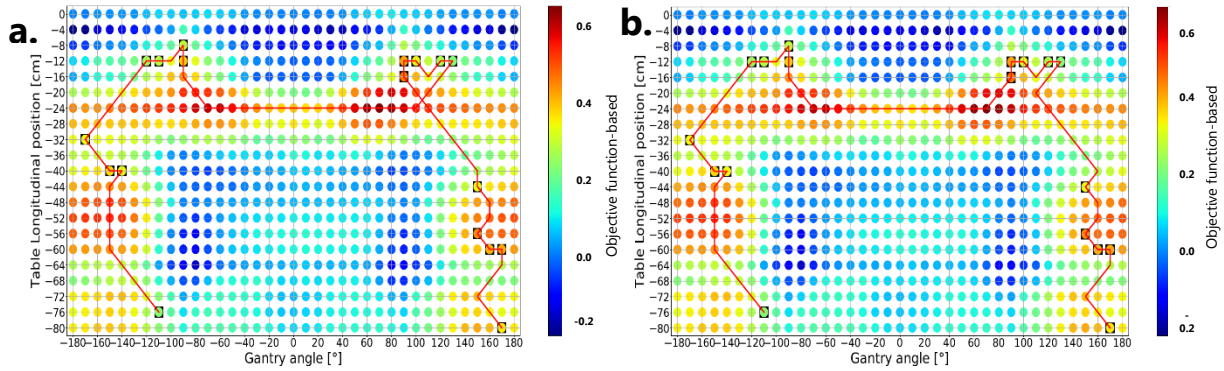

Figure 27: The DTRT paths generated when using the two TSP solver algorithms implemented, are presented in a red line. Paths generated by the use of a) greedy and b) hybrid TSP solver algorithms are shown. Each point on the graphs represents an available beam direction of a gantry and table angle. Points marked in black squares express the anchor points, while the colour bar presents the scoring of each map point by the objective function-based quantity.

The two DTRT paths generated look almost the same following a scheme as described in 3.1.1.2. Although, the path coming out by using the greedy algorithm, makes a loop at the end of the arc around the patient's head. This loop, as it can be seen, causes the path to go through more red areas which correspond to preferable beam directions. Treatment plans were created based on these paths, while the paths were doubled to create the plan. The resulting DVHs for specific structures, which were produced after a H-DAO, are shown in **Figure 28**, while the objective function values, different dose values referring to the selected structures and calculation times, are presented in **Table 13**.

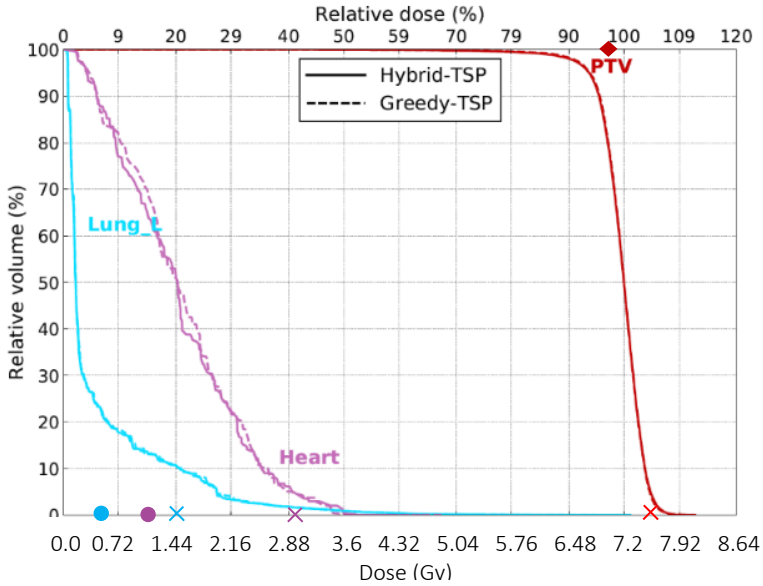

Figure 28: A comparison of DVHs for the PTV (red), heart (pink) and the left lung (light blue) between the use of the greedy algorithm and the hybrid TSP solver algorithm for the ordering of map points. Upper dose objectives are marked with a cross, lower dose objectives are marked with a rhombus and mean dose objectives are marked with a circle.

Table 13: A comparison of DVHs for the PTV (red), the left lung (light blue) and the heart (pink) between a path generated using the greedy algorithm and a path using the hybrid TSP solver algorithm. Upper and lower dose objectives are marked with a cross, while mean dose objectives are marked with a circle.

	Greedy algorithm	Hybrid TSP solver algorithm
Objective function value	0.131548	0.144413
Anchor points generation calc time [s]	9074.336	9074.336
DTRT Path calc time [s]	0.000	7297.400
H-DAO calc time [s]	3213.081	1304.414
PTV $D_{98\%}$	90.8%	90.3%
PTV $D_{2\%}$	105.6%	105.9%
Left Lung Mean Dose	6.4%	6.3%
Left Lung Max Dose	100.2%	101.2%
Heart Mean Dose	21.1%	20.6%
Heart Max Dose	67.7%	65.0%

The plan created by using the greedy algorithm shows a reduced objective function value, while the rest of the results are approximately the same for the two plans. That loop in the path that the greedy algorithm produces, leads to the reduction of the objective function value, as the loop goes through beam directions that are significant for the decrease of the objective function value. Using the greedy algorithm can give the resulting path immediately as it is not checking many different connections of the anchor points.

3.1.4.Map points and grid points scoring

In this section the two different map points scoring quantities are investigated. The plans presented were created by selecting a threshold of 10%, using the Hybrid TSP solver for the ordering of the anchor points, while for the brain case 15 anchor points were used and 18 for the craniospinal irradiation case.

3.1.4.1. Brain case

Characterizing each available beam direction based on these two quantities and then eliminating based on them, lead to the paths shown in **Figure 29**.

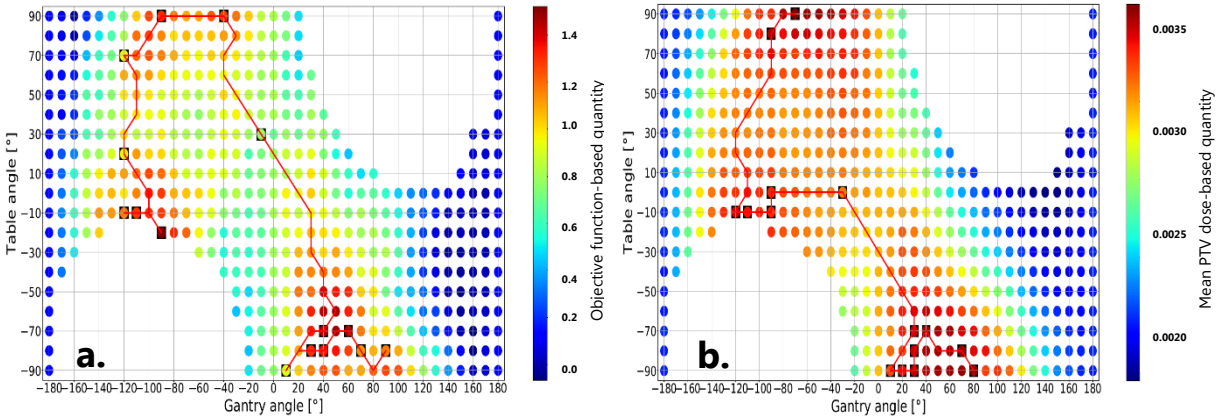

Figure 29: The DTRT paths generated when using the two scoring quantities for the map points, are presented in a red line. Paths generated using the a) Objective function-based quantity and the b) mean PTV dose-based quantity, are shown. Each point on the graphs represents an available beam direction of a gantry and table angle. White areas demonstrate inaccessible beam directions due to collisions of the treatment machine units. Points marked in black squares express the anchor points.

The two DTRT paths follow a different scheme. It is clear that, using these 2 different quantities, different map points are considered as more important or less important to deliver the beam. Even though the paths created differ, similar beam directions were chosen as anchor points.

Treatment plans were created based on the paths shown in the aforementioned figure. The resulting DVHs for specific structures, which were produced after a H-DAO, are shown in **Figure 30**, while the objective function values, different dose values referring to the selected structures and calculation times, presented in **Table 14**.

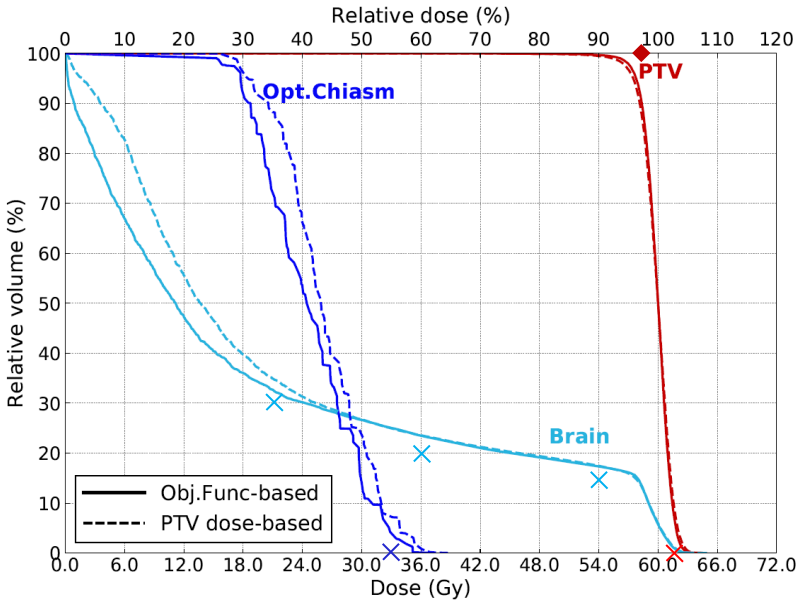

Figure 30: A comparison of DVHs for the PTV (red), the optic chiasm (blue) and the brain (light blue) between the plans based on map points scored by the objective function-based quantity and the mean dose-based quantity. Upper dose objectives are marked with a cross and lower dose objectives are marked with a rhombus.

Table 14: The objective function value of the plans and dose values for the selected structures for plans created using the objective function-based quantity and the mean PTV dose-based quantity.

	Objective function-based	Mean PTV dose-based
Objective function value	0.024322	0.035455
Anchor points generation calc time [s]	1928.566	2294.330
DTRT Path calc time [s]	14.701	17.701
H-DAO calc time [s]	752.122	529.504
PTV $D_{98\%}$	94.9%	94.1%
PTV $D_{2\%}$	103.6%	104.1%
Brain Mean Dose	34.0%	37.2%
Brain Max Dose	108.0%	107.7%
Optic Chiasm Max Dose	61.9%	64.9%

The plan which uses the objective function-based quantity produces a plan with a lower objective function value. The tumor control between the two plans is approximately the same, while the brain and the optic chiasm are more spared for the plan relying on the objective function-based quantity. The DTRT path generated by using the objective function-based quantity follows a scheme as described in **3.1.1.1**. The algorithms, used to create the DTRT plan, perform the calculations in short calculation times for every threshold case investigated.

3.1.4.2. Craniospinal Irradiation case II

Characterizing each available beam direction based on these two quantities and then eliminating based on them, lead to the paths shown in **Figure 31**.

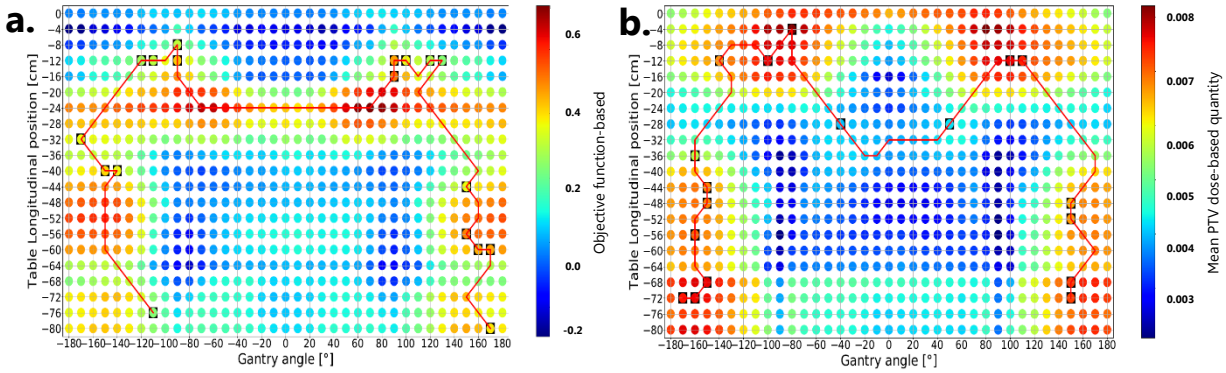

Figure 31: The DTRT paths generated when using the two scoring quantities for the map points, are presented in a red line. Paths generated using the a) Objective function-based quantity and the b) mean PTV dose-based quantity, are shown. Each point on the graphs represents an available beam direction of a gantry and table angle. Points marked in black squares express the anchor points.

The two DTRT paths have different form, although they share similarities. It is clear that, using these 2 different quantities, different map points are considered as more important or less important to deliver the beam. The path generated by the use of the objective function-based quantity starts the radiation from the lowest part of the spinal cord, travels along the spinal cord towards the patient's head, makes a partial arc radiating the brain and then travels back to the lowest part of the spinal cord. The path generated by the use of the other quantity has a similar trend, but it is important to focus on the fact that anchor points were not generated at the lowest part of the spinal cord.

Treatment plans were created based on the paths shown in the aforementioned figure. The resulting DVHs for specific structures, which were produced after a H-DAO, are shown in **Figure 32**, while the objective function values, different dose values referring to the selected structures and calculation times, are presented in **Table 15**.

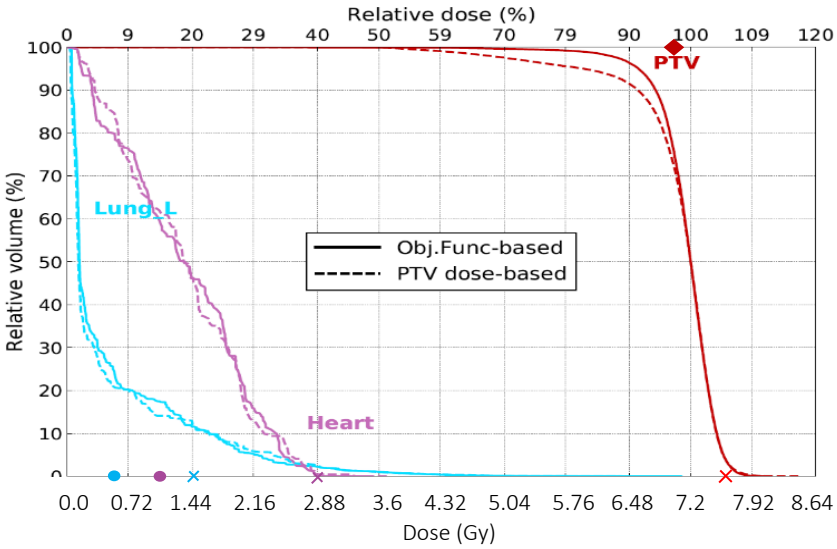

Figure 32: A comparison of DVHs for the PTV (red), the heart (pink) and the left lung (light blue) between the use of the greedy algorithm and the hybrid TSP solver algorithm for the ordering of map points. Upper dose objectives are marked with a cross, lower dose objectives are marked with a rhombus and mean dose objectives are marked with a circle.

Table 15: The objective function value of the plans and dose values for the selected structures for plans created using the objective function-based quantity and the mean PTV dose-based quantity.

	Objective function-based	Mean PTV dose-based
Objective function value	0.259579	0.645055
Anchor points generation calc time [s]	9074.336	7677.468
DTRT Path calc time [s]	7297.400	93.676
H-DAO calc time [s]	1304.414	2145.973
PTV $D_{98\%}$	87.1%	67.7%
PTV $D_{2\%}$	106.5%	106.6%
Left Lung Mean Dose	7.1%	6.7%
Left Lung Max Dose	98.5%	94.3%
Heart Mean Dose	18.7%	18.8%
Heart Max Dose	48.2%	51.8%

The plan which uses the objective function-based quantity produces a plan with a lower objective function value. A DTRT plan relying on the objective function-based quantity leads to a more homogeneous dose to the PTV, while the brain and the optic chiasm are more spared. The DTRT path generated by using the objective function-based quantity follows a scheme as described in **3.1.1.1**. The favorable dosimetric results of the DTRT plan using the objective function-based quantity come with a calculation time cost of the path generation.

3.2. Cases investigated with a fixed isocenter position

This section presents a DTRT TPP, as explained in **Materials and Methods**, generated for a brain case, a head and neck case, a breast case and a prostate case and each case was investigated by a doubled path that the path-finding algorithm produced. In order to validate the performance of the developed DTRT TPP, a comparison of the dosimetric results achieved, using different treatment modalities, was performed.

3.2.1.Brain case

In **Figure 33** the DTRT paths, generated for the dosimetrically motivated DTRT and geometrically motivated DTRT plans, are illustrated.

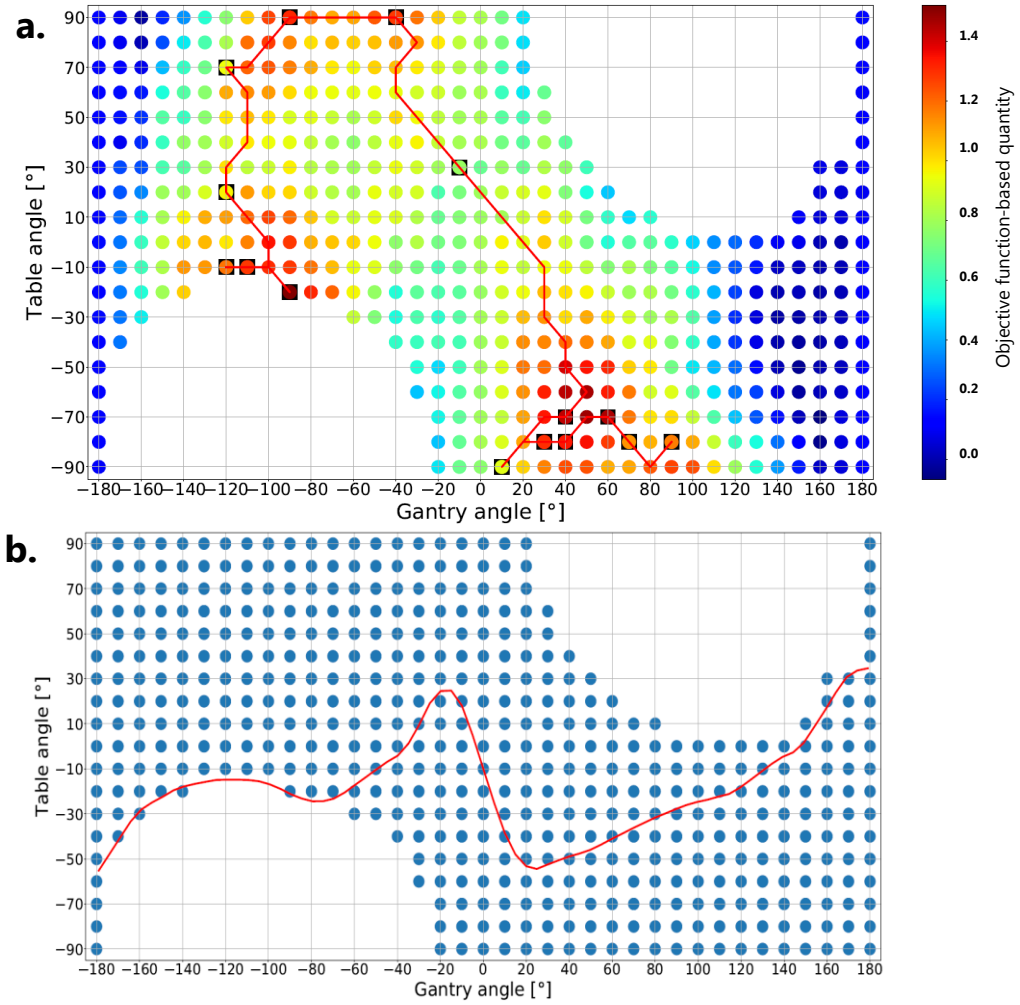

Figure 33: The DTRT paths generated for the a) dosimetrically motivated DTRT plan and b) geometrically motivated DTRT plan regarding a brain case.

This dosimetrically motivated DTRT path starts with the table slightly rotated clockwise (-10°) and the gantry at an angle below the patient and on his right side (-120°). The table then begins a counter clockwise until the patient is fully rotated to a horizontal position, while the gantry makes small shifts around the initial angle. After that, both the table and gantry rotate clockwise. At the very end of the path slight shifts at both gantry and table rotations occur, leading to the gantry radiating from the left side of the patient (90°) and the table rotated to an almost horizontal position (-80°). The gantry stays close to the patient's head during the path. The path-finding algorithm calculation time was 0.25 minutes.

The geometrically motivated DTRT path is described by a continuous clockwise rotation of the gantry starting below the patient and finishing below the patient. The treatment couch is initially rotated approximately by 50° clockwise (-50°). While the gantry starts its clockwise rotation, the table is rotating counter clockwise. When the gantry is rotated right above the patient, the table is placed in a straight position. The gantry then continues its clockwise rotation, and the table rotates to reach an angle of 60° clockwise (-60°). This position of the table will be achieved by the time the gantry is rotated at a 20° angle. After that, the table starts a counter clockwise rotation until the end of the path.

A VMAT plan using 2 partial arcs, a DTRT dosimetrically motivated plan using 2 paths and a geometrically motivated DTRT plan using 2 paths were created and the corresponding DVHs for certain structures are shown in **Figure 34**. In **Table 16,** the objective function values and dose values for selected structures are shown regarding the treatment method used, while in **Figure 35** the dose distributions calculated for each treatment method are visualised.

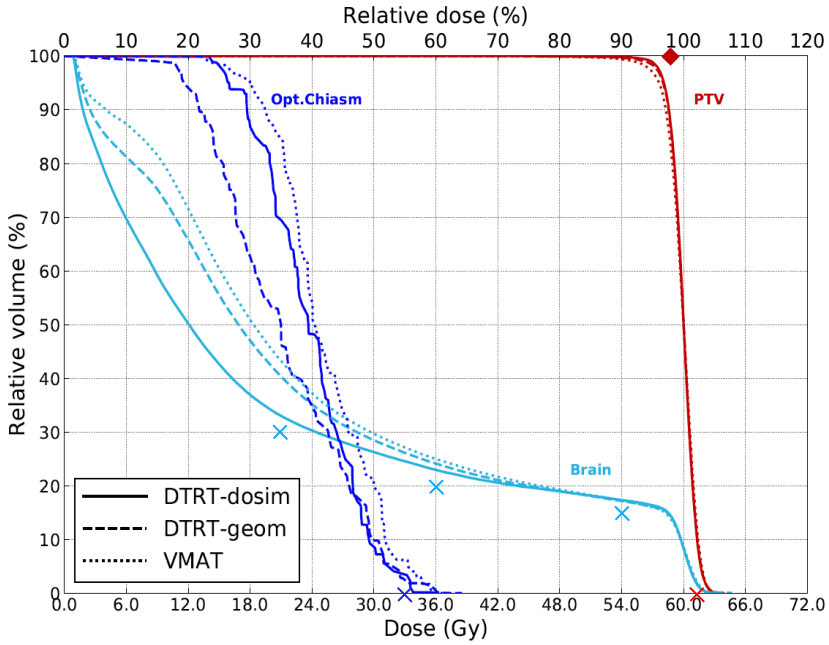

Figure 34: A comparison of DVHs for the PTV (red), the optic chiasm (blue) and the brain (light blue) between the plans of a VMAT, a dosimetrically motivated DTRT and a geometrically motivated DTRT treatment plans. Upper dose objectives are marked with a cross and lower dose objectives are marked with rhombus.

Table 16: The objective function value of the plans and dose values for the selected structures for plans of different treatment modalities.

	Dosimetrically motivated DTRT	Geometrically motivated DTRT	VMAT
Objective function value	0.020999	0.037159	0.059761
Delivery time [min]	4.93	3.53	1.73
Anchor points generation calc time [s]	1928.566	-	-
DTRT Path calc time [s]	14.701	-	-
H-DAO calc time [s]	2852.253	2135.393	1326.276
PTV $D_{98\%}$	95.7%	95.3%	94.0%
PTV $D_{2\%}$	103.5%	103.5%	103.5%
Brain Mean Dose	34.9%	39.5%	41.6%
Brain Max Dose	105.8%	107.8%	106.0%
Optic Chiasm Max Dose	60.1%	64.2%	61.1%

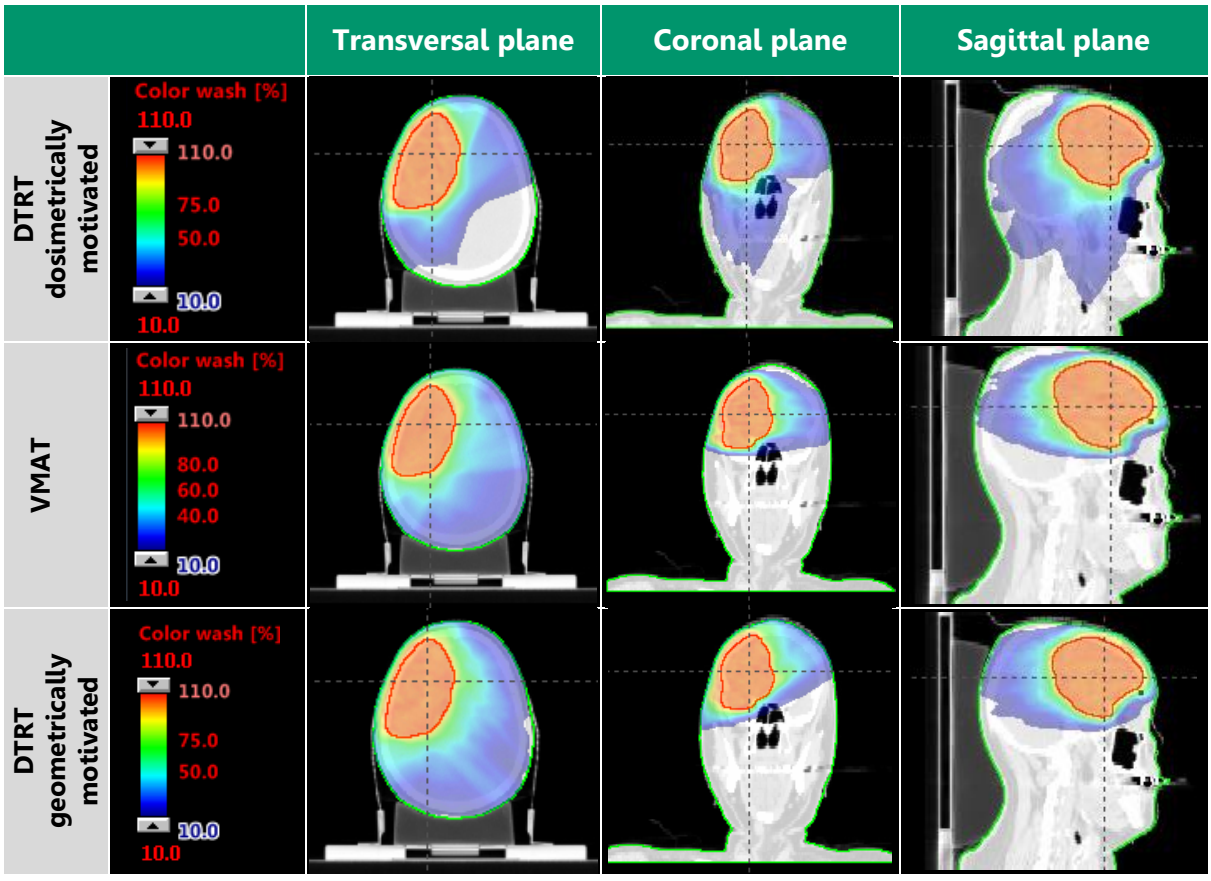

Figure 35: An illustration of the calculated dose distribution for the treatment plans studied. Red indicates 100% and blue indicates 10 % of the prescribed dose.

The dosimetrically motivated DTRT plan has a lower objective function value, while the dose delivered to the target is slightly more homogeneous and the OARs are more spared compared to the other plans. These favorable dosimetric results come with a delivery time cost.

3.2.2.Head & Neck case

In **Figure 36** the DTRT paths, generated for the dosimetrically motivated DTRT and geometrically motivated DTRT plans, are illustrated.

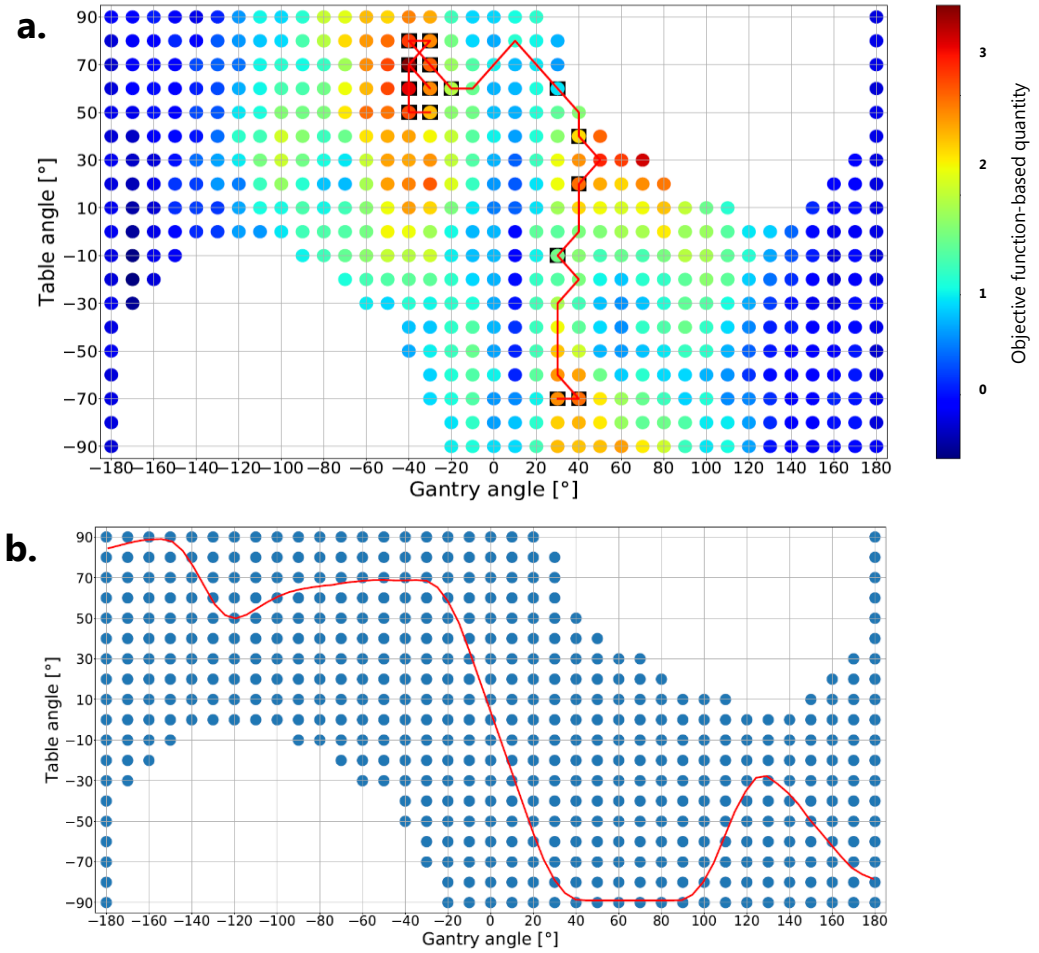

Figure 36: The DTRT paths generated for the a) dosimetrically motivated DTRT plan and b) geometrically motivated DTRT plan regarding a nasopharyngeal case.

The DTRT path starts with both the gantry (-30°) and the table (+50°) rotated counter clockwise. With the gantry approximately still, the table makes a short counter clockwise rotation and then comes back. Then a clockwise rotation of the gantry begins until it achieves a slight angle on the left side of the patient. The table is then rotated clockwise until the patient is placed to an almost horizontal position (-70°). The path-finding algorithm calculation time was 1.78 minutes.

The geometrically motivated DTRT path is described by a continuous clockwise rotation of the gantry starting below the patient and finishing again at a position below the patient. The treatment couch is initially rotated to approximately a horizontal position counter clockwise (80°). While the gantry starts its clockwise rotation, the table is rotating also clockwise. When the gantry is rotated right above the patient, the table reaches a straight position. The gantry then continues its clockwise rotation, and the

table rotates to reach a horizontal position on the other side (clockwise). When the gantry starts going below the patient (100°), the table starts a 60° counter clockwise rotation and then returns back to an almost horizontal position (clockwise) by the end of the path.

A VMAT plan using 2 partial arcs, a DTRT dosimetrically motivated plan using 2 paths and a geometrically motivated DTRT plan using 2 paths were created and the corresponding DVHs for certain structures are shown in **Figure 37**. In **Table 17** the objective function values and the maximum doses for the selected structures are shown regarding the treatment method used, while in **Figure 38** the dose distributions calculated for each treatment method are visualised.

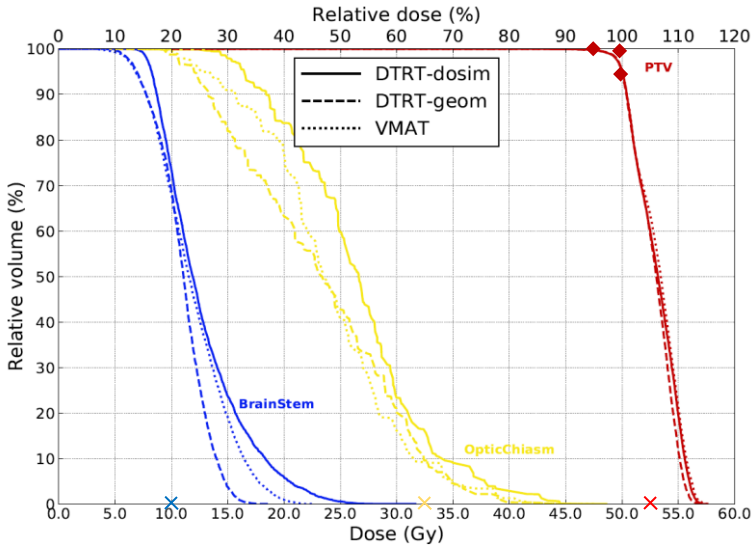

Figure 37: A comparison of DVHs for the PTV (red), the optic chiasm (yellow) and the brainstem (blue) between the plans of a VMAT, a dosimetrically motivated DTRT and a geometrically motivated DTRT treatment plans. Upper dose objectives are marked with a cross and lower dose objectives are marked with a rhombus.

Table 17: The objective function value of the plans and dose values for the selected structures for plans of different treatment modalities.

	Dosimetrically motivated DTRT	Geometrically motivated DTRT	VMAT
Objective Function value	0.017248	0.011614	0.018010
Delivery time [min]	2.99	4.48	1.76
Anchor points generation calc time [s]	1978.646	-	-
DTRT Path calc time [s]	106.511	-	-
H-DAO calc time [s]	394.071	642.528	474.319
PTV $D_{98\%}$	98.8%	99.0 %	98.9%
PTV $D_{2\%}$	112.7%	111.8%	113.0%
Optic Chiasm Max Dose	97.2%	92.4%	95.5%
Brainstem Max Dose	63.3%	37.4%	45.4%

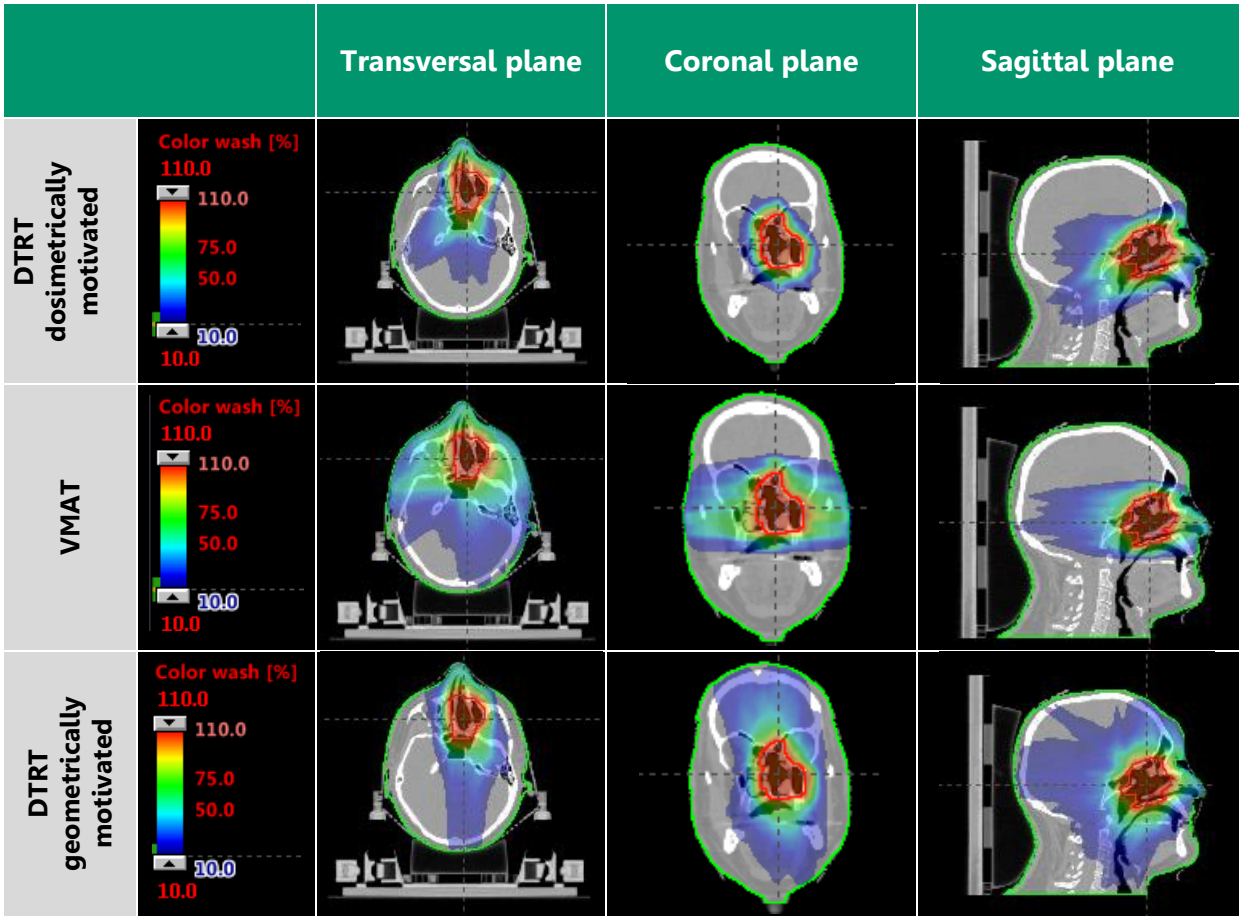

Figure 38: An illustration of the calculated dose distribution for the treatment plans studied. Red indicates 100% and blue indicates 10 % of the prescribed dose.

The dosimetrically motivated DTRT plan produces a homogeneous dose to the tartget, but this comes with a high cost on the maximum dose delivered to the OARs. It seems that for the nasopharyngeal case, the geometrically motivated DTRT plan generates the most favorable dosimetric results, while the delivery time is increased.

3.2.3.Breast case

In **Figure 39** the DTRT paths, generated for the dosimetrically motivated DTRT and geometrically motivated DTRT plans, are illustrated.

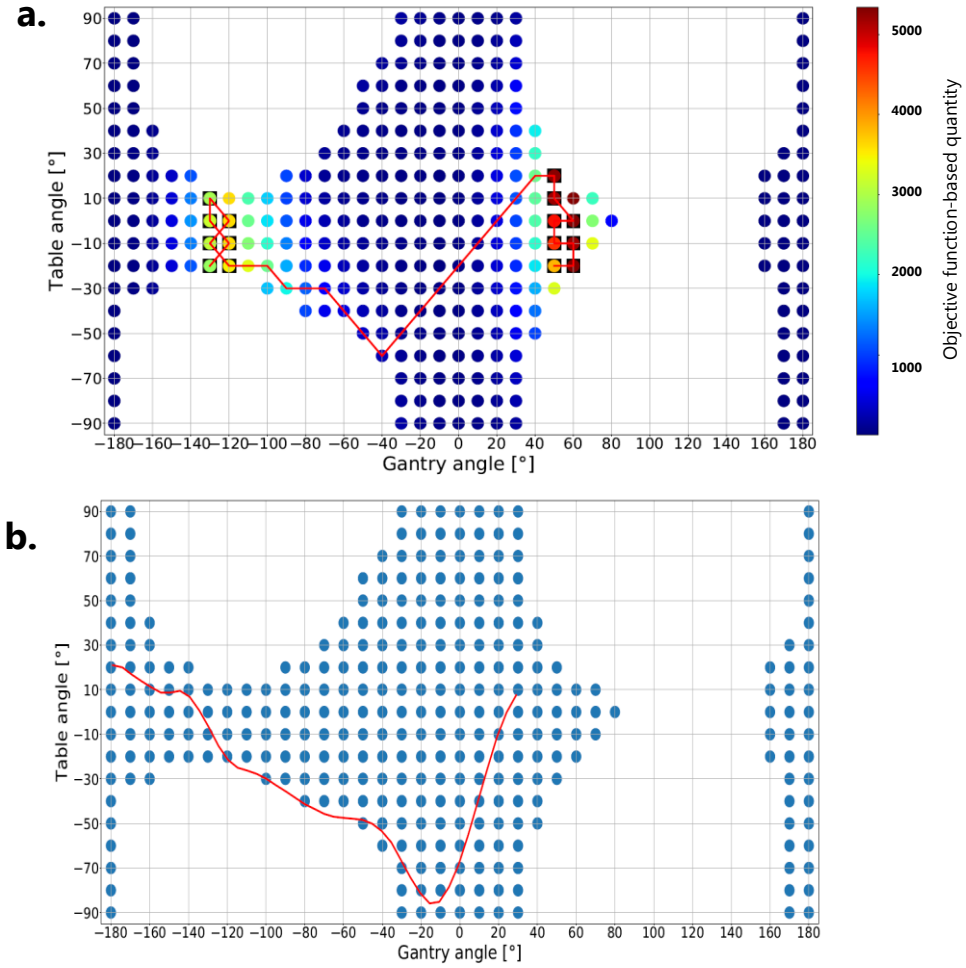

Figure 39: The DTRT paths generated for the a) dosimetrically motivated DTRT plan and b) geometrically motivated DTRT plan regarding a breast case.

The DTRT path has the gantry initially placed below the patient at a certain angle on his right side (-130°), while the table is slightly rotated clockwise (-20°). In this position, the tumor is radiated by tangential beam directions to the patient's body, meaning that the brest is radiated while OARs such as the heart and the spinal cord are avoided. At approximately this position, several beam directions are included in the path. Then the gantry begins a clockwise rotation until it stops to an angle above the patient and on her left side (50°). During the gantry rotation, the table makes a short clockwise and counter clockwise rotation ending up at the same position as before. At this position, the tumor breast is again radiated by a tangential beam direction to the patient's body, only now it is radiated from the other side of the patient. At approximately this position, several beam directions are again included in

the path. The DTRT path makes great use of tangential beam direction to the patient's body. The path-finding algorithm calculation time was 2.03 minutes.

The geometrically motivated DTRT path is described by a continuous clockwise rotation of the gantry starting below the patient and finishing at a 30° angle on the left side of the patient. The treatment couch is initially rotated to approximately 20° counter clockwise (20°). While the gantry starts its clockwise rotation, the table is rotating also clockwise until it reaches approximately a horizontal position (-85°). The table reaches this position by the time the gantry is approximately above the patient (-10°). Between this gantry position and its final position (30°), the table rotates counter clockwise to reach an approximately straight position (10°).

A VMAT plan using 2 partial arcs with the field split technique, a DTRT dosimetrically motivated plan using 2 paths and a geometrically motivated DTRT plan using 2 paths with the field split technique, were created and the corresponding DVHs for certain structures are shown in **Figure 40**. In **Table 18** the objective function values and the maximum doses for the selected structures are shown regarding the treatment method used, while in **Figure 41** the dose distributions calculated for each treatment method are visualised.

The dosimetrically motivated DTRT plan and the VMAT plan produce similar dosimetric results, as the dose to the target is similarly homogeneous and the OARs are equally spared. The VMAT plan has an advantage on the delivery time.

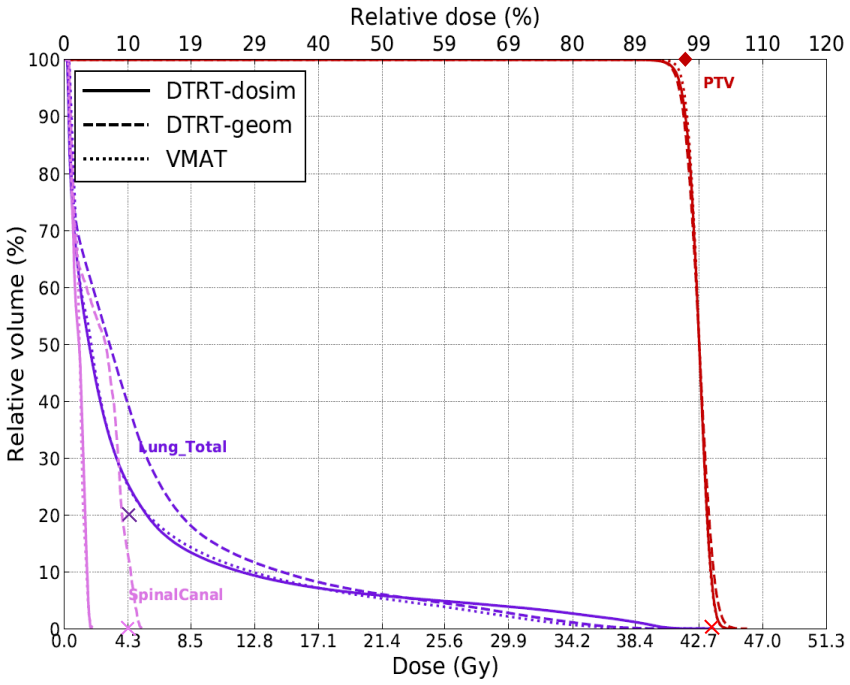

Figure 40: A comparison of DVHs for the PTV (red), the two lungs (purple) and the spinal canal (pink) between the plans of a VMAT, a dosimetrically motivated DTRT and a geometrically motivated DTRT treatment plans. Upper dose objectives are marked with a cross and lower dose objectives are marked with a rhombus.

Table 18: The objective function value of the plans and dose values for the selected structures for plans of different treatment modalities.

Treatment modality	Dosimetrically motivated DTRT	Geometrically motivated DTRT	VMAT
Objective function value	0.012876	0.023630	0.007765
Delivery time [min]	3.01	2.76	1.92
Anchor points generation calc time [s]	3509.711	-	-
DTRT Path calc time [s]	121.663	-	-
H-DAO calc time [s]	1902.006	637.494	838.637
PTV $D_{98\%}$	96.2%	95.9%	96.9%
PTV $D_{2\%}$	102.8%	103.6%	102.8%
Both Lungs Mean Dose	10.8%	13.0%	10.5%
Both Lungs Max Dose	102.2%	102.0%	101.8%
Spinal Canal Max Dose	4.3%	12.3%	4.8%

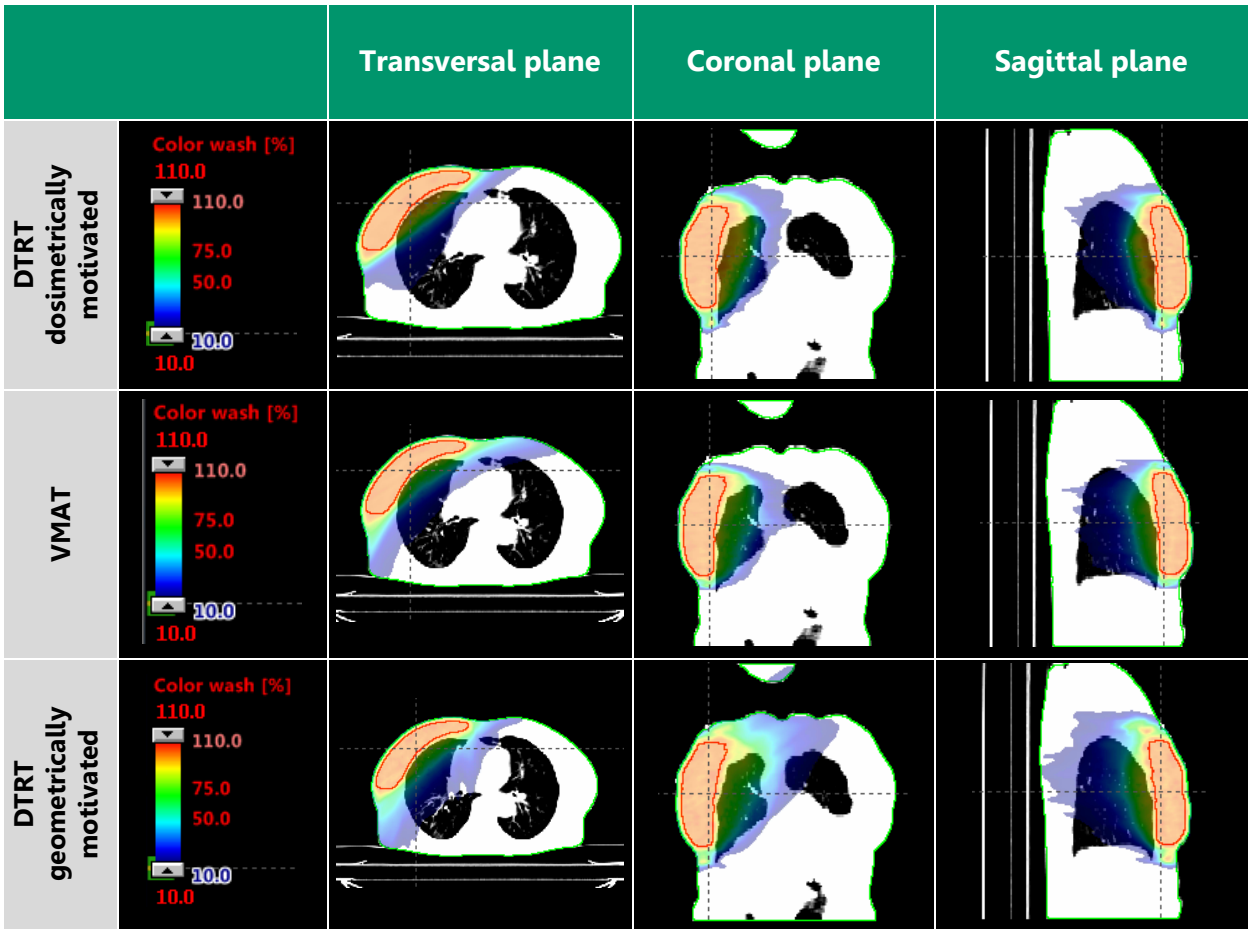

Figure 41: An illustration of the calculated dose distribution for the treatment plans studied. Red indicates 100% and blue indicates 10 % of the prescribed dose.

3.2.4.Prostate case

In **Figure 42**, the DTRT paths, generated for the dosimetrically motivated DTRT and geometrically motivated DTRT plans, are illustrated.

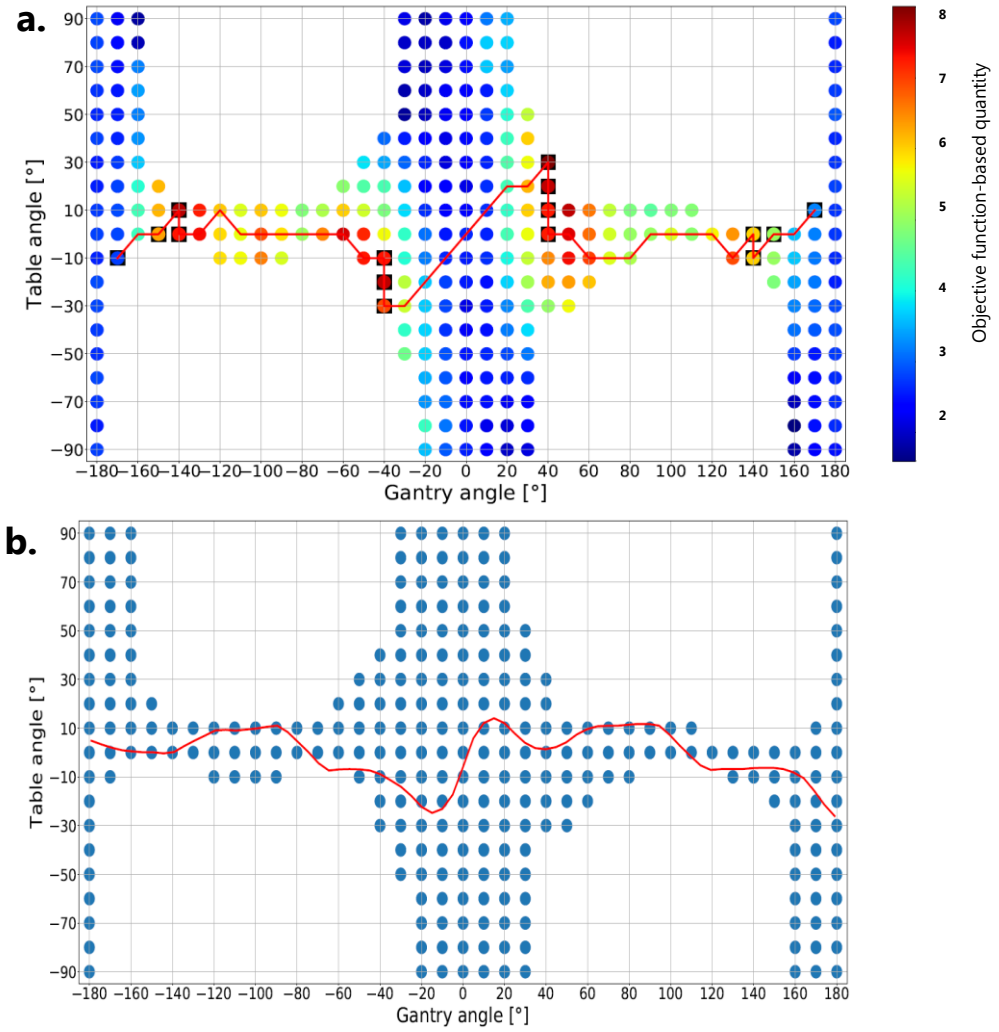

Figure 42: The DTRT paths generated for the a) dosimetrically motivated DTRT plan and b) geometrically motivated DTRT plan regarding a prostate case.

The dosimetrically motivated DTRT path generated is similar to a VMAT arc, only with some shifts on the table rotation angle. Although, it is clear that the path-finding algorithm did not choose the path to have a static treatment couch. Based on that it is expected that dosimetric results will differ at some point between a VMAT treatment plan and a dosimetrically motivated DTRT plan. The path-finding algorithm calculation time was 0.08 minutes. Regarding the geometrically motivated DTRT path, it also has a similar scheme as a VMAT arc, only with some shifts on the treatment couch rotation.

A VMAT plan using 2 partial arcs, a DTRT dosimetrically motivated plan using 2 paths and a geometrically motivated DTRT plan using 2 paths were created and the

corresponding DVHs for certain structures are shown in **Figure 43.** In **Table 19** the objective function values and the maximum doses for the selected structures are shown regarding the treatment method used, while in **Figure 44** the dose distributions calculated for each treatment method are visualised.

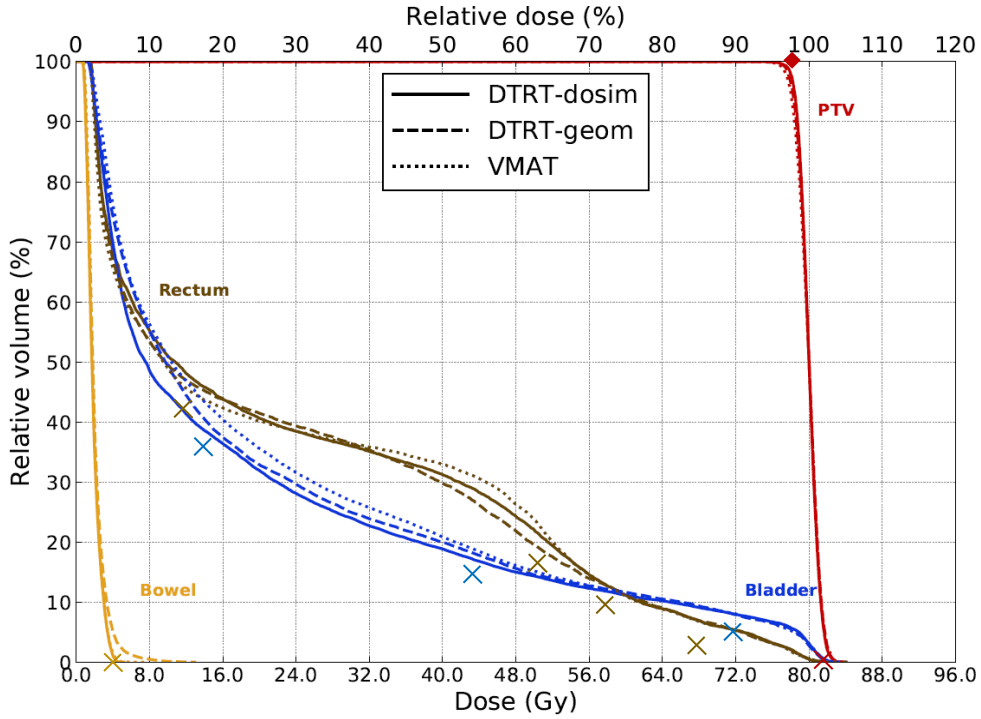

Figure 43: A comparison of DVHs for the PTV (red), the bladder (blue), the rectum (brown) and the bowel (orange) between the plans of a VMAT, a dosimetrically motivated DTRT and a geometrically motivated DTRT treatment plans. Upper dose objectives are marked with a cross and lower dose objectives are marked with a rhombus.

Table 19: The objective function value of the plans and dose values for the selected structures for plans of different treatment modalities.

Treatment modality	Dosimetrically motivated DTRT	Geometrically motivated DTRT	VMAT
Objective function value	0.003743	0.004729	0.004999
Delivery time [min]	3.75	2.72	2.25
Anchor points generation calc time [s]	1218.911	-	-
DTRT Path calc time [s]	4.520	-	-
H-DAO calc time [s]	1247.397	853.614	972.753
PTV $D_{98\%}$	97.5%	97.2%	96.8%
PTV $D_{2\%}$	102.5%	102.7%	102.5%
Rectum Mean Dose	30.3%	29.8%	30.3%
Rectum Max Dose	105.0%	103.6%	104.2%
Bladder Mean Dose	25.1%	26.3%	27.3%
Bladder Max Dose	104.1%	103.8%	103.9%
Bowel Max Dose	6.5%	16.4%	9.6%

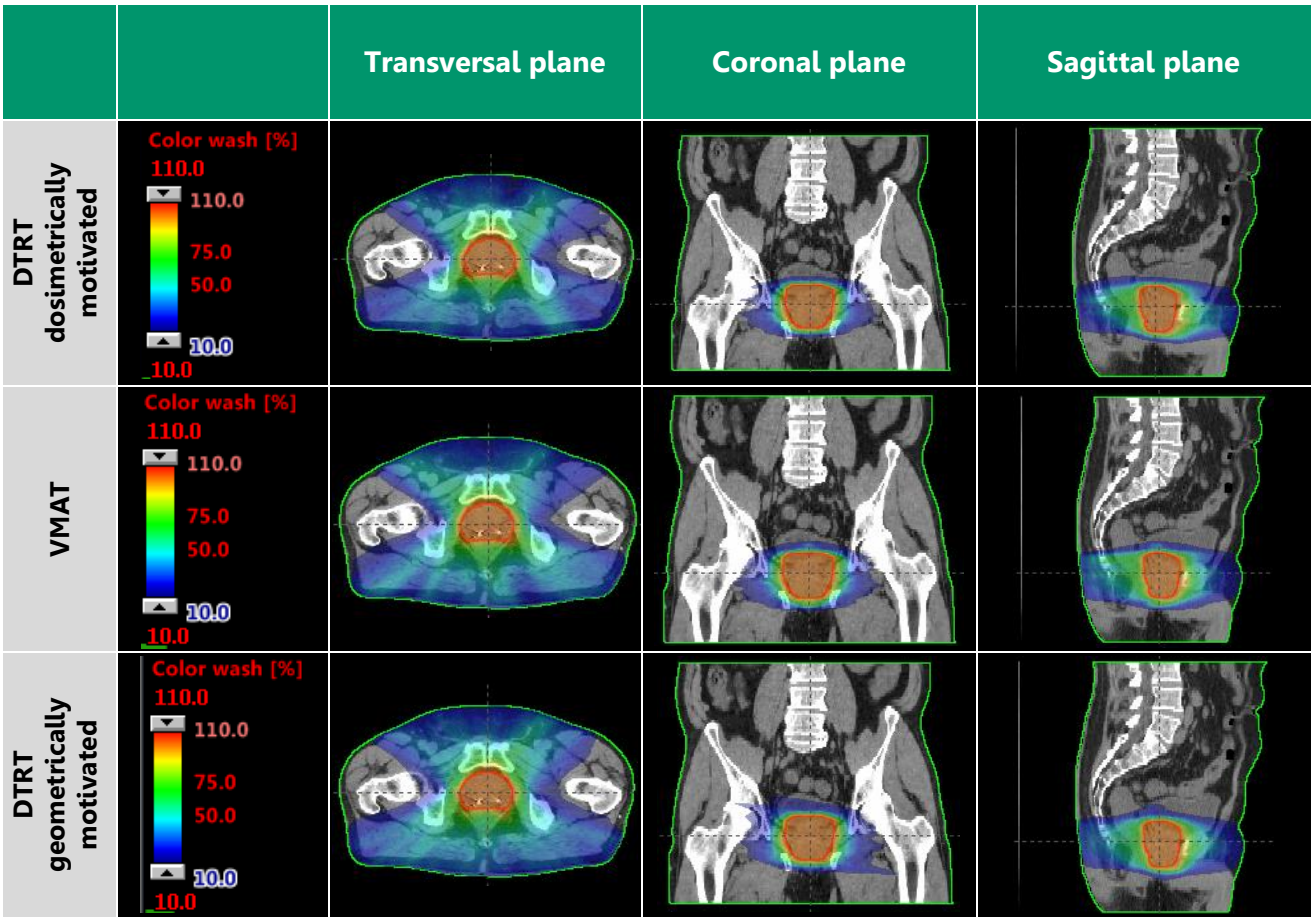

Figure 44: An illustration of the calculated dose distribution for the treatment plans studied. Red indicates 100% and blue indicates 10 % of the prescribed dose.

The dosimetrically motivated DTRT plan produces a lower objective function value, while the dosimetric results for the OARs are similar between the 3 plans. An important difference between the 3 plans regarding the OARs, is that the maximum dose at the bowel is substantially decreased for the dosimetrically motivated DTRT plan. The favorable dosimetric results of the dosimetrically motivated DTRT plan, come with a cost on the delivery time.

3.3. Cases investigated with a continuously changing isocenter position

This section presents a complete DTRT TPP, as explained in **Materials and Methods**, generated for two craniospinal irradiation cases and a bilateral breast case. Each case was investigated by a doubled path that the path-finding algorithm produced and in order to evaluate the dosimetrically motivated DTRT treatment plan that was developed, a comparison of the dosimetric results achieved using different treatment modalities was performed.

3.3.1. Craniospinal Irradiation case I

In **Figure 45**, the DTRT paths, generated for the dosimetrically motivated DTRT and manually defined DTRT plans, are illustrated. The craniospinal tumor in question, is a long tumor having the shape of the brain along with the spinal cord of the patient. In terms of absolute table longitudinal positions, the tumor is located in a range of -83 cm up to -5 cm.

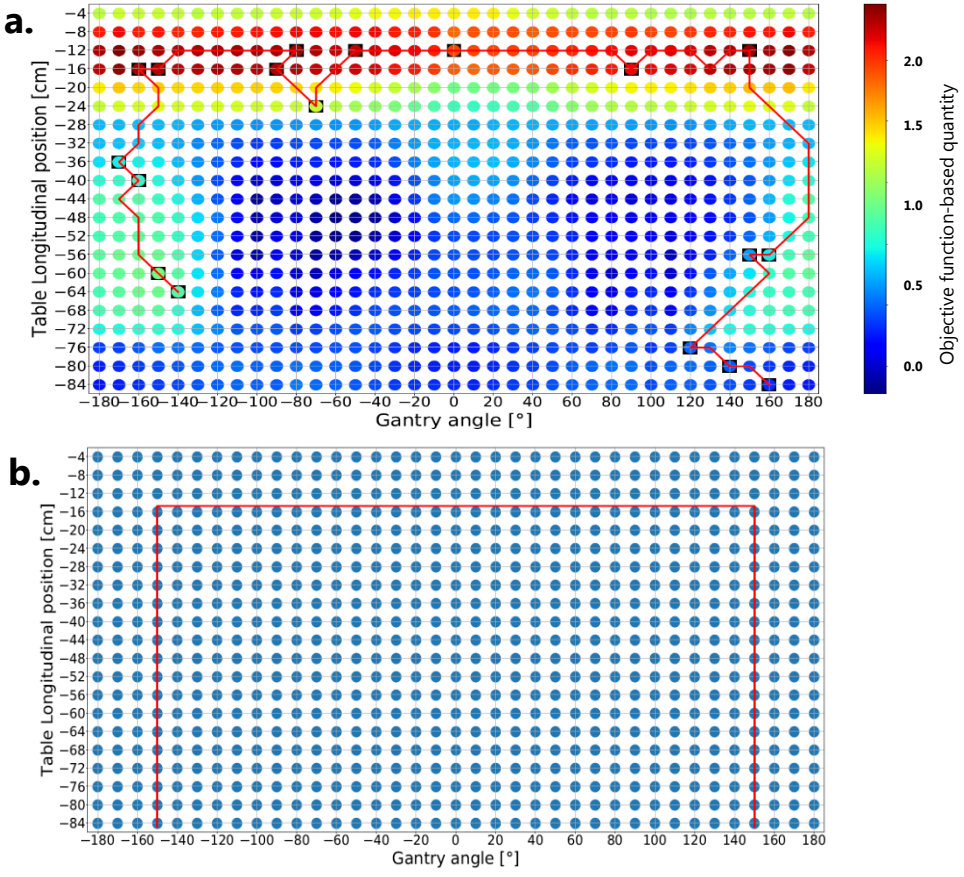

Figure 45: The DTRT paths generated for the a) dosimetrically motivated DTRT plan and b) manually defined DTRT plan regarding a craniospinal case.

In the figure above, the x-axis represents the gantry rotation angle, and the y-axis shows the longitudinal position of the treatment couch. The dosimetrically motivated DTRT path generated, starts at a -64 cm absolute longitudinal table position, where the abdomen area of the patient is located. The gantry is set to an angle of -140^{o}, which means that the radiation beam will be delivered from the bottom side of the patient. The table starts moving until the isocenter points the brain area, following by a partial arc of the gantry around the head of the patient. The arc stops at a gantry angle of 150^{o} and then the table starts moving again so that the beam will be delivered along the tumor shape up until the end of the spinal cord, while minor shifts at the gantry angle are allowed. It is important to point out that along the generated path, the lower part of the tumor, which is located at the bottom of the spinal cord, is only radiated by a small part of the path. The path-finding algorithm calculation time was 54.12 minutes.

The manually defined DTRT path starts with a gantry rotation angle below the patient and on his right side (-150^{o}) while the table is moved to the longitudinal direction so that the beam is focused on the lower part of the spinal cord. The gantry stays still at this angle and the table moves on the longitudinal direction until the isocenter is focused on the brain region. This motion of the table leads the radiation beam along the PTV. An arc is then performed until the gantry reaches the exact symmetric position on the left side of the patient (150^{o}). Then, the table moves again on the longitudinal axis and the path stops when the beam is again focused on the lower part of the spinal cord.

An IMRT plan using 6 fields, a VMAT plan using 3 full arcs, a DTRT dosimetrically motivated plan using 2 paths and a manually defined DTRT plan using 2 paths were created and the corresponding DVHs for certain structures are shown in **Figure 46**. In **Table 20** the objective function values and the maximum doses for the selected structures are shown regarding the treatment method used, while in **Figure 47** the dose distributions calculated for each treatment method are visualised.

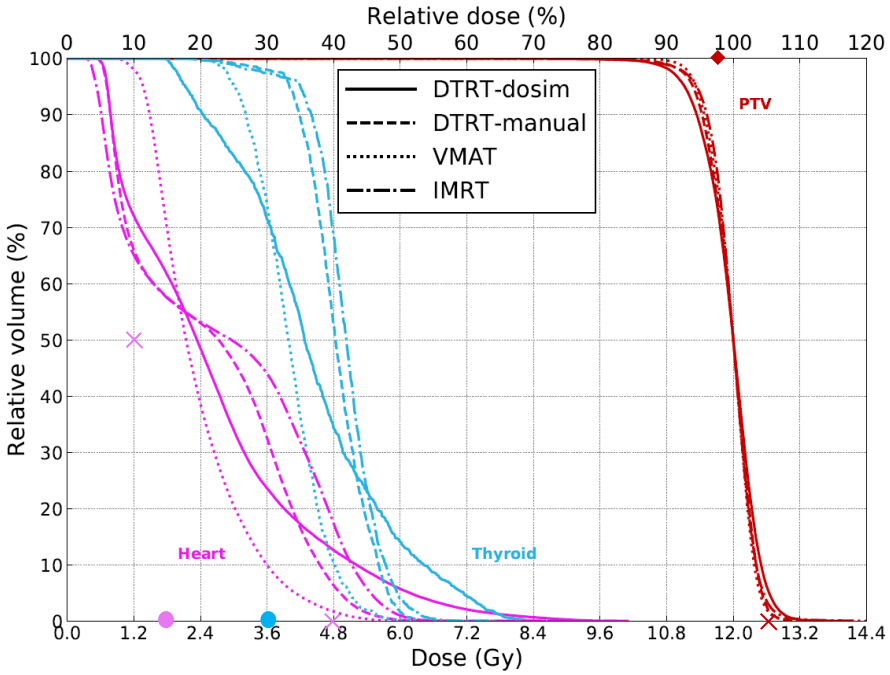

Figure 46: A comparison of DVHs for the PTV (red), the thyroid (light blue) and the heart (pink) between the plans of a dosimetrically motivated DTRT, a manually defined DTRT, a VMAT and an IMRT treatment plan. Upper dose objectives are marked with cross, lower dose objectives are marked with a rhombus and mean dose objectives are marked with a circle.

Table 20: The objective function value of the plans and dose values for the selected structures for plans of different treatment modalities.

Treatment modality	Dosimetrically motivated DTRT	Manually defined DTRT	VMAT	IMRT
Objective function value	0.195704	0.136080	0.057007	0.159724
Delivery time [min]	5.07	4.64	3.58	9.53
Anchor points generation calc time [s]	12680.053	-	-	-
DTRT Path calc time [s]	3247.120	-	-	-
H-DAO calc time [s]	22123.070	28971.354	17770.244	1108.170
PTV $D_{98\%}$	90.4%	92.0%	93.0%	92.1%
PTV $D_{2\%}$	106.8%	105.2%	105.0%	105.9%
Heart Mean Dose	21.9%	21.4%	19.7%	23.3%
Heart Max Dose	84.1%	76.3%	54.3%	82.5%
Thyroid Mean Dose	36.7%	40.5%	33.4%	41.9%

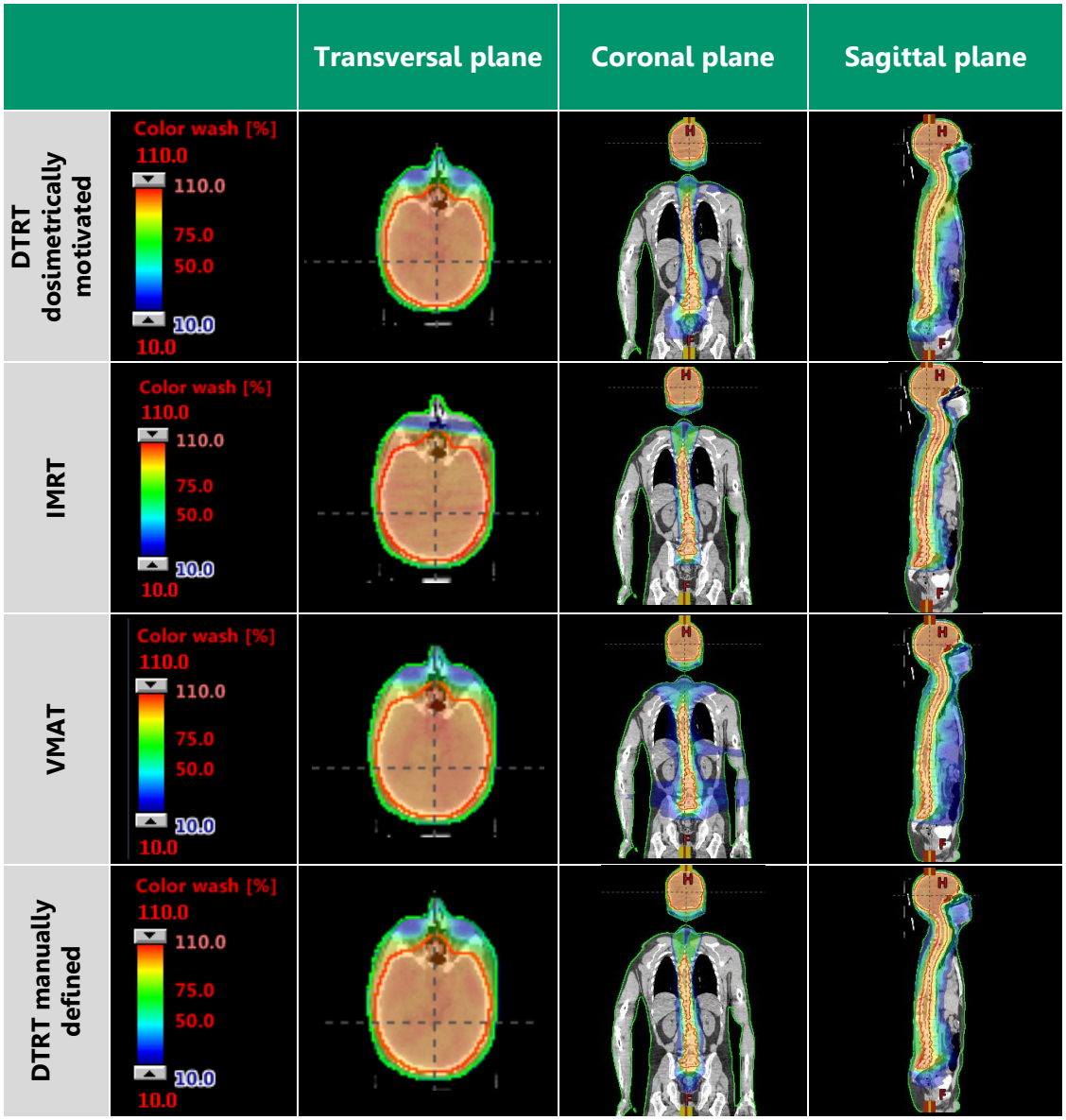

Figure 47: An illustration of the calculated dose distribution for the treatment plans studied. Red indicates 100% and blue indicates 10 % of the prescribed dose.

The dosimetrically motivated DTRT plan and the manually defined DTRT plan produce similar dosimetric results. It seems that the VMAT plan utilizing 3 arcs is more advantageous regarding dose homogeneity to the target, sparing of the OARs and plan delivery time compared to the other plans.

3.3.2.Craniospinal case II

In **Figure 48**, the DTRT paths, generated for the dosimetrically motivated DTRT and manually defined DTRT plans, are illustrated. The craniospinal tumor in question, is a long tumor having the shape of the brain along with the spinal cord of the patient. In terms of absolute table longitudinal positions, the tumor is located in a range of -80 cm up to -2 cm.

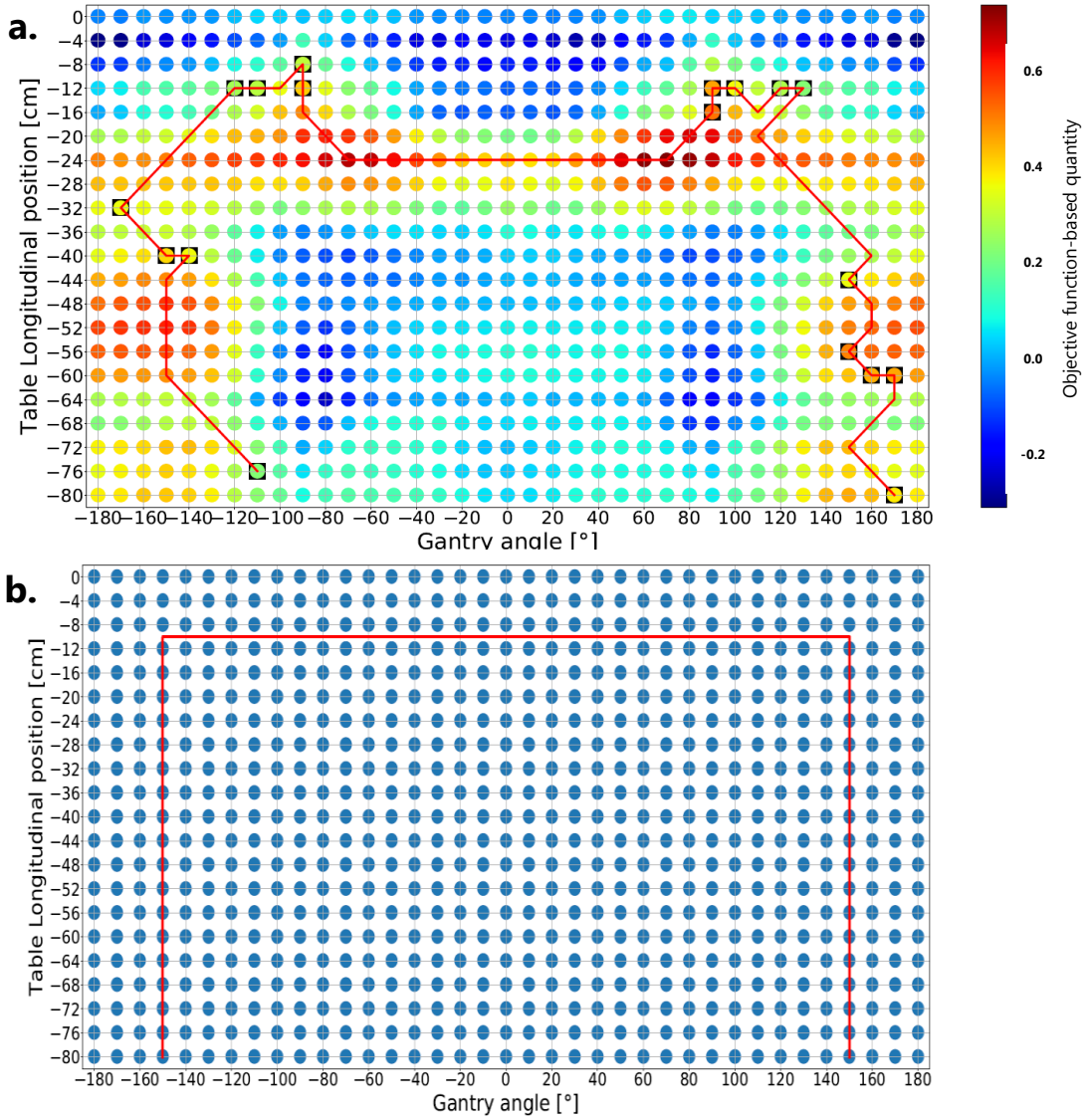

Figure 48: The DTRT paths generated for the a) dosimetrically motivated DTRT plan and b) manually defined DTRT plan regarding a craniospinal case.

The DTRT path generated, starts at a -76 cm absolute longitudinal table position, where the lower part of the spinal cord of the patient is located. The gantry is set to an angle of -110°, which means that the radiation beam will be delivered from the bottom side of the patient. The table starts moving until the isocenter points the brain area, while the gantry rotates counter clockwise up to a degree of -170° and then starts a clockwise rotation. A partial arc follows around the head of the patient. The

table then, starts moving again so that the beam will be delivered along the tumor shape up until the end of the spinal cord, while minor shifts at the gantry angle are allowed. The path-finding algorithm calculation time was 2.03 hours. The manually defined DTRT path follows the same scheme as explained in **Craniospinal Irradiation case I**.

An IMRT plan using 6 fields, a VMAT plan using 3 full arcs and a DTRT dosimetrically motivated plan using 2 paths, were created and the corresponding DVHs for certain structures are shown in **Figure 49**. In **Table 21** the objective function values and the maximum doses for the selected structures are shown regarding the treatment method used, while in **Figure 50** the dose distributions calculated for each treatment method are visualised.

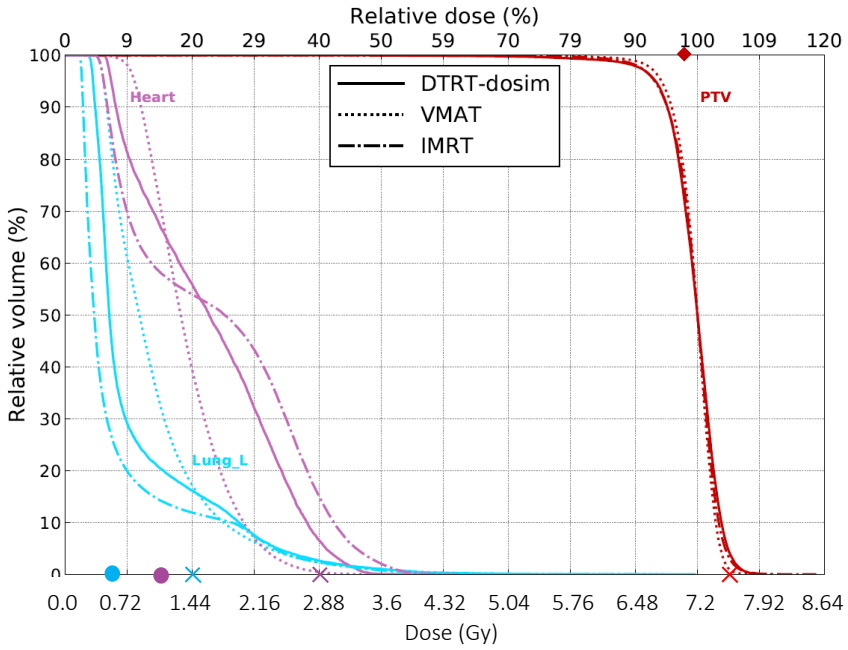

Figure 49: A comparison of DVHs for the PTV (red), the thyroid (light blue) and the heart (pink) between the plans of a dosimetrically motivated DTRT, a VMAT and an IMRT treatment plan. Upper dose objectives are marked with a cross, lower dose objectives are marked with a rhombus and mean dose objectives are marked with a circle.

The dosimetrically motivated DTRT plan produces a lower objective function value and a lower plan delivery time than the IMRT plan representing the clinical treatment of this patient. On the other hand, the VMAT plan utilizing 3 arcs is more advantageous regarding dose homogeneity to the target, sparing of the OARs and plan delivery time compared to the other plans.

Table 21: The objective function value of the plans and dose values for the selected structures for plans of different treatment modalities.

Treatment modality	Dosimetrically motivated DTRT	VMAT	IMRT
Objective function value	0.180078	0.104674	0.212574
Delivery time [min]	4.75	3.61	9.07
Anchor points generation calc time [s]	9074.336	-	-
DTRT Path calc time [s]	7297.401	-	-
H-DAO calc time [s]	4291.946	17625.955	946.049
PTV $D_{98\%}$	90.0%	92.1%	90.4%
PTV $D_{2\%}$	106.0%	104.4%	105.7%
Heart Mean Dose	22.9%	19.3%	23.8%
Heart Max Dose	62.0%	50.2%	62.1%
Left Lung Mean Dose	11.4%	14.2%	8.6%
Left Lung Max Dose	99.6%	94.6%	92.5%

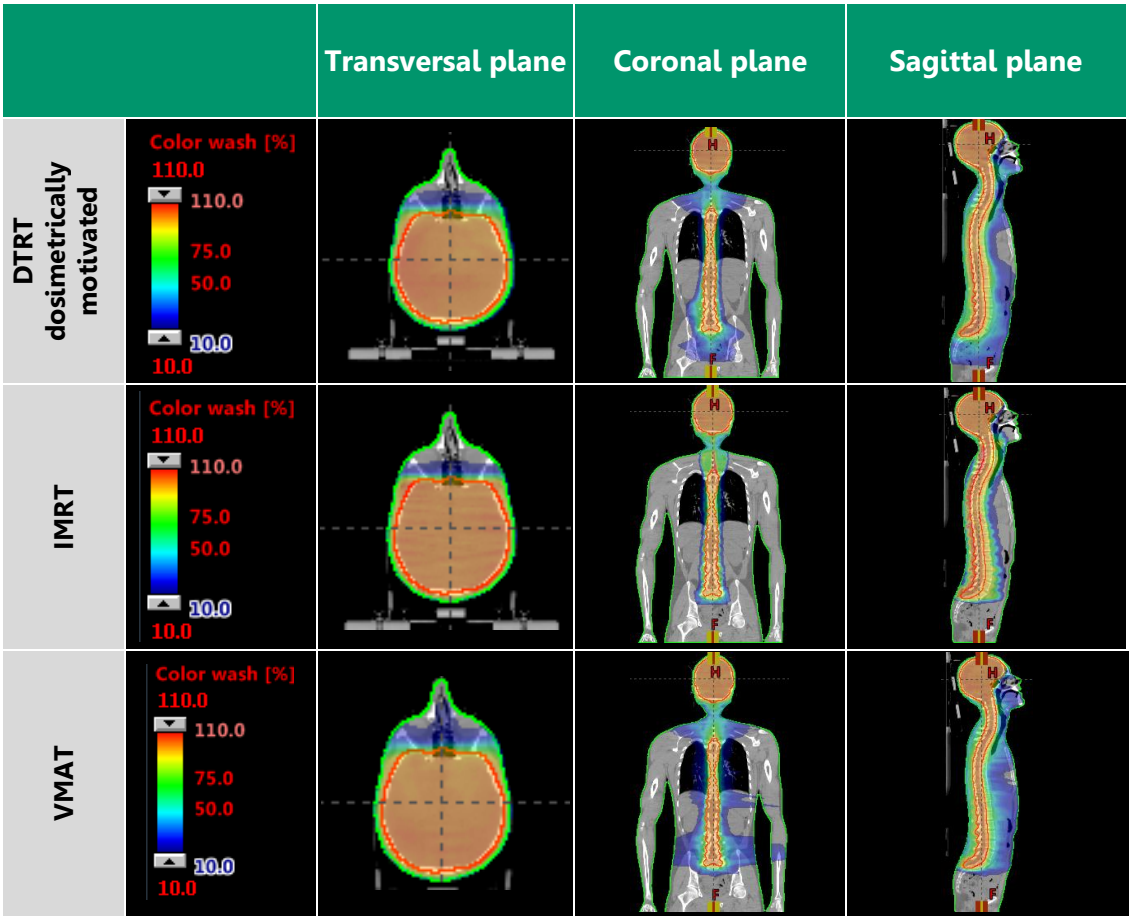

Figure 50: An illustration of the calculated dose distribution for the treatment plans studied. Red indicates 100% and blue indicates 10 % of the prescribed dose.

3.3.3.Bilateral breast case

In **Figure 51** the DTRT paths, generated for the dosimetrically motivated DTRT and manually defined DTRT plans, are illustrated. The bilateral breast tumor in question, is a concave shaped tumor following the shape of the two breasts of the patient. In terms of absolute table lateral positions, the tumor is located in a range of -20 cm up to 18 cm.

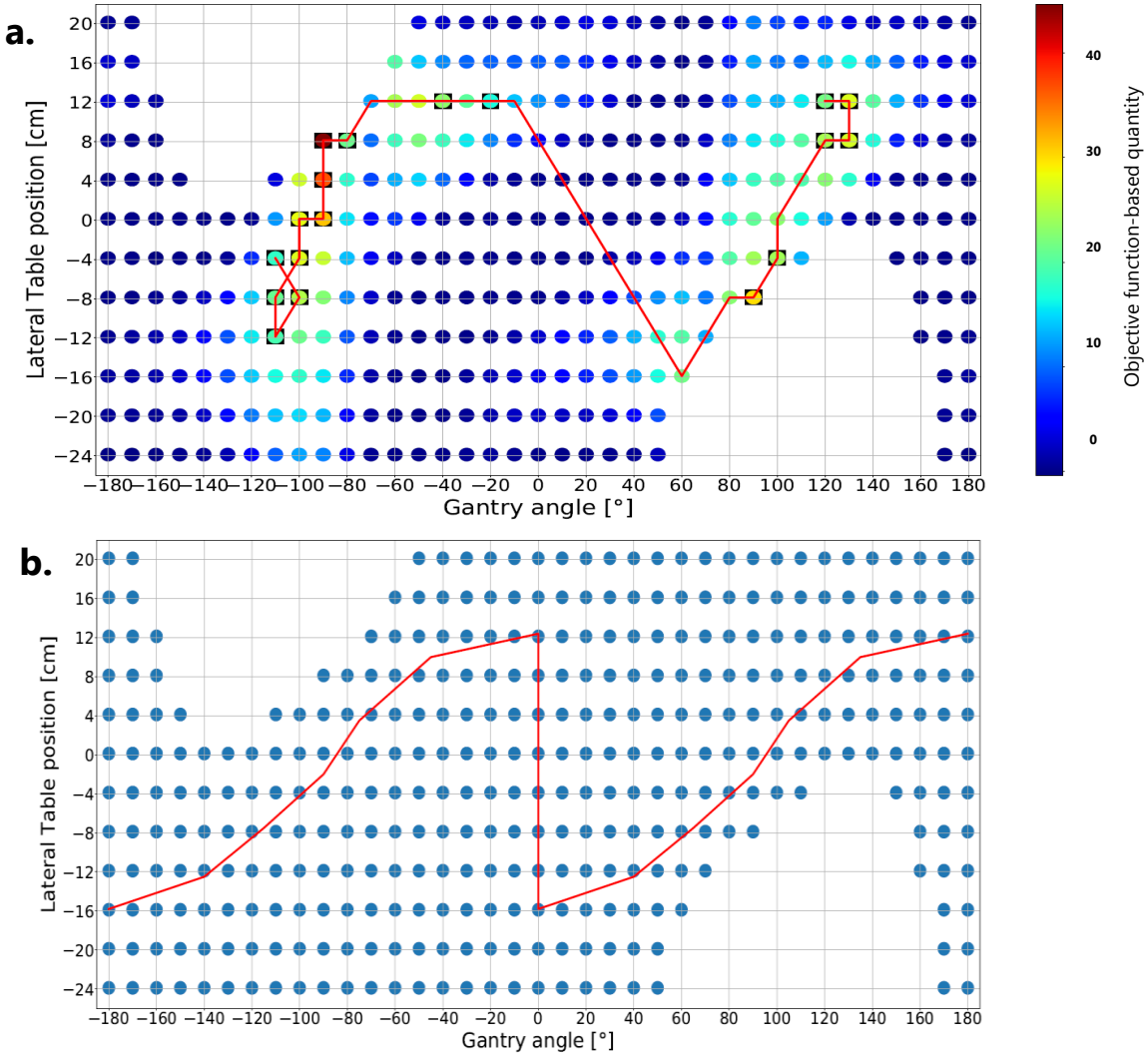

Figure 51: The DTRT paths generated for the a) dosimetrically motivated DTRT plan and b) manually defined DTRT plan regarding a bilateral breast case.

The DTRT path generated, starts at a -4 cm absolute lateral table position. This position leads the isocenter to point at the tumor located at the right breast and more specifically to the edge of the tumor towards the diaphragm. The gantry is set to the left side of the patient at an angle of -110°, which means that the radiation beam will be delivered at a tangential direction to the left breast. The table starts moving towards -12cm absolute position, meaning that the isocenter position moves along the right breast tumor. A clockwise rotation of the gantry starts until the end of the beam delivery. While the gantry is rotating, the table moves on the opposite direction so that

the isocenter will be focused on the left breast leading to multiple tangential beam directions on the left breast. The gantry then continues its rotation towards the right side of the patient at a 60° angle, while the table moved back to a -16 cm position. The radiation is now pointing to the right breast. After that, the table starts moving so that the isocenter will point to the left breast. While the table moves to this direction, the gantry rotates from 60° to 130° leading to multiple tangential beam directions on the right breast. The path-finding algorithm calculation time was 7.51 minutes.

The manually defined DTRT path can be described in 2 parts. The first part begins with the gantry rotated right below the patient (-180°) and the table moved on the right so that the isocenter is placed at the right breast. The gantry starts a clockwise rotation until it reaches a position right above the patient (0°) and while the gantry is rotating, the table is moving on the left. When the gantry is right above the patient, the table is moved so that the isocenter focuses on the left breast. For the second part of the path, the table moves on the right so that the isocenter focuses again on the right breast, while the gantry stays still right above the patient. Then a clockwise rotation of the gantry continues until the gantry goes right below the patient and during this rotation, the table moves on the left so that the beam will be delivered firstly at the right breast and then at the left breast.

A VMAT plan using 4 partial arcs, with 2 of them focusing on the left breast and the rest to the right breast, a DTRT dosimetrically motivated plan using 2 paths and a manually defined DTRT plan using 2 paths were created and the corresponding DVHs for certain structures are shown in **Figure 52**. In **Table 22** the objective function values and the maximum doses for the selected structures are shown regarding the treatment method used, while in **Figure 53** the dose distributions calculated for each treatment method are visualised.

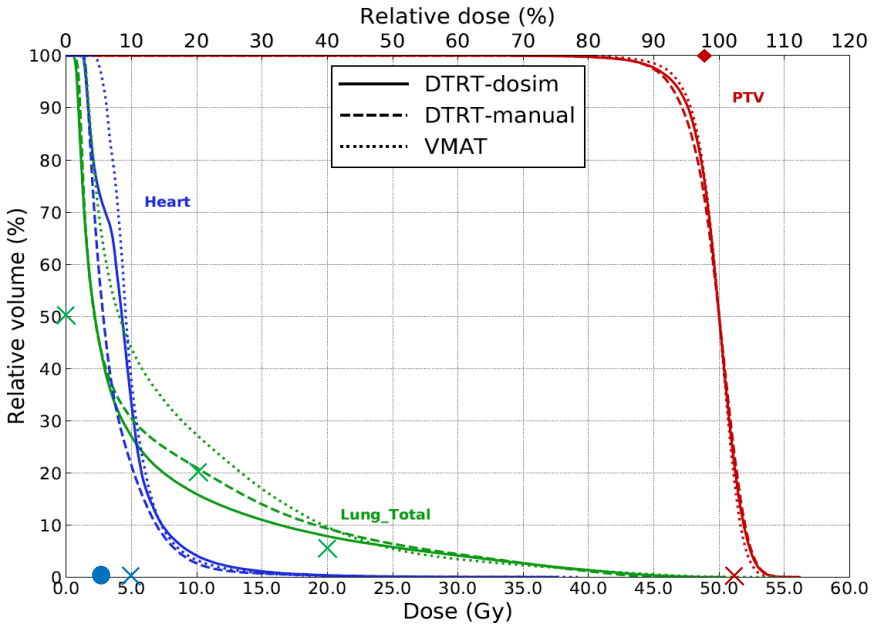

Figure 52: A comparison of DVHs for the PTV (red), the two lungs (green) and the heart (blue) between the plans of a dosimetrically motivated DTRT, a manually defined DTRT and a VMAT. Upper dose objectives are marked with a cross, lower dose objectives are marked with a rhombus and mean dose objectives are marked with a circle.

Table 22: The objective function value of the plans and dose values for the selected structures for plans of different treatment modalities.

Treatment modality	Dosimetrically motivated DTRT	Manually defined DTRT	VMAT
Objective function value	0.086317	0.088667	0.092634
Delivery time [min]	2.47	2.51	3.84
Anchor points generation calc time [s]	2280.604	-	-
DTRT Path calc time [s]	450.763	-	-
H-DAO calc time [s]	8383.276	2162.575	12014.740
PTV Max Dose	89.4%	89.1%	91.0%
PTV Min Dose	105.9%	106.0%	105.2%
Both Lungs Mean Dose	11.6%	13.0%	16.0%
Both Lungs Max Dose	100.5%	96.9%	109.1%
Heart Mean Dose	9.1%	7.4%	10.1%
Heart Max Dose	75.3%	70.4%	78.4%

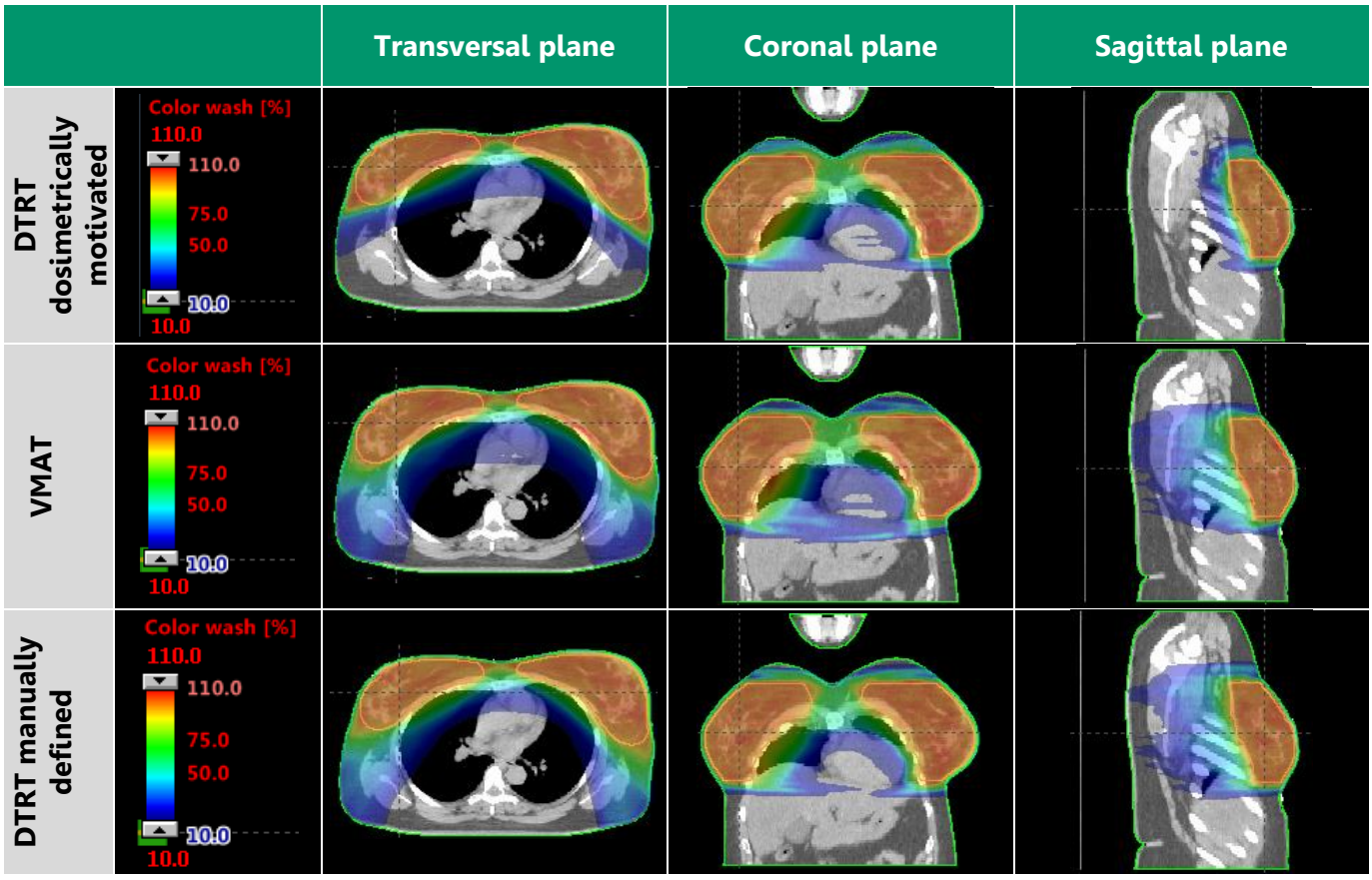

Figure 53: An illustration of the calculated dose distribution for the treatment plans studied. Red indicates 100% and blue indicates 10 % of the prescribed dose.

The dosimetrically motivated DTRT plan produces a lower objective function value, a more homogeneous dose to the PTV, better sparing of the OARs and a lower plan delivery time than the other plans.

4. Discussion

A TPP for creating non-isocentric DTRT plans was successfully developed and the set of parameters that affect the DTRT path generation were investigated. To validate the developed TPP, four unique tumor cases were studied. These cases were referring to a brain tumor, a nasopharyngeal tumor, a breast tumor and a prostate tumor, as each one of them was investigated with a static isocenter position. Validation of the proper functionality of the TPP was successful by comparing the dosimetric results of the dosimetrically motivated DTRT plan with a VMAT and a geometrically motivated DTRT plan for each case. To further understand the advantages and drawbacks of the new TPP, more tumor cases were investigated utilizing multiple isocenter positions, such us two craniospinal cases and a bilateral breast case.

According to the parameter investigation performed, a threshold of 10% during FMO & Elimination process was selected as the best option. A lower amount of map points to be eliminated in each iteration leads to a more accurate elimination method, because in each iteration, FMO is performed for the remaining map points. Looking at the number of anchor points, it can be said that after a certain amount of anchor points, the dosimetric results saturate. For the DTRT plans created by an isocentric approach, a number of 15 anchor points was selected, while for the plans utilizing a non-isocentric approach 18 anchor points were used. The path-finding algorithm calculation time sharply increases after a certain amount of anchor points and so in order to investigate DTRT paths with higher number of anchor points, the path-finding algorithm should be improved to calculate the path faster. Another parameter for the DTRT path generation, that was investigated, is the TSP solver algorithm. While for the isocentric approach, the dosimetric results were approximately the same by using either the greedy algorithm or the hybrid TSP solver, the non-isocentric cases showed a decrease of the objective function value when greedy algorithm was used. On the other hand, the path created by the hybrid TSP solver avoids sharp shifts of the treatment machine components along the path up to a certain level. The hybrid TSP solver algorithm was used for further investigations in this study. The last parameter investigated was the scoring quantity of the map points. An objective function-based quantity and a mean PTV dose-based quantity were used. Plans using the objective function-based quantity showed better dosimetric results, so the treatment plans created were based on this scoring quantity.

To validate the proper functionality of the developed DTRT TPP, treatment plans were created for a brain case, a nasophryngeal case, a breast case and a prostate case. Dosimetric results were compared with VMAT plans and geometrically motivated DTRT plans. Looking at the brain case, a lower objective function value was obtained from the developed DTRT plan, while more conformal dose to the PTV and better sparing of the brain were achieved. In addition, the maximum dose delivered to the optic chiasm was kept at a lower value. Observing a nasopharyngeal tumor, tumor control and sparing of the optic chiasm was achieved at similar levels with the other plans. Focusing

on the brainstem it seems that the dosimetrically motivated DTRT plan led to a significant increase to the maximum dose delivered to the brainstem. Analysing a right breast tumor case, the dosimetrically motivated DTRT plan showed a similar tumor control and a better sparing of the lungs and the spinal canal, compared to the geometrically motivated DTRT plan. The dosimetric results compared with the VMAT plan were similar. The last isocentric case studied was a prostate case, where tumor control and sparing of the rectum showed similar results among the three plans. Considering the sparing of the bladder and the bowel, the developed DTRT plan showed better dosimetric results. In summury, the developed dosimetrically motivated DTRT TPP shows positive dosimetric results for tumor cases investigated with a fixed isocenter position.

Scaling up to the main purpose of the project, which is to investigate the performance of the developed DTRT TPP for non-isocentric cases, two craniospinal cases and a bilateral breast case were investigated. For the first craniospinal case, an IMRT plan representing the clinical treatment performed, a VMAT plan and manually defined DTRT plan were created in order to identify the dosimetric advantages and drawbacks of the dosimetrically motivated DTRT plan. A lower tumor control was achieved by the developed DTRT plan, while a better sparing of the heart and the thyroid was accomplished comparing to the IMRT clinical treatment. Comparing to the manually defined DTRT plan, the two plans showed similar sparing of the heart, while the dosimetrically motivated DTRT plan showed better sparing of the thyroid. Among the 4 plans, VMAT showed the best dosimetric results and had a shorter plan delivery time. This is probably due to the fact that each part of the tumor was radiated by a full arc. The dosimetrically motivated DTRT plan delivers the beam to the tumor located at the lower part of the spinal cord only by a short pathlength. The pathlength radiating each part of the tumor could possibly affect the dosimetric results as intensity modulation along a longer pathlength could be more effective. The second craniospinal case was also treated clinically by an IMRT plan. For this case an IMRT and a VMAT plan where produced in addition to the dosimetrically motivated DTRT plan. Similar tumor control and a slightly better heart sparing was achieved by the dosimetrically motivated DTRT plan comparing to the IMRT plan. On the other hand, the VMAT plan showed higher tumor control and heart sparing. Looking at the mean dose at the left lung, the dosimetrically motivated DTRT plan performed better than the VMAT plan, while the IMRT plan performed even better. As said before, the pathlength covering each part of the tumor probably affects the plan quality. In addition, the delivery time for the VMAT plan was much shorter. The last tumor case studied for non-isocentric DTRT plans, was a bilateral breast case, which was clinically treated by a VMAT plan. In addition, a manually defined DTRT plan was produced. Similar tumor control was achieved from the three plans, while better sparing of the lungs was achieved by the dosimetrically motivated DTRT plan. Looking at the sparing of the heart, better dosimetric results were achieved compared to VMAT, while the manually defined DTRT plan showed even better dosimetric results. A lower objective

function value and a shorter delivery time was obtained by the dosimetrically motivated DTRT plan.

A method used, which might limit the plan quality of the developed TPP, is the anchor points generation during FMO & Elimination process. We try to find the anchor points and then produce the DTRT path which connects them. As we saw in the first craniospinal case, a part of the tumor is only radiated by a small part of the path because of the anchor points created. This means that the method used for the anchor points generation still has room for improvement. Another limitation of the developed TPP lies on the path-finding algorithm. As we see in many paths produced, sharp loops can be produced along the path. These loops are avoided up to a point using the hybrid TSP solver instead of the greedy algorithm, but this comes with a calculation time cost. An additional question that needs to be answered for the developed TPP is whether the treatment beam can indeed be delivered along the DTRT path calculated. Mechanical constraints of the motion of the treatment machine units should be taken into consideration for this purpose. Furthermore, fair comparison between treatment plans of different treatment modalities, could be performed by forcing the same pathlength or delivery time. However, the current TPP does not allow to control the pathlength or delivery time explicitly.

To further improve the dosimetrically motivated non-isocentric DTRT TPP, methods to influence the location of the generated anchor points should be produced. An idea of such an improvement could be to insert a sparser grid of the available map points into the path-finding algorithm. This could possibly lead to sparser located anchor points and then a longer path would be generated delivering the treatment beam from an increased amount of beam directions. Another idea to advance the path-finding algorithm is to utilize a k-optimization algorithm [26] in order to prevent crossings along the path. This would make the path smoother meaning that it would be much easier for the treatment machine units to move along the produced path. Either a combination of the greedy algorithm with the k-optimization algorithm, or a combination of the k-optimization algorithm with the hybrid TSP solver could be introduced to produce the DTRT path. The connection of the greedy algorithm with a k-optimization algorithm could potentially lead to a faster calculation of the DTRT path. An additional advancement of the path-finding algorithm could be the introduction of source to target distance (STD) as an extra DoF. As investigated by Guyer et al. [8], increasing STD could lead to the decrease of the collision areas and so beam delivery could be performed by previously inaccessible beam directions. Another DoF which could be studied is the MLC rotation. In this project, the MLC was set static at a certain angle for the non-isocentric plans. MLC rotation could be further introduced to the path-finding algorithm, finding optimal MLC rotation angles along the path. To further improve the dosimetric results achieved by the developed DTRT TPP, more paths could be used in a single treatment plan. This would lead to an intensity modulation along 4 paths and potentially to better dosimetric results, with a cost of delivery time.

5. Conclusions

By integrating dynamic table translations during beam on, a TPP for non-isocentric DTRT is developed including investigation of suitable parameter values describing the TPP. Four different cases were investigated for an isocentric approach of the developed DTRT TPP in order to validate the performance of the TPP. Similar or even more favorable dosimetric results were obtained by the developed TPP. Three different applications of non-isocentric DTRT are described, including the evaluation of the developed DTRT TPP. Improved dosimetric plan quality was achieved for the bilateral breast case, while the plans generated for the two craniospinal cases showed similar dosimetric results with treatment plans using other treatment modalities. The developed TPP seems to be well-functioning as the promising first results motivate further research in the field of non-isocentric DTRT.

References

[1] F. M. Khan, J. P. Gibbons, and P. W. Sperduto, *Khan's treatment planning in radiation oncology*.

[2] S. Mueller *et al.*, "A hybrid column generation and simulated annealing algorithm for direct aperture optimization," *Phys Med Biol*, vol. 67, no. 7, Apr. 2022, doi: 10.1088/1361-6560/ac58db.

[3] M. K. Fix *et al.*, "Part 1: Optimization and evaluation of dynamic trajectory radiotherapy," *Med Phys*, vol. 45, no. 9, pp. 4201–4212, Sep. 2018, doi: 10.1002/mp.13086.

[4] M. K. Fix, P. Manser, D. Frei, W. Volken, R. Mini, and E. J. Born, "An efficient framework for photon Monte Carlo treatment planning," *Phys Med Biol*, vol. 52, no. 19, Sep. 2007, doi: 10.1088/0031-9155/52/19/N01.

[5] C. Nutting, D. P. Dearnaley, and S. Webb, "Intensity modulated radiation therapy: a clinical review."

[6] M. Teoh, C. H. Clark, K. Wood, S. Whitaker, and A. Nisbet, "Volumetric modulated arc therapy: A review of current literature and clinical use in practice," *British Journal of Radiology*, vol. 84, no. 1007. pp. 967–996, Nov. 2011. doi: 10.1259/bjr/22373346.

[7] G. Smyth, J. C. Bamber, P. M. Evans, and J. L. Bedford, "Trajectory optimization for dynamic couch rotation during volumetric modulated arc radiotherapy," *Phys Med Biol*, vol. 58, no. 22, pp. 8163–8177, Nov. 2013, doi: 10.1088/0031-9155/58/22/8163.

[8] G. Guyer *et al.*, "Enabling non-isocentric dynamic trajectory radiotherapy by integration of dynamic table translations," *Phys Med Biol*, vol. 67, no. 17, Sep. 2022, doi: 10.1088/1361-6560/ac840d.

[9] D. W. O. Rogers, B. Walters, and I. Kawrakow, "BEAMnrc Users Manual," 2023.

[10] I. Kawrakow, D. W. O. Rogers, and B. R. B. Walters, "Large efficiency improvements in BEAMnrc using directional bremsstrahlung splitting," *Medical Physics*, vol. 31, no. 10. John Wiley and Sons Ltd, pp. 2883–2898, 2004. doi: 10.1118/1.1788912.

[11] T. Bortfeld, "IMRT: A review and preview," *Physics in Medicine and Biology*, vol. 51, no. 13. Jul. 07, 2006. doi: 10.1088/0031-9155/51/13/R21.

[12] C. Ju, Q. Luo, and X. Yan, "Path Planning Using an Improved A-star Algorithm," in *Proceedings - 11th International Conference on Prognostics and System Health Management, PHM-Jinan 2020*, Institute of Electrical and Electronics Engineers Inc., Oct. 2020, pp. 23–26. doi: 10.1109/PHM-Jinan48558.2020.00012.

[13] F. Duchon *et al.*, "Path planning with modified A star algorithm for a mobile robot," in *Procedia Engineering*, Elsevier Ltd, 2014, pp. 59–69. doi: 10.1016/j.proeng.2014.12.098.

[14] "Two new variants of Christofides heuristic for the Static TSP and a computational study of a nearest neighbor approach for the Dynamic TSP".

[15] G. Tang, C. Tang, C. Claramunt, X. Hu, and P. Zhou, "Geometric A-Star Algorithm: An Improved A-Star Algorithm for AGV Path Planning in a Port

Environment," *IEEE Access*, vol. 9, pp. 59196–59210, 2021, doi: 10.1109/ACCESS.2021.3070054.
[16] R. Mohan, M. Arnfield, S. Tong, Q. Wu, and J. Siebers, "The impact of fluctuations in intensity patterns on the number of monitor units and the quality and accuracy of intensity modulated radiotherapy," *Med Phys*, vol. 27, no. 6, pp. 1226–1237, 2000, doi: 10.1118/1.599000.
[17] D. M. Shepard, M. A. Earl, X. A. Li, S. Naqvi, and C. Yu, "Direct aperture optimization: A turnkey solution for step-and-shoot IMRT," *Med Phys*, vol. 29, no. 6, pp. 1007–1018, 2002, doi: 10.1118/1.1477415.
[18] E. Heath *et al.*, "Implementation and experimental validation of a robust hybrid direct aperture optimization approach for mixed-beam radiotherapy," *Med Phys*, vol. 48, no. 11, pp. 7299–7312, Nov. 2021, doi: 10.1002/mp.15258.
[19] H. E. Romeijn, R. K. Ahuja, J. F. Dempsey, and A. Kumar, "A column generation approach to radiation therapy treatment planning using aperture modulation," *SIAM Journal on Optimization*, vol. 15, no. 3, pp. 838–862, 2005, doi: 10.1137/040606612.
[20] S. Webb, "Optimisation of conformal radiotherapy dose distribution by simulated annealing Optimisation of conformal radiotherapy dose distributions by simulated annealing," 1989. [Online]. Available: http://iopscience.iop.org/0031-9155/34/10/002
[21] U. Oelfke and W. Schlegel, "New concepts for beam angle selection in IMRT treatment planning: From heuristics to combinatorial optimization Referees."
[22] R. Jeraj, P. J. Keall, and J. V Siebers, "The effect of dose calculation accuracy on inverse treatment planning INSTITUTE OF PHYSICS PUBLISHING PHYSICS IN MEDICINE The effect of dose calculation accuracy on inverse treatment planning," 2002. [Online]. Available: http://iopscience.iop.org/0031-9155/47/3/303
[23] J. L. Bedford and A. P. Warrington, "Commissioning of Volumetric Modulated Arc Therapy (VMAT)," *Int J Radiat Oncol Biol Phys*, vol. 73, no. 2, pp. 537–545, Feb. 2009, doi: 10.1016/j.ijrobp.2008.08.055.
[24] M. K. Fix *et al.*, "Part 1: Optimization and evaluation of dynamic trajectory radiotherapy," *Med Phys*, vol. 45, no. 9, pp. 4201–4212, Sep. 2018, doi: 10.1002/mp.13086.
[25] M. J. D Powell *et al.*, "The gradient projection method for nonlinear programming, pt. I, linear constraints," 1968.
[26] K. Helsgaun, "General k-opt submoves for the Lin-Kernighan TSP heuristic," *Math Program Comput*, vol. 1, no. 2–3, pp. 119–163, 2009, doi: 10.1007/s12532-009-0004-6.